Dilution of the Antarctic Ozone Hole into Southern Midlatitudes

A thesis
submitted in partial fulfilment
of the requirements for the Degree
of
Doctor of Philosophy in Physics
in the
University of Canterbury
by
Jelena Ajtic

Department of Physics and Astronomy
University of Canterbury
2003

Abstract

Reduction in ozone levels in southern midlatitudes, caused by the transport of ozone-depleted air from the Antarctic polar vortex, is examined. The problem is approached from two different, but complementary, directions. First, a case study examining an atypical vertical profile of ozone in December 1998, caused by the presence of vortex air is presented. Second, the overall dilution effect in spring- and summer time in the years 1998, 1999, and 2000 is quantified.

In the first approach, an ozonesonde profile over the Network for Detection of Stratospheric Change (NDSC) site at Lauder (45.0° S, 169.7° E), New Zealand, for 24 December 1998 showing atypically low ozone centered around 24 km altitude (600 K potential temperature), is analyzed. The origin of the anomaly is explained using reverse domain filling (RDF) calculations combined with a PV/O_3 fitting technique applied to ozone measurements from the Polar Ozone and Aerosol Measurement (POAM) III instrument.

The RDF calculations for two isentropic surfaces, 550 K and 600 K, show that ozone-poor air from the Antarctic polar vortex reached New Zealand on 24–26 December 1998. The vortex air on the 550 K isentrope originated in the ozone hole region, unlike the air on 600 K, where low ozone values were the result of dynamical effects.

High-resolution ozone maps are generated, and their examination shows that the vortex remnant situated above New Zealand was the cause of the altered ozone profile on 24 December. The maps also illustrate mixing of the vortex filaments into southern midlatitudes, whereby the overall midlatitude ozone levels are decreased.

In the second approach, to quantify the full impact of the dilution of the Antarctic ozone hole into southern midlatitudes in spring and summer of the years 1998, 1999 and 2000, diabatic RDF calculations are performed for parcels between 30 ° S and 60 ° S, initialized on a 1 ° longitude by 1 ° latitude grid, on seven potential temperature surfaces, between 400 K and 700 K. In each year, the trajectories are run back to 10 October, at which time the ozone depletion processes in the Antarctic vortex have largely ceased. Two distinct regions in the vortex, the core and the edge region, are taken into account.

The reduction in ozone due to the presence of vortex parcels in southern midlatitudes is calculated in the layer between 375 K and 725 K, thus encompassing the stratospheric region where most of ozone depletion occurs and where ozone is most abundant. The calculations are performed under the assumption that the volume mixing ratio of depleted ozone (the difference between undepleted ozone and observed ozone) does not change along the trajectories. To mitigate non-conservation of mass arising from the employment of a

Lagrangian model, a scaling method is introduced.

The results for the years 1998–2000 show that on average, between 15 October and 15 January of the following year, 17–19 % of the midlatitude air parcels originate inside the Antarctic vortex. The corresponding reduction in ozone is 15–18 DU. The reduction caused by the presence of the air parcels originating in the vortex edge region is significant, especially in the early part of the period under examination. The results for four subregions in midlatitudes (spanning longitude regions of 90°, starting from 0°) are also presented, and they indicate that, on average, in the region encompassing New Zealand and Australia ozone reduction is less than in other subregions in the months of October and November, but from mid-December to mid-January the reduction is effectively the same in all subregions.

Furthermore, tests to examine the sensitivity of the results to uncertainties in the wind fields, and to the choice of the initial day, are performed for the year 1998. The results indicate that the method is more sensitive to the initial conditions, including the size of the vortex and the amount of filamentation, than to introduced perturbations in the winds. The corresponding uncertainties in the midlatitude ozone reduction are 38 % and 5 %, respectively. The uncertainties are generally larger for subregions, and range from 37–65 %, and 4–14 %, respectively.

The calculated ozone reduction is compared to the Total Ozone Mapping Spectrometer (TOMS) measurements of ozone column to derive relative changes in the total ozone. The results show that without the dilution effect, ozone levels in southern midlatitudes would be 4–6 % higher during spring- and summertime. Moreover, a comparison of the calculated ozone reduction with ozone levels in 1979 demonstrates that on average, approximately 50–60 % of the change can be attributed to the dilution effect. These results present a lower limit of the impact, as dilution in the lowermost stratosphere and troposphere is not captured in the calculations presented here.

Acknowledgements

XBAΛA!

Contents

Figures

Tables

Chapter 1

Introduction

Ozone depletion represents one of the major global environmental issues of the last three decades. Since the ozone hole was discovered in 1985 (*Farman et al.*, 1985), much scientific research has been conducted in order to understand the intricate processes that drive this phenomenon. Extensive monitoring of the atmosphere using highly sophisticated satellite, aircraft and ground-based instruments, offers data for the detailed analysis of the state of the atmosphere. A great number of atmospheric models have been developed with the aim to clearly distinguish all the causes and pathways leading to ozone depletion. It is now widely accepted that human release of chlorofluorocarbons and some bromine compounds plays the main role in ozone destruction (*WMO*, 2003). However, the incomplete agreement between the observations and the results of existing models indicates that the problem is not yet fully understood.

The ozone hole, which was first described as severe ozone depletion in the Antarctic atmosphere, provoked great concern for life on the Earth. Although ozone is a minor atmospheric constituent, its role for life on the Earth is invaluable since it absorbs biologically harmful ultra-violet radiation. It has been shown that increased exposure to ultra-violet radiation causes damage to the eyes, the immune system and the skin in both humans and animals (*UNEP*, 1998). Moreover, materials such as naturally-occurring and synthetic polymers, i.e. wood and plastics, are adversely affected by the ultra-violet content in sunlight. In addition, atmospheric circulation and climate depend on the amount of ozone present in the stratosphere. Hence, the amount of ozone in the atmosphere has both direct and indirect influence on life on the Earth as we know it.

There have been some suggestions for mitigating ozone loss by direct input of ozone into the atmosphere. Making enough ozone to artificially replace even small amounts is an extremely expensive venture (*Solomon* (1999) and references therein). Alternative schemes involving interference with the chemistry of chlorofluorocarbons have also been shown to be impractical (*Viggiano et al.*, 1995). Therefore, the only practical approach to recovery of the ozone layer is the reduction of global emission of chlorofluorocarbons. This fact was recognized in 1987 when the Montreal Protocol on Substances that Deplete the Ozone Layer was agreed. Since then, it has been ratified by over 160 countries. The research that followed showed that the initial controls were insufficient to prevent further

build up of ozone depleting substances in the atmosphere, and subsequent amendments to the Montreal Protocol strengthened the control.

The imposed control on ozone depleting substances has been successful in one respect – total chlorine carried by chlorofluorocarbons has ceased to increase in the lower stratosphere (*WMO*, 2003). Nevertheless, severe ozone depletion still occurs every austral spring over the Antarctic and the Arctic ozone losses have become significant (*WMO*, 2003). Furthermore, the global mean total column of ozone over the 1997–2001 period, was around 3 % below the pre-1980 average value (*WMO*, 2003). Hence ozone depletion, which was first recognized as a highly localized phenomenon, has become an issue of global importance.

Furthermore, another atmospheric phenomenon caused by human activity, the greenhouse effect, has been shown to be coupled with ozone depletion (*Austin et al.*, 1992). While greenhouse gases warm the Earth's surface they cool the stratosphere and therefore affect the chemical reactions responsible for ozone destruction. Research done in this area shows that these two phenomena are not independent and hence should not be treated as such. Some models predict that in spite of the control of ozone depleting substances, and due to the influence of greenhouse gases, the recovery of the ozone layer may take place later than expected (*Shindell et al.*, 1998).

In the work presented here, only one aspect of the ozone depletion in southern midlatitudes is analyzed – the change in spring- and summertime ozone levels caused by the transport of ozone-depleted air from the Antarctic vortex. An attempt is made to quantify how much of the ozone change compared to the pre-1980 period, is caused purely by transport.

The thesis is organized as follows. In Chapter 2, a short description of the chemical and dynamical processes governing the amount and distribution of ozone in the atmosphere is presented. An emphasis is given on the phenomenology of the Antarctic ozone hole. The ozone changes is midlatitudes are also briefly discussed.

Chapters 3 and 4 give an overview of the data and tools used in this work. A case study of the influence of Antarctic ozone hole on ozone levels in New Zealand, in late December 1998, is presented in Chapter 5. Much of the material in that chapter has been accepted for publication (*Ajtić et al.*, 2003).

A method for quantifying the ozone reduction in midlatitudes, caused by the presence of the Antarctic vortex parcels, is given in Chapter 6. The results for the years 1998, 1999 and 2000, along with a validation of the method used, and sensitivity tests, are presented in Chapter 7. Chapter 8 provides concluding remarks.

Chapter 2

Ozone Depletion

This chapter gives a short introduction to ozone depletion. The chemical and dynamical processes that control the ozone amounts and distribution are presented first. Then, the polar vortex and the ozone hole are described briefly. Finally, the ozone changes in midlatitudes are considered. As the goal of this work is to quantify the influence of the Antarctic ozone hole on the ozone levels in southern midlatitudes, emphasis is given to the Southern Hemisphere.

2.1   Ozone in the Atmosphere

Ozone's molecular structure consists of three oxygen atoms. The most outstanding feature of ozone is absorbtion of solar ultra-violet (UV) radiation in the wavelengths which are harmful to living systems on the Earth. Proteins and nucleic acids are damaged by radiation of wavelengths shorter than about 290 nm. While some major components of the atmosphere, especially oxygen, filter out solar radiation of less than 230 nm, ozone is the only atmospheric species capable of attenuating radiation of 230–290 nm (*Wayne*, 1992). In this wavelength region, ozone has a strong absorption, and thus represents an effective filter despite its relatively small concentration.

Most of ozone molecules reside in the stratosphere (Figure 2.1), in a layer below 35 km (*Brasseur and Solomon*, 1986). The typical ozone concentration in the stratosphere is 10 parts per million by volume (ppmv). In the troposphere (Figure 2.1), ozone is harmful to both animal and plant life and is considered a pollutant. In urban air, the concentrations of ozone can be as high as 0.35 ppmv (*Jacobson*, 1999). The typical amount of ozone in the troposphere is approximately 10 % of the total column ozone[1] (*WMO*, 2003), but it can be as low as 5 % in unpolluted areas (*McKenzie et al.*, 2003).

The absorption of solar ultra-violet and the outgoing infrared radiation by ozone results in heating of the stratosphere. As temperature gradients influence transport in the stratosphere, ozone is also responsible for the atmospheric circulation.

---

[1]The unit for total column ozone is a Dobson unit (DU) which represents the thickness, measured in hundredths of a millimetre, that the ozone column would occupy at standard temperature and pressure.
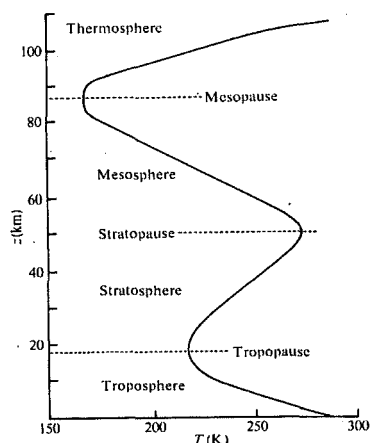
Figure 2.1: Temperature–altitude profile of the atmosphere [from *Wayne* (1992)]. The stratosphere is a part of atmosphere in which temperature increases with altitude. Its boundaries are roughly between 12 and 50 km, depending on latitude (in polar regions, the lower boundary is about 9 km). The existence of the stratosphere is a direct consequence of the absorption of solar radiation by ozone. The lower part of the atmosphere, in which temperature decreases with altitude, is the troposphere.

2.1.1   Ozone Chemistry

Chapman (1930) was the first to propose natural pathways of ozone formation and destruction. These reactions are now known as the Chapman cycle (Table 2.1).

During the 1960s it became clear that the Chapman cycle reactions were insufficient to explain the observed levels of stratospheric ozone. *Crutzen* (1970, 1971) showed that the additional reactions of ozone destruction included the HO_x family ($HO_x = OH + HO_2$) and NO_x family ($NO_x = NO + NO_2$) (Table 2.1). In the 1970s, the ClO_x family ($ClO_x = Cl + ClO$) and BrO_x family ($BrO_x = Br + BrO$) were also recognized as ozone depleting substances (Table 2.1). Even though there are many natural processes that produce chlorine at ground level (e. g. sea salt and volcanic emission of hydrogen chloride), these compounds are efficiently removed in precipitation due to their high solubility (*Solomon*, 1999). Hence, chlorine atoms in the stratosphere are mainly produced by the photolysis of chlorofluorocarbons (CFCs) (*Molina and Rowland*, 1974), while bromine atoms are mainly produced from halons.[2,3] Hydrogen chloride emitted from spacecraft motors directly into the stratosphere also represents a source of active chlorine.

The common feature of ozone destruction reactions is that all depleting substances act as catalysts. Therefore, even small concentrations of these substances can destroy a great number of ozone molecules. For example, in the middle and upper stratosphere (35–40 km), ClO_x can act as a catalyst in a thousand ozone destroying reactions before it is removed by reaction with another gas (*Jacobson*, 1999).

---

[2]Halons are brominated CFCs.

[3]Since chlorine and bromine ozone depleting reactions are coupled, they are often called halogen chemistry.

Chapman Chemistry	$O_2 + h\nu \, (\lambda < 242 \, \text{nm}) \rightarrow 2\,O\,(^3P)$
	$O\,(^3P) + O_2 + M \rightarrow O_3 + M$
	$O\,(^1D) + M \rightarrow O\,(^3P) + M$
	$O\,(^3P) + O\,(^3P) + M \rightarrow O_2 + M$
	$O\,(^3P) + O_3 \rightarrow 2\,O_2$
	$O_3 + h\nu \, (\lambda < 336 \, \text{nm}) \rightarrow O\,(^1D) + O_2$
HO_x Catalytic Cycles	$O\,(^3P) + OH \rightarrow O_2 + H$
	$H + O_2 + M \rightarrow HO_2 + M$
	$O\,(^3P) + HO_2 \rightarrow O_2 + OH$
	Net Cycle: $O\,(^3P) + O\,(^3P) + M \rightarrow O_2 + M$
	$OH + O_3 \rightarrow HO_2 + O_2$
	$HO_2 + O_3 \rightarrow OH + 2\,O_2$
	Net Cycle: $2\,O_3 \rightarrow 3\,O_2$
NO_x Catalytic Cycles	$NO + O_3 \rightarrow NO_2 + O_2$
	$O\,(^3P) + NO_2 \rightarrow NO + O_2$
	Net Cycle: $O\,(^3P) + O_3 \rightarrow 2\,O_2$
ClO_x Catalytic Cycles	$Cl + O_3 \rightarrow ClO + O_2$
	$ClO + O\,(^3P) \rightarrow Cl + O_2$
	Net Cycle: $O\,(^3P) + O_3 \rightarrow 2\,O_2$
	$Cl + O_3 \rightarrow ClO + O_2$
	$ClO + ClO + M \rightarrow Cl_2O_2 + M$
	$Cl_2O_2 + h\nu \rightarrow Cl + ClO_2$
	$ClO_2 + M \rightarrow Cl + O_2 + M$
	Net Cycle: $2\,O_3 \rightarrow 3\,O_2$
$Cl - Br$ Catalytic Cycles	$Cl + O_3 \rightarrow ClO + O_2$
	$Br + O_3 \rightarrow BrO + O_2$
	$BrO + ClO \rightarrow Br + ClO_2$
	$ClO_2 + M \rightarrow Cl + O_2 + M$
	Net Cycle: $2\,O_3 \rightarrow 3\,O_2$
Coupling and Reservoir Reactions	$ClO + NO \rightarrow Cl + NO_2$
	$Cl + CH_4 \rightarrow HCl + CH_3$
	$HO_2 + ClO \rightarrow HOCl + O_2$
	$ClO + NO_2 + M \rightarrow ClONO_2 + M$
	$BrO + NO_2 + M \rightarrow BrONO_2 + M$
	$OH + NO_2 + M \rightarrow HNO_3 + M$
Heterogeneous Reactions	$HCl + ClONO_2 \rightarrow HNO_3 + Cl_2$
	$N_2O_5 + H_2O \rightarrow 2\,HNO_3$
	$ClONO_2 + H_2O \rightarrow HNO_3 + HOCl$
	$HCl + HOCl \rightarrow H_2O + Cl_2$
	$BrONO_2 + H_2O \rightarrow HNO_3 + HOBr$
	$HCl + BrONO_2 \rightarrow HNO_3 + BrCl$
	$HCl + HOBr \rightarrow H_2O + BrCl$

Table 2.1: Some illustrative chemical processes in ozone gaseous and heterogeneous chemistries [from *Solomon* (1999)]. In these reactions, M represents a third body, e.g. O_2 or N_2.

On the other hand, ozone depleting substances also react with each other, and other molecules, to produce reservoir species.[4] For example, chlorine can react with methane, the only organic sufficiently long-lived to reach the stratosphere, to produce hydrogen chloride, a temporary reservoir from which active chlorine can be regenerated. Bromine is particularly effective in destroying ozone because unlike chlorine atoms, atomic bromine does not react rapidly with methane, thus it spends more time in its catalytically active form. Such a potential of bromine to destroy ozone is mitigated by the fact that in the stratosphere, bromine is about 200 times less abundant than chlorine (*Schauffler et al.*, 1993).

The ozone production rates maximize in the stratosphere, where the solar intensity is high, and the abundance of molecular oxygen is sufficient to yield large rates of the photolysis reaction in which atomic oxygen is formed (Table 2.1). As the intensity of UV radiation peaks in the tropics, the tropical stratosphere is where most ozone is produced.

The reaction rates of the ozone destruction cycles also depend on the altitude region in which the reactions take place. Hence, the photochemical lifetime of ozone depends on altitude. In the upper stratosphere and lower mesosphere, ozone is very short-lived, while below approximately 30 km, ozone is long-lived, and is dynamically controlled (*Brasseur and Solomon*, 1986). In other words, below ∼30 km, transport plays a major role in the ozone distribution.

2.1.2   Ozone Distribution

Transport in the lower and middle stratosphere, where ozone is a long-lived species, determines the global distribution of ozone. Large-scale stratospheric circulation, which is characterized by rising motion in the tropics and descending motion in middle and high latitudes, transports ozone from the tropical region where ozone production is at maximum, to middle and high latitudes. As a consequence, the total column ozone peaks in higher latitudes, in the Northern Hemisphere around 75°N, and in the Southern Hemisphere between 50°S and 60°S in spring (*Brasseur and Solomon*, 1986). The general circulation pattern was recognized by *Dobson* (1930) who used it to explain the discrepancy between the location of the maximum ozone production and of the maximum ozone abundance. These results were later confirmed by *Brewer* (1949). The current understanding of the stratospheric large-scale motion agrees with the early findings (*Holton et al.*, 1995).

Seasonal and latitudinal variations in the vertical distribution of ozone influence the total column ozone. As an example, the standard vertical distributions of ozone in Southern Hemisphere (SH) midlatitudes (30°–60°S) and polar region (60°–90°S), for the months

---

[4]Reservoir species represent inactive form of ozone depleting substances, i. e. they do not participate in catalytic cycles.

of March, June, September and December, are plotted in Figure 2.2.
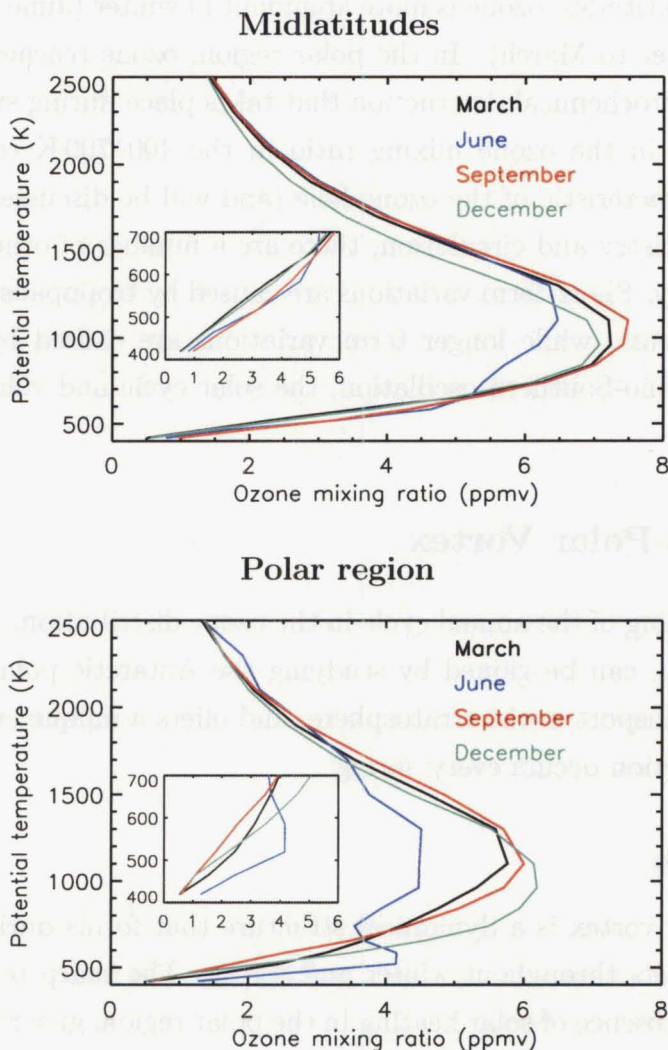
Figure 2.2: Standard ozone mixing ratio (ppmv) as a function of potential temperature (K), in southern midlatitudes (top) and polar region (bottom) for the months of March, June, September and December. The ozone vertical profile between 400 K and 700 K is enlarged in the smaller plots. The data were obtained from the UARS Reference Atmospheric Project web page, http://code916.gsfc.nasa.gov/Public/Analysis/UARS/urap/home.html.

A complete understanding of the vertical distribution in midlatitudes and the polar region requires a detailed discussion of all the processes influencing ozone levels, including the Antarctic ozone hole (Section 2.2.2). Here, it is worth mentioning a few things.

The volume mixing ratio of ozone (which is a relative quantity, and represents the ratio of the number of ozone molecules and the number of molecules of dry air, see Section 6.2) is higher at all altitudes in midlatitudes, resulting in a larger total column ozone in midlatitudes than in the polar region. Even though the volume mixing ratio of ozone peaks around 1000 K, the number of ozone molecules is at maximum lower in the stratosphere, roughly between the potential temperature surfaces of 400 K and 700 K, where the atmosphere is more dense (small plots in Figure 2.2). In this region, even small

changes in the ozone mixing ratio reflect significant changes in the total amount of ozone.

In southern midlatitudes, ozone is more abundant in winter (June to September), than in summer (December to March). In the polar region, ozone reaches seasonal minimum in autumn, after photochemical destruction that takes place during summer (*Brühl et al.*, 1998). The change in the ozone mixing ratio in the 400–700 K region, from June to September, is a characteristic of the ozone hole (and will be discussed in Section 2.2.2).

Apart from chemistry and circulation, there are a number of other factors that influence ozone variability. Short-term variations are caused by tropopause folding and stratospheric warming events, while longer term variations are caused by the quasi-biennial oscillation, the El Niño-Southern oscillation, the solar cycle and volcanic effects (*WMO*, 1999).

2.2 Antarctic Polar Vortex

A better understanding of the annual cycle in the ozone distribution, both in midlatitudes and the polar region, can be gained by studying the Antarctic polar vortex. The polar vortex influences transport in the stratosphere, and offers a unique environment in which severe ozone destruction occurs every spring.

2.2.1 Description

The Antarctic polar vortex is a dynamical structure that forms during autumn over the Antarctic, and persists throughout winter and spring. The sharp temperature gradients that develop in the absence of solar heating in the polar region, give rise to strong westerly winds which isolate the air inside the vortex.

Some studies on the degree of the vortex isolation showed that the vortex air is continuously mixed with the surrounding air (*Tuck*, 1989; *Proffitt et al.*, 1989b), in other words, that the vortex behaves like a "flowing processor". On the other hand, the model results of *Juckes and McIntyre* (1987) showed that the exchange of material between the vortex and the surrounding air is only one-way. Although some material from the vortex can be eroded into the surrounding air, the intrusion of the surrounding air into the vortex is much less likely. The isolation of the vortex is due to the strong gradient of potential vorticity (PV) at the edge of the vortex, which acts as a barrier to mass exchange. This idea of the vortex behaving as a "containment vessel" has been supported by a number of studies (e.g. *Bowman*, 1993; *Pierce and Fairlie*, 1993; *Norton*, 1994; *Sutton*, 1994; *Rosenfield and Schoeberl*, 2001).

Still, in the lowermost stratosphere, the vortex is not as well isolated as higher up. The transition altitude where the dynamical character of the vortex changes is around 400 K (*Schoeberl et al.*, 1992; *Bowman*, 1993; *Chen et al.*, 1994; *Chen*, 1994; *Haynes and*

Shuckburgh, 2000b). Below this altitude, there is a substantial exchange of mass across the vortex boundary.

A definition of the vortex boundary, or edge, is a necessary prerequisite for analyzing the vortex. Some of the definitions use the wind maximum of the circumpolar jet (e.g. *Kent et al.*, 1985), or the steep horizontal gradient in tracer fields (e.g. *Proffitt et al.*, 1989a), or the maximum of kinetic energy (*Paparella et al.*, 1997) . A definition introduced by *Nash et al.* (1996), taking into account both the steep gradient of PV and the strong winds associated with the boundary of the vortex, is widely used.

Inside the vortex, there are two distinctly different regions: the vortex core, where mixing is relatively strong, and the vortex edge region (region between the vortex core and the exterior of the vortex) of weak mixing (*Lee et al.*, 2001; *Öllers et al.*, 2002). The size and the position of the vortex edge region change with seasons. In winter, the vortex core and the edge region are of almost equal size (*Lee et al.*, 2001).

The temperatures inside the vortex are extremely low (below $-80\,^\circ$C) due to the absence of solar heating, as well as to isolation (preventing intrusion of warmer air masses). The temperatures in the vortex edge region are usually higher than in the vortex core (*Tao and Tuck*, 1994).

During winter, the vertical motion throughout the vortex is downwards. Various methods have been used to estimate descent rates in the vortex (*WMO*, 2003). Due to higher temperatures and increased cooling to space, descent is stronger in the upper stratosphere than in the lower stratosphere (*Rosenfield et al.*, 1994). Since there is very little exchange of air between the vortex and the surrounding air, diabatic descent plays a key role in the winter ozone distribution inside the vortex.

Randall et al. (1995), *Godin et al.* (2001) and *Hoppel et al.* (2002) discussed the vertical distribution of ozone in the vortex observed during winter. They noted that the subsidence of air from the altitudes where ozone mixing ratio peaks (Figure 2.2), brings ozone-rich air to the region around and below $500\,$K (small plot in the bottom panel of Figure 2.2). As a result, in that altitude region, the ozone mixing ratios in the vortex are higher than in other seasons, but also higher than in the surrounding midlatitude air.

On the other hand, at the altitudes above $500\,$K, winter ozone mixing ratios inside the vortex are less than in other seasons (Figure 2.2). This is caused by diabatic descent of air above the ozone mixing ratio peak which reduces ozone levels in this region (*Bevilacqua et al.*, 1997), and by the isolation of the vortex which prevents intrusion of ozone-rich air. At the same time, horizontal mixing of ozone-rich air outside the vortex leads to accumulation of ozone in midlatitudes (*Manney et al.*, 1995; *Mariotti et al.*, 2000). Hence, the ozone mixing ratios above $500\,$K in midlatitudes are higher than inside the vortex.

In spring, when solar heating raises the temperatures in the polar region, the winds driven by the temperature gradients weaken, and the vortex becomes less stable. In the

process of breaking up, the vortex is not as well isolated, and the mixing regime between the vortex and midlatitude air changes, allowing for two-way mass exchange to occur (*Bowman*, 1993).

The polar vortex in the Northern Hemisphere is generally smaller, warmer, less stable and breaks up earlier in spring than its Antarctic counterpart (e.g. *Waugh*, 1997; *Waugh and Randel*, 1999; *Waugh et al.*, 1999).

2.2.2   Antarctic Ozone Hole

Gas-phase chemistry, outlined in Section 2.1.1, coupled with transport, was sufficient to describe the pre-1980 global distribution of ozone. Some of the first chemical models of ozone depletion were developed during the 1970s (*Crutzen*, 1974). These models encompassed gas-phase chemical reactions of ozone destruction and predicted ozone depletion in the region around the altitude of 40 km, where ClO was calculated to have a maximum. Soon afterwards, the ClO maximum was confirmed by observations (e.g. *Parrish et al.*, 1981), whereas ozone depletion at that altitude was confirmed later by observations of the northern midlatitude ozone profile trends (*Solomon et al.*, 1997). The early models of ozone depletion did not predict the findings of *Farman et al.* (1985), reporting a severe ozone depletion in the austral spring at the British Antarctic Survey station at Halley, Antarctica.

Hofmann et al. (1987) showed that at some altitudes (roughly between 10 km and 20 km) in the lower stratosphere ozone can be almost completely removed (Figure 2.3), while the total amount of ozone becomes significantly smaller than the winter amounts. These observations were quickly confirmed by ground-based measurements from other Antarctic sites and by satellite measurements. In addition, it was confirmed that the depletion extended over almost the entire continent. This phenomenon became known as the Antarctic ozone hole.

These findings were completely unanticipated. First, the observed depletion was far larger than ever expected. Second, the altitudes at which the depletion occurred were lower in the stratosphere than the existing models suggested. Finally, the predictions did not identify the Antarctic as a site of particular significance for ozone depletion. The available observations of the Antarctic ozone and other chemical species as well as meteorological properties were limited at the time of the discovery. As a result, a variety of different theories were proposed as plausible explanations (*Solomon* (1999) and references therein).

Many campaigns, including intensified ground-based measurements and satellite observations in the Antarctic atmosphere, have been undertaken since 1985. The early research showed greatly enhanced ClO concentrations in the Antarctic stratosphere, and the follow-
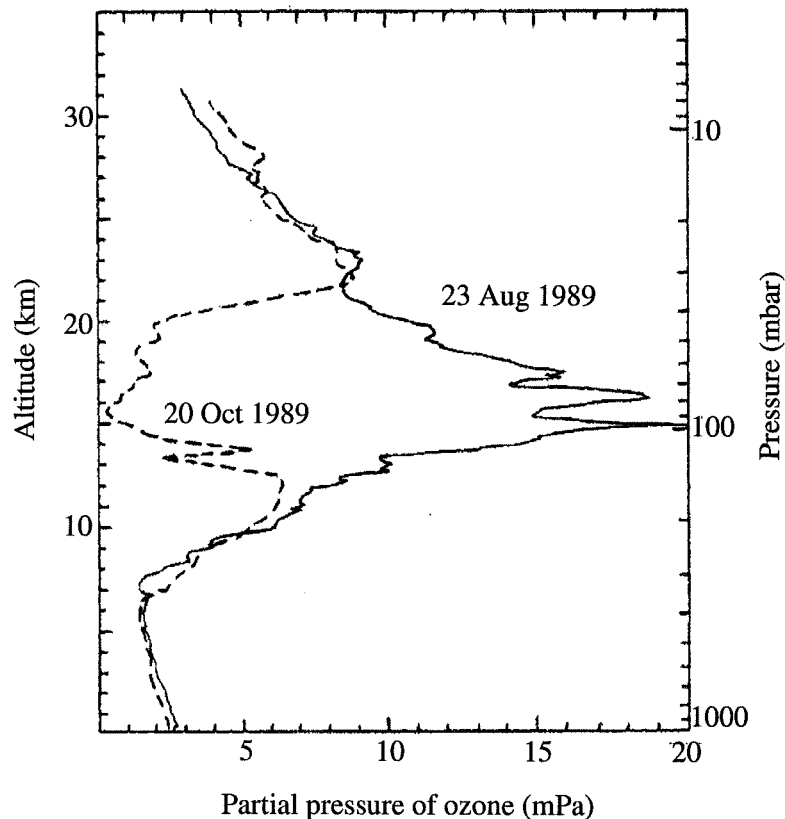
Figure 2.3: Ozone vertical profiles over McMurdo station, Antarctica, in winter (August) and spring (October) 1989. The winter profile shows the typical shape of ozone layer where ozone is most abundant (between 14 km and 22 km). The spring profile shows a drastic drop in ozone concentration, with the reduction in ozone being 98 % at 15 km [from *Deshler et al.* (1990)].

ing studies were directed towards chlorofluorocarbons (CFCs) in the stratosphere, polar stratospheric clouds (PSCs) and heterogeneous chemistry. Here, only a short description of the current understanding of the ozone depletion processes is given.

CFCs are almost completely insoluble in water (*Solomon*, 1999) and are chemically inert in the troposphere. As a consequence, they are evenly distributed in the troposphere (through rapid mixing), in spite of the fact that the main sources are in the Northern Hemisphere. An upward motion in the tropics (*Holton et al.*, 1995) lifts CFCs into the stratosphere, and from there they are transported polewards. Hence, although there are no sources of CFCs in the Antarctic, observations show that above the South Pole they are present in nearly the same amounts as above the industrialized regions. Once in the stratosphere, CFCs are photolyzed by solar radiation and produce reactive chlorine, which takes part in the catalytic reactions of ozone destruction (Table 2.1). Still, for severe ozone depletion to occur, reactive chlorine has to be present in large amounts, which are not readily available purely from the gas-phase chemical reactions. This preconditioning of the polar stratosphere is achieved when the temperatures are low enough for PSCs to

form.

Two types of PSCs are found in the stratosphere, at altitudes of approximately 12–25 km (*Collins et al.*, 1993; *Fromm et al.*, 1997). Type I PSCs form when the temperature drops to below about 195 K (*Jacobson*, 1999), and they contain nitric acid (*WMO*, 2003). Denitrification of the stratosphere is a consequence of adsorption of nitric acid to type I PSCs, whereby nitric acid is first removed from the gas phase, and then sedimented out along with the PSC particles to lower regions of the stratosphere. Type II PSCs form when the temperature is below 187 K and they are mostly water ice (*WMO*, 1999).

Heterogeneous chemical reactions take place on PSC surfaces. The products of these reactions are adsorbed species, which can either remain adsorbed or can desorb. Some key heterogeneous reactions are presented in Table 2.1. For example, molecular chlorine, a product of the HCl and $ClONO_2$ reaction, desorbs and can start gas-phase catalytic reactions that destroy ozone.

In short, even though PSCs do not take part in the actual ozone depleting reactions, they play a key role in the availability of ozone depleting substances. On one hand, heterogeneous reactions on PSC surfaces convert relatively inactive forms of chlorine into photochemically active forms. On the other hand, the formation of chlorine reservoir species (e. g. in a reaction with NO_2, see Table 2.1) is hindered due to the denitrification of the stratosphere caused by the presence of PSCs. Therefore, during the course of polar night, active chlorine species accumulate in the altitude region where PSCs are present.

The ozone hole forms in spring, when sunlight returns to the polar regions abundant in active forms of ozone depleting substances. The cycle involving the ClO dimer, Cl_2O_2, and the Cl–Br cycle (Table 2.1), are thought to be the cycles responsible for over 90% of the ozone removal (*Solomon* (1999) and references therein).

Throughout the vortex core, the temperatures are low enough for PSCs to form and to persist until October (e.g. *Cacciani et al.*, 1997; *Fromm et al.*, 1997). The observed ozone decline is steepest in September, when the vortex is exposed to large amounts of sunlight. The time when depletion processes cease is determined by the amount of active substances (which in turn are largely controlled by the presence of PSCs) and the amount of ozone "available" for destruction. Usually, the depletion ends around late September or early October (e.g. *Godin et al.*, 2001). With the temperatures in the vortex edge region being usually warmer than in the vortex core (*Tao and Tuck*, 1994), PSCs are less frequent and there is less reactive chlorine. However, the edge region is exposed to more sunlight, resulting in a significant ozone depletion in the edge region (*Lee et al.*, 2001).

The Arctic ozone hole is generally smaller than its Southern Hemisphere counterpart. The main reason behind this is the difference in meteorology of the Antarctic and the Arctic vortex. As already mentioned, the Arctic vortex is warmer, hence the occurrences of PSCs are less frequent, and with the Arctic vortex being less stable, and breaking up

earlier, the resulting ozone depletion is not as severe. Nevertheless, large ozone depletion above the Arctic has been reported in especially cold winters, e. g. in the winter of 1999–2000 (*WMO*, 2003).

Ozone depletion inside the vortices has been a subject of extensive studies. A number of methods, including calculations based on observations as well as purely modelling studies, have been presented; e. g. *MacKenzie et al.* (1996), *Schoeberl et al.* (1996), *Godin et al.* (2001) in the SH, and e. g. *Salawitch et al.* (1990), *von der Gathen et al.* (1995), *Manney et al.* (1996), *Knudsen et al.* (1998b), *Hoppel et al.* (2002) in the NH. A detailed comparison of the Arctic ozone loss techniques is given by *Harris et al.* (2002).

Some studies of the Arctic ozone loss show that the modelled ozone loss is less than the observed loss, and suggest that the polar ozone-depleting chemistry is not fully understood (*Hansen et al.*, 1997; *Deniel et al.*, 1998; *Becker et al.*, 1998; *Woyke et al.*, 1999; *Becker et al.*, 2000; *Rex et al.*, 2003). On the other hand, *Wu and Dessler* (2001) showed a good agreement between the modelled and observed ozone loss in the Antarctic, and argued that the discrepancies in the Arctic could be caused by the simplified representation of the dynamics.

The reduction of ozone levels inside the vortex decreases solar heating, and in turn, strengthens the lower vortex (*Mahlman et al.*, 1994). Consequently, the decrease in the vortex temperatures leads to a longer lasting vortex (*Kiehl et al.*, 1988). *Waugh et al.* (1999) and *Zhou et al.* (2000) found that the break up of the Antarctic vortex in the 1990's was delayed by about two weeks, compared to the early 1980's. On the other hand, *Bodeker et al.* (2002) showed that over the 1981–2000 period, the size of the Antarctic vortex did not change. Inside the vortex, though, the ozone hole both increased in size, and deepened.

The analysis of changes in the total column ozone between November 1978 and December 2000 presented in *WMO* (2003) shows that over the September–November period in the SH polar region, the ozone trends are of order −2.5 %/year. This trend is more negative than in any other season and region.

2.3   Ozone Reduction in Midlatitudes

Global observations of the total column ozone show decreases in ozone levels not only in the polar regions, but also in midlatitudes. In southern midlatitudes (35 °–60 ° S), total ozone is 5–6 % lower than in the early 1980's, with the maximum decrease in spring- and summertime (*WMO*, 2003).

Chemical and dynamical processes both contribute to ozone reduction in midlatitudes; they are coupled and the full understanding requires a simultaneous analysis. Chemical processes include in situ destruction of ozone. Dynamical processes include transport of

ozone-poor air into midlatitudes, and changes in the stratospheric and tropospheric circulation and in tropopause height (*WMO*, 2003). Here, chemical destruction and transport of ozone-poor air are discussed briefly.

In situ chemical destruction of ozone includes a number of pathways. For example, heterogeneous reactions on sulfate aerosols can yield sufficient amounts of active chlorine for significant ozone loss (*Hofmann and Solomon*, 1989), both in midlatitudes and in polar regions (e.g. *Bregman et al.*, 1997; *Knight et al.*, 1998). In addition to direct chlorine activation on aerosols, the hydrolysis reaction of N_2O_5 has an indirect influence on ozone depletion as it reduces concentrations of NO_x (*Solomon* (1999) and references therein). On the other hand, midlatitude in situ ozone destruction can also be initiated by active forms of depleting substances transported from the polar vortices (e.g. *Prather and Jaffe*, 1990; *Norton and Chipperfield*, 1995). Instances of vortex air, in the vertical region where ozone depletion occurs, reaching midlatitudes during winter are ample for the Northern Hemisphere (e.g. *Orsolini et al.*, 1995; *Schoeberl and Newman*, 1995; *Godin et al.*, 2002). Since the Arctic vortex is less stable than the Antarctic vortex, the likelihood of these events is higher in the Northern Hemisphere. Nevertheless, *Brinksma et al.* (1998) reported that in the winter of 1997, very low ozone values in New Zealand were in part caused by the presence of Antarctic vortex air at altitudes above $\sim$25 km. It is important to note that at these altitudes vortex air is poor in ozone due to vertical descent (as discussed in Section 2.2.1), and not because of the chemical depletion.

Transport of vortex air into midlatitudes plays another key role in midlatitude ozone levels. If transport occurs after the onset of ozone depletion inside the vortex, then transport reduces ozone not only through ensuing chemical depletion caused by any remaining active substances, but also through another two mechanisms. First, the mere presence of isolated ozone-depleted air masses causes a transient ozone reduction over the geographical region where they are located (e.g. *Kirchhoff et al.*, 1997; *Pérez et al.*, 2000; *Brinksma et al.*, 2002; *Ajtić et al.*, 2003). A longer lasting, and not as conspicuous effect takes place once vortex ozone-depleted air is diluted in midlatitude air.

Due to more severe ozone depletion inside the Antarctic vortex, the midlatitude ozone levels in the Southern Hemisphere, compared to the Northern Hemisphere, are likely to be more affected by transport, especially during and after vortex breakdown, when large vortex air masses reach midlatitudes.

2.4   Scope of This Work

The aim of the work presented here is to examine the impact of transport of ozone-depleted air into southern midlatitudes. There are two distinct parts in the study. In Chapter 5, a transient event of vortex remnants reaching New Zealand in December 1998,

is examined. A more comprehensive study of the impact, encompassing three months during spring-summer season in 1998, 1999 and 2000, is given in Chapter 7.

There have been some studies partially covering the second objective. For example, purely modelling works of *Prather et al.* (1990), *Mahlman et al.* (1994), *Eckman et al.* (1996) and *Chipperfield* (1999) showed a decrease of 2–5 % in midlatitude total ozone, as a consequence of dilution. In northern midlatitudes, *Knudsen and Grooß* (2000) used the 1997 winter ozone depletion inside the Arctic vortex (*Knudsen et al.*, 1998b) to show that dilution in May of that year was responsible for 40 % of the total ozone change from 1979. The study of *Li et al.* (2002) indicated that ~10 % of the September–October southern midlatitude ozone trends is caused by the presence of the Antarctic vortex air.

Still, as stated in *WMO* (2003), Chapter 4: "It is also well established that some of the chemical depletion that occurs during spring in high latitudes must eventually lead to a decrease (or "dilution") of ozone at midlatitudes when the polar vortices break down. However, this process is poorly quantified at present.". This thesis will hopefully shed more light on the topic.

Chapter 3

Trajectory Scheme

In this chapter, details of the trajectory scheme and meteorological data used in the calculations are given. Two modes of trajectory calculations, isentropic and diabatic, are described. Heating rates used in diabatic trajectory calculations are also discussed briefly. The applications of trajectory calculations are illustrated, particularly for the isentropic case. Finally, computational errors in trajectory calculations, and the errors arising from the meteorological data used, are discussed.

3.1 Introduction

There are two frames of reference in which time evolution of an atmospheric species can be followed. In the Eulerian frame of reference, the distribution of the species at any given point of time, is examined on a set of stationary grid points. On the other hand, in the Lagrangian frame of reference, the distribution is examined on a pre-chosen set of points, which follow the motion of the atmosphere. The possibility of tracking each air parcel and examining its motion in the atmosphere that is the basis of the Lagrangian frame of reference, is used in this work.

A trajectory scheme computes the change in the distribution of a species due to transport, either by prevailing winds (advection) or by turbulent mixing (diffusion), or both. In the Lagrangian frame of reference, time evolution of each air parcel is analyzed by solving the displacement equation

$$\frac{d\mathbf{x}}{dt} = \mathbf{v}, \tag{3.1}$$

where $\mathbf{x}$ is the position vector and $\mathbf{v}$ is the velocity of the parcel, for each time-step t. There are two steps in solving the above equation. The first one is calculating the velocity vector at current parcel locations, and the other one is the actual integration of the equation. In the code used in this work, the velocities away from the pole (see below) are determined through bilinear interpolation of input wind fields, and the fourth-order Runge-Kutta method is used to integrate the equation.

The coordinate system of the trajectory code is spherical apart from regions near the poles where it is polar-stereographic. Near the poles, the wind vectors become singular and the polar cap latitude-longitude grid boxes are no longer even approximately rectan-

gular. To overcome these problems, the trajectory scheme has the capacity to convert the wind vectors to polar-stereographic coordinates and carry out the interpolation in these coordinates. This procedure can be turned on by choosing a polar-cap radius. All parcels which begin a time step poleward of the chosen radius are advected in polar-stereographic coordinates, and at the completion of the time step, the parcels are returned to latitude-longitude coordinates. The polar-stereographic cap of 25° radius is used in this work.

The trajectory code has been designed to accept input data in various formats, including aircraft and satellite data, as well as data from an assimilation system. In the current work, data from the United Kingdom Meteorological Office are used.

3.2   Met Office Data and Analysis

A data assimilation system that has been developed at the United Kingdom Meteorological Office (Met Office) is the main source of meteorological data in this work. The Met Office data assimilation system provides a self-consistent sequence of three-dimensional grid point analyses of the atmosphere (*Swinbank and O'Neill*, 1994).

The observational data for the assimilation system represent a heterogeneous set of measurements from the Upper Atmosphere Research Satellite (UARS)[1] and also from a variety of other sources. The main type of non-UARS observations are temperature soundings from the Television Infra Red Observation Satellites (TIROS-N) series of polar orbiter satellites operated by the National Oceanic and Atmospheric Administration (NOAA) and radiosonde soundings of temperatures and winds. Additional observational sources include aircraft winds and temperatures, satellite cloud-track winds, and surface observations of pressure.

The numerical model used by the assimilation system is the Met Office Unified Model (UM). This model has been designed for a variety of applications, including operational weather forecasting and climate simulations. The output grid of the model has a latitude resolution of 2.5° and longitude resolution of 3.75°. There are 42 levels in the vertical coordinate, with resolution in the stratosphere of approximately 1.6 km. The levels near the ground follow the terrain. The top level of the model is at 0.28 hPa.

The process of data assimilation consists of the following steps. First, UARS and non-UARS data are acquired. These data then undergo an observation quality control whereby they are checked against values taken from a numerical forecast at the location of the observation. If a statistical test, based on numerical values and expected errors in

---

[1]UARS was launched in 1991 and a number of instruments on board are still operational. The Met Office data assimilation system uses only a subset of observations conducted on UARS – measurements of temperature and stratospheric winds. Nonetheless, chemical observations from UARS, that include measurements of source gases, reservoir gases and radicals, have proven to be extremely valuable in the study of ozone depletion processes.

the observations, labels an observation as likely to be incorrect, it is not passed to the assimilation. The statistical test allows for a group of independent observations which are consistent with each other, but do not agree with the forecast data, to be accepted. Next, the assimilation is run by integrating the UM in data assimilation mode, in which numerical fields, as they are being integrated, are adjusted towards the observed data. This way the state of the numerical model is a realistic representation of the state of the atmosphere within the assumed errors. Apart from this assimilation mode, the UM can also be run in forecast mode, in which case the evolution of the state of the atmosphere is governed solely by the model equations. The output from the forecast mode is used to run the observation quality control, as mentioned above.

The model is first run for 24 h in data assimilation mode, immediately followed by 24 h in forecast mode. At the end of the assimilation period, the UM writes out a set of analyzed fields and a copy of the complete model state is taken as initial data for the next 24 h of assimilation.

Met Office assimilated data for temperatures, zonal and meridional wind components, and geopotential height are used in this work. Global-average estimated root mean square (RMS) errors and estimated bias for those properties are given in Table 3.1. The tem-

	Temperature (K)		Wind (m/s)		Geopotential height (m)
Pressure (hPa)	RMS	bias	RMS	bias	RMS
1000	1.0	<0.3	6.0	<1.0	(10)
tropopause	1.5		9.0		
100	1.0	<0.3	6.0	<1.0	(20)
10	1.0	<0.3	(8.0)		(70)
1	2.0	<0.5	(12.0)		(100)

Table 3.1: Estimated root mean square errors and bias for the Met Office temperatures, winds and geopotential height. Indicative estimates are given in brackets [from UK Met Office Correlative Analyses: Data Quality, on the British Atmospheric Data Centre web page www.badc.rl.ac.uk].

perature and wind errors are expected to be greater in winter and during dynamically active times such as stratospheric warmings. The errors in winds are also larger for high latitudes and around the equator.

The trajectory code used in this work interpolates data from the Met Office assimilation analyses, changing the grid to 5° longitude by 5° latitude. The new vertical coordinate has 30 levels, with log pressure height from 2 km to 60 km in 2 km increments.

3.3   Isentropic Trajectory Calculations

Over a period of a few days, diabatic warming or cooling in the stratosphere can be neglected (e.g. *Holton et al.*, 1995; *Schoeberl and Sparling*, 1995). As there is no significant

change in the potential temperature of air parcels, their motion can be viewed as motion on an isentropic surface (a surface of constant potential temperature θ). If the observed winds for this period of time are interpolated to such surfaces to produce isentropic winds, then Equation 3.1 needs to be integrated only in two dimensions. In this approach, the change in the physical height associated with the vertical motion of the isentropes, is excluded from the analysis (*Sparling et al.*, 1997). This way, air parcels can easily be advected in time, and tracked along their trajectories.

Furthermore, by advecting a long-lived tracer, high spatial resolution of the tracer field can be obtained. In atmospheric research, it is desirable to have high-resolution data as well as global coverage. The existing methods for probing the atmosphere do not satisfy both of the criteria. For example, satellite measurements give good spatial coverage with low spatial resolution data, whereas aircraft measurements give high spatial resolution and poor spatial coverage. The first step in combining the available data in one set of measurements with a satisfactory spatial resolution and a global coverage is done by the Met Office data assimilation system. A further step in the same direction can be done by a computational method which obtains high-resolution fields from low-resolution fields with good spatial coverage, and relies on advecting in time a long-lived tracer. For stratospheric motion, long-lived tracers include two dynamical quantities, potential temperature (in an adiabatic flow), and potential vorticity (in an adiabatic and frictionless flow), and a number of chemical species with a relatively long lifetime, such as CH_4, N_2O, and the chlorofluorocarbons F-11 and F-12 (*Schoeberl and Lait*, 1992).

On an isentropic surface, a high-resolution tracer field can be obtained by initializing air parcels on a high-resolution grid and advecting them either forward or backward in time. In forward advection, the parcels tend to disperse irregularly causing gaps in the final field, whereas in backward advection, air parcels are regularly spaced at the time when the distribution is analyzed. In this case, Equation 3.1 is solved for the reversed sign of velocity vector. At their positions earlier in time, the advected parcels are labelled with the corresponding values of the tracer, derived from a low-resolution field. If the analyzed tracer is long-lived, then the labelled values of the tracer can be advected unchanged to their final positions. The higher resolution field at some later time can thus be calculated using a low-resolution field from an earlier time. The horizontal resolution of the initial field does not directly limit the resolution of the derived field, because stratospheric advection is dominated by the large-scale flow and in most circumstances small-scale features not present in low-resolution input data can be produced (*Waugh and Plumb*, 1994). However, these calculations can miss some of the details of fine-scale structure which are sensitive to the small-scale details of the flow.

The above idea is the basis of the "reverse domain filling" (RDF) technique. It was introduced by *Sutton et al.* (1994), where a high-resolution field of N_2O in the middle

stratosphere was produced from a low-resolution satellite field. The same technique was applied by *Schoeberl and Newman* (1995), using PV as a conserved tracer, to investigate the three-dimensional structure of vortex filaments. *Sutton et al.* (1994) found that five-day integrations were sufficient to capture the most important high-resolution features. *Schoeberl and Newman* (1995) found that in some cases, longer integrations were needed for extremely fine-scale features to be captured, and concluded that ten-day integrations were adequate for most dynamical situations.

An example of low-resolution and high-resolution PV fields on the 600 K potential temperature surface, on 24 December 1998 is given in Figure 3.1. The low-resolution Met
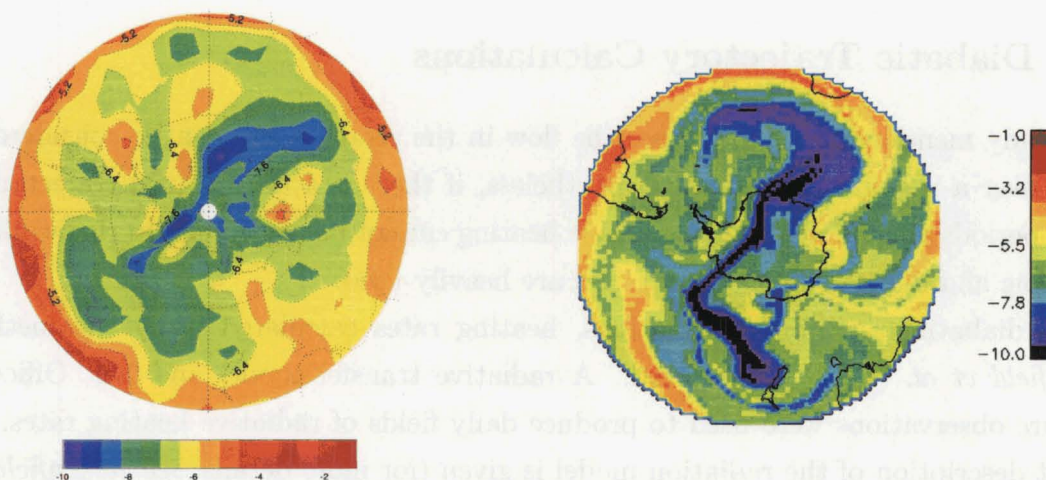
Figure 3.1: Polar-stereographic view (30°–90° S) of low-resolution (left) and high-resolution (right) PV field (in $10^{-5}\,\mathrm{K\,kg^{-1}\,m^2\,s^{-1}}$) on 600 K, on 24 December 1998.

Office PV field presented is on a 5° longitude by 5° latitude grid. The high-resolution field was produced assuming that the flow was adiabatic and frictionless. The trajectories of the parcels initialized on a 1° longitude by 1° latitude grid were run backwards in time for 5 days. The wind fields were interpolated on the isentropic surface using cubic spline interpolation (in *Schoeberl and Sparling* (1995) this method for interpolation of winds in the vertical is recommended).

The uses of trajectory modelling (especially isentropic trajectories, with their low computational demands) are numerous. *Waugh and Plumb* (1994) and *Norton* (1994) introduced the "contour advection with surgery" technique which produces fine-scale features of tracer contours. The disadvantage of this method (compared to the RDF technique) is that in order to produce a high-resolution global field, a large number of contours need to be advected simultaneously. *Pierce et al.* (1994) used air mass trajectories advected forward or backward in time, to create synoptic maps from asynoptically gathered measurements (the so called "trajectory mapping" technique). *Morris et al.* (2000) used trajectory mapping to validate satellite measurements of trace gases. *Danilin et al.* (2002) utilized air parcel trajectories in the so called "trajectory hunting technique" to compare

measurement from different instruments. *Schoeberl et al.* (1992) examined the structure of the polar vortices using trajectory calculations. Trajectories can be used to model the dispersion of injected pollutants such as bomb debris, volcanic sources or aircraft emission (*Schoeberl and Sparling*, 1995). Moreover, trajectory modelling enables a detailed examination of the chemical processes undergone in an air parcel. For example, *Schoeberl et al.* (1993) analyzed back-trajectories of Arctic and Antarctic aircraft data to confirm that the high ClO concentrations were associated with polar stratospheric cloud encounters.

As powerful as they may seem, trajectory calculations do have their limitations. These are discussed in Section 3.5.

3.4 Diabatic Trajectory Calculations

As already mentioned, in most cases the flow in the stratosphere can be considered adiabatic over a period of few days. Nevertheless, if there is a need to run trajectories for longer periods of time, diabatic cooling or heating cannot be neglected. In this work, both isentropic and diabatic RDF trajectories are heavily used.

For diabatic trajectory calculations, heating rates calculated using the method of *Rosenfield et al.* (1994) are utilized. A radiative transfer model and Met Office temperature observations were used to produce daily fields of radiative heating rates. Here, a short description of the radiation model is given (for more details, see *Rosenfield et al.* (1994) and *Rosenfield and Schoeberl* (2001)).

Solar heating and radiative heating and cooling of three major species, carbon dioxide, water vapour and ozone, were included in the radiation model. Solar heating in the near-infrared region was treated with the formulations of *Ramanathan and Cess* (1974) for carbon dioxide and *Lacis and Hansen* (1990) for water vapour, while solar heating due to ozone was computed with the parametrization of *Strobel* (1978). Infrared heating due to carbon dioxide was calculated using transmission function parametrization of *Chou and Kouvaris* (1991). The parametrization of *Chou* (1984) was used for water vapour bands, and of *Rosenfield* (1991) for ozone.

The volume mixing ratio of carbon dioxide was taken as 330 ppmv. Water vapour values were monthly, zonally averaged values from the Nimbus-7 Limb Infrared Monitor of the Stratosphere, except for the Antarctic region during July through to October. For this time period, the time and zonally averaged latitude-height fields reconstructed from water vapour measured during the 1987 Antarctic Airborne Ozone Experiment (AAOE) by *Kelly et al.* (1989) were used. Ozone values were monthly, zonally averaged profiles for 1979 derived from the solar backscattered ultraviolet instrument on Nimbus-7 (*McPeters et al.*, 1984), except for the Antarctic region from 23 August to 31 October, when daily latitude-height fields reconstructed (*Schoeberl et al.*, 1989; *Lait et al.*, 1990) from ozone

values measured during AAOE by *Proffitt et al.* (1989c) were used.

Output from the radiation model consists of daily global fields of change in temperature with time, dT/dt, on a $3.75°$ longitude by $2.5°$ latitude grid, on 18 pressure levels, from 1000 to 0.4 hPa. The trajectory code used in this work carries out the calculations with potential temperature as the vertical coordinate. Hence, the rates dT/dt were first converted into change in potential temperature with time, $d\theta/dt$, on constant pressure levels, using the definition of potential temperature, θ, and log pressure height, Z:

$$\theta = T_\theta \left(\frac{p_S}{p_\theta}\right)^{R/c_P},\qquad(3.2)$$

$$Z = -H\,ln\left(\frac{p_\theta}{p_S}\right),\qquad(3.3)$$

where p_S is standard pressure, R is the gas constant for dry air, c_P is the specific heat of dry air at constant pressure, and H is the scale height. Combining the above equations yields

$$\left(\frac{d\theta}{dt}\right) = \left(\frac{dT}{dt}\right)e^{RZ/c_P H}.\qquad(3.4)$$

The change in potential temperature with time was then linearly interpolated onto constant potential temperature surfaces (hereinafter referred to as heating rates). Linear interpolation of the heating rates in the vertical was performed since cubic splines can give rise to spurious extrema (Joan Rosenfield, private communication).

Throughout this work, "heating" will refer to positive heating rates, and "cooling" to negative heating rates. In other words, those two terms commonly used to describe the change in temperature, will be used here to describe the change in potential temperature.

As already mentioned, RDF calculations performed in this work were carried out with potential temperature as the vertical coordinate. An advantage of this choice is that it allows an analysis of the vertical motion of air parcels in which the physical height is irrelevant. In that sense, air parcels ascend if they move to isentropes with higher potential temperature (i.e. if the heating rates are positive), even though in the physical space they may actually move downwards (*Holton et al.*, 1995; *Schoeberl and Sparling*, 1995).

3.5 Errors in Trajectory Calculations

The physical accuracy of trajectory modelling depends primarily on two factors. First, the method for numerical integration of the displacement equation can give rise to computational errors. Second, measurement uncertainties, both in the initial field and in meteorological data used to advect air parcels, can lead to an unrealistic final field, and

to incorrect locations of individual parcels.

Schoeberl and Sparling (1995) examined the computational errors by performing a forward-backward test, in which the model was first run forward moving the parcels to some point, and then the same parcels were advected backward from the ending point. The test was run for a day, for different time-steps, and the start and end point of the advected parcels were compared. The results showed that the fourth-order Runge-Kutta method gave very satisfactory results. The differences between starting and ending points, both in longitude and latitude, increased with an increasing time-step. For a time-step of 10^{-1} day, those differences were less than 10^{-2} degrees/day. Hence, in our trajectory scheme, where the fourth-order Runge-Kutta method is used, and a time-step of 2 hours, the computational errors are expected to be negligible.

Indeed, a one day forward-backward trajectory test performed for parcels in the Southern Hemisphere (initialized on a $1°$ longitude by $1°$ latitude grid, on 7 isentropic surfaces of 400–700 K, with a 50 K difference) showed the mean differences in longitude, latitude and potential temperature, between the starting and ending point, of zero. A non-zero displacement in longitude and latitude was observed only for parcels with trajectories in the vicinity of the polar cap (with maximum absolute differences of $\sim0.2°$ and $\sim0.03°$ in longitude and latitude, respectively). This pattern was not seen in the potential temperature differences. The likely cause for the pattern is a change in coordinate system introduced when a parcel crosses the polar cap parallel (Section 3.1), and tests performed with different polar cap radii confirmed this.

Trajectory errors arising from measurement uncertainties have two components. The first one is the uncertainty in the initial field, which is inherent in the field and is constant in trajectory calculations. For example, in the process of generating a high-resolution PV field as described in Section 3.3, all of the errors in the initial low-resolution field are simply carried forward in time, and the final PV values have the same uncertainties as the initial values.

The measurement uncertainties of the meteorological data, i. e. of the wind fields, used to advect air parcels, accumulate with each trajectory calculation. The errors in individual trajectories can increase rapidly with time, particularly when a parcel is advected through chaotic flow or high wind shear (*Morris et al.*, 1995). Furthermore, the wind fields in the region around the Antarctic are expected to have larger errors because their values are derived from far fewer observations than in other regions. A typical position error of 20 % of the travel distance is expected in the calculations of individual trajectories (*Stohl*, 1998). On the other hand, fields produced from large ensembles of trajectories have much smaller uncertainties (*Morris et al.*, 1995). *Newman et al.* (1996) examined the sensitivity of RDF calculations in producing high-resolution PV maps, to different wind field analyses (one of which was Met Office), and found that although the exact positioning of fine-scale

features differed, all of the analyses showed similar large-scale features, and concluded that no particular analysis showed superiority. *Morris et al.* (1995) also performed a test of sensitivity to wind field analyses, the results of which again confirmed that the uncertainties in a large number of trajectories were less than in individual trajectories.

Another source of errors in isentropic trajectory calculations is the assumption of isentropic flow. At different potential temperature surfaces, air parcels encounter different horizontal winds, both in magnitude and in direction. In regions of large vertical wind shear, the differences between isentropic and diabatic trajectories can grow rapidly. The tests done by *Schoeberl and Sparling* (1995), for parcels in the Northern Hemisphere, in January 1992 on the 500 K isentrope, showed that the upper limit on the validity of the isentropic approximation in the stratosphere was 10–15 days. *Morris et al.* (1995) derived the same conclusions for the Northern Hemisphere parcels in January 1992 on the 800 K isentrope, and for Southern Hemisphere parcels in July 1992 on the 800 K isentrope. The validity of the isentropic approximation depends strongly on the region and season examined. Generally speaking, the approximation is valid when the time for heat to flow into or out of the system is long compared to the dynamical time scales.

In this work, the errors in trajectories introduced by the approximation of adiabatic flow are addressed for each particular case.

Chapter 4

Ozone Data

In this chapter, the sources of ozone data used in this work are depicted. A description of two spaceborne instruments, the Total Ozone Mapping Spectrometer and the Polar Ozone and Aerosol Measurement III, and their observation geometries is given. The instruments' retrieval algorithms, data uncertainties, and validation are briefly outlined.

In this work, pre-calculated values of ozone depletion inside the Antarctic vortex are used. A method through which the data were generated, as well as the results, is given at the end of the chapter.

4.1 TOMS

The Total Ozone Mapping Spectrometer (TOMS) is a spaceborne instrument designed to measure the total column ozone in the atmosphere (*McPeters et al.*, 1998). One of the TOMS products are maps of global total column ozone on a $3°$ longitude by $3°$ latitude grid. The data products from TOMS measurements are processed by the National Aeronautics and Space Administration, and archived at the Goddard Space Flight Center Distributed Active Archive Center.

TOMS was launched on the Earth Probe (EP) Satellite on 2 July 1996, and is still operational. EP/TOMS is a continuation of TOMS instruments aboard Nimbus-7 and Meteor-3 satellites, which were operational between 31 October 1978 and 28 December 1994. EP/TOMS is expected to remain operational until sometime in the year 2004 when a follow-on instrument, the Ozone Monitoring Instrument (OMI) onboard the Earth Observing System Aura satellite, is launched.

In this section, brief descriptions of the TOMS instrument, the observations, and the retrieval algorithm are given.

4.1.1 Instrument Characteristics

TOMS measures incident solar radiation and backscattered ultraviolet sunlight. In its primary operating mode, scan mode, the backscattered sunlight is sampled for different scenes (see below details of observations). In solar calibration mode, solar irradiance is measured. The primary quantity derived from these measurements and used to derive

the total column ozone, is the normalized radiance. Normalized radiance represents the ratio of backscattered and solar irradiance; any instrument sensitivity changes affecting both of the measured quantities cancel in this ratio.

In scan mode, backscattered light enters the optical system through an entrance slit. TOMS uses a single, fixed monochromator, with exit slits at six near-ultraviolet wavelengths, given in Table 4.1. The slit functions are triangular, with a nominal 1-nm band-

Wavelength	Albedo Cal. Const.
(nm)	(steradian^{-1})
308.60	0.087
313.50	0.088
317.50	0.089
322.30	0.088
331.20	0.091
360.40	0.094

Table 4.1: EP/TOMS wavelengths [from *McPeters et al.* (1998)].

width. A chopper wheel, with openings at different distances from the centre of the wheel, determines the order of individual measurements.

In solar calibration mode, a diffuser reflects sunlight into the instrument. In EP/TOMS, a three-diffuser system is deployed to reduce the exposure and degradation of the diffuser. The system allows calibration through comparison of signals reflected off diffusers with different rates of exposure. In addition, solar diffuser reflectance is monitored. A phosphor light source with peak emission over the TOMS wavelength range is used to illuminate the exposed diffuser surface, and the signal thus obtained is compared to the signal obtained when the phosphor surface is viewed directly. The ratio of these two signals is a measure of relative diffuser reflectance.

As mentioned above, the primary product of TOMS measurements is the ratio of backscattered and solar irradiance. The ratio of the instrument calibration constants for these quantities, the so called albedo calibration constant, is critical for correct measurements. The prelaunch values of the albedo constant, for all TOMS wavelengths, are given in Table 4.1. A quantity which is essential for time-dependant calibration of the normalized radiance, is the diffuser plate reflectivity, hence the need to monitor it.

Some other operating modes of TOMS include standby mode, wavelength monitoring mode and electronic calibration mode. TOMS is in standby mode during the nighttime part of the orbit. The scan mirror points into the instrument, at a black surface. In wavelength monitoring mode, any changes produced by excessive temperature differentials or mechanical displacements due to shock or vibration are tracked. In electronic calibration mode, gain ratios from three electronic amplifiers (fed by the current from the

photo-multiplier tube) are monitored in order to determine the instrument linearity.

4.1.2 Observations

The mean altitude of the Earth Probe Satellite is 739 km. The orbital period is 99.7 min, and the inclination is 98.4°. The mean local time of the ascending node is 11:16 am. The TOMS instantaneous field of view is 3° longitude by 3° latitude. Scans last 8 seconds, during which time the mirror scans perpendicularly to the orbital plane in 3° steps, from 51° on the left side of spacecraft nadir to 51° on the right (relative to direction of flight), totalling 35 samples in one scan. At the end of each scan, the mirror returns to the first position, without making measurements on the retrace.

4.1.3 Retrieval Algorithm

Atmospheric constituents, such as ozone and aerosols, absorb solar radiation that penetrates the Earth's atmosphere. Incoming radiation also undergoes scattering in the troposphere by clouds and aerosols, and at the ground by surfaces of varying reflectivity. The detected backscattered irradiance depends on the total column ozone. At all of the TOMS wavelengths (Table 4.1), it consists primarily of the solar radiation that is reflected back by the dense tropospheric air, clouds, aerosols and the Earth's surface. The three shortest wavelengths are strongly absorbed by ozone, and absorption by other atmospheric components is negligible.

In the TOMS retrieval algorithm, the calculations of irradiances are based on the work of *Dave* (1964). The calculations are performed at approximately 0.05-nm intervals across each of the TOMS slits. For each wavelength, absorption coefficients and temperature dependance are taken from *Paur and Bass* (1985). Ozone and temperature profiles are constructed using a climatology based on solar backscatter ultraviolet measurements above 15 km, and on balloon ozonesonde measurements (*Klenk et al.*, 1983) for lower altitudes.

In the retrieval algorithm, it is assumed that reflected radiation comes from two levels, ground and cloud. Pressure profiles are obtained from the National Oceanic and Atmospheric Administration National Meteorological Center average ground terrain heights, which are converted to pressure using a U. S. Standard Atmosphere. Monthly averages of snow/ice cover probabilities are used from the Air Force Global Weather Center. For cloud heights, a climatology based on the International Satellite Cloud Project data set is used.

The calculations of the total column ozone are based on parameters called N-values, defined as

$$N = -100 \, log_{10} \left(\frac{I}{F} \right) \tag{4.1}$$

where I is the measured backscattered irradiance and F is solar irradiance. In the TOMS retrieval algorithm, first detailed calculations of N-values for different viewing geometries, the total column ozone and ozone vertical distribution, and two choices of pressure at the reflecting surface are performed. The N-values for a given scene are then derived through interpolation of pre-calculated N-values.

An initial estimate of the total column ozone is calculated by comparing N-values for two wavelengths, 317.6 nm and 331.3 nm. The first wavelength is strongly absorbed by ozone, the other one is insensitive to ozone. The initial estimate of ozone is then used to calculate N-values for the rest of the wavelengths. The residuals, that is, the differences between the measured and calculated N-values, for a specific triplet of wavelengths, are used to correct the initial estimate of ozone and pre-calculated radiances. The triplet of wavelengths consists of two wavelengths which are most sensitive to ozone at the optical path length of the measurement, and of the 360 nm wavelength, which is insensitive to ozone. The residuals indicate how well the assumed atmospheric and surface conditions agree with the real conditions, and are used to investigate the validity and quality of TOMS data.

4.1.4   Data Uncertainties and Validation

In TOMS ozone measurements, there are three sources of possible uncertainties: the accuracy and precision of the radiance measurements, the results of the radiative transfer model, and the retrieval process. The errors associated with the uncertainties are classed as an absolute error, which is independent of time, a random error and a time-dependent drift. For EP/TOMS total ozone, the absolute error is 3 %, the random error is 2 %, and the drift estimated after 1.5 years of operation was less than 0.6 % (*McPeters et al.*, 1998).

There are some particular measurement scenes that can introduce significant errors into TOMS measurements. For example, in the Arctic and Antarctic, the presence of polar stratospheric clouds above the ozone peak, can cause TOMS retrieved ozone to be underestimated by up to 50 %, depending on the type of polar stratospheric clouds (*McPeters et al.*, 1998).

A comparison of EP/TOMS ozone with ground-based measurements of total column ozone in northern midlatitudes, showed that TOMS retrieved ozone is approximately 1.0 % higher (*McPeters et al.*, 1998). A study of *Bodeker et al.* (2001), in which EP/TOMS data were compared to 67 stations with Dobson instruments distributed over the whole globe, confirmed a good agreement in northern midlatitudes. On the other hand, the differences between the measurements are higher in other regions. On average, in southern midlatitudes and polar region, TOMS measurements are up to 6% and 18 %, respectively, higher than the Dobson.

EP/TOMS is still operational, but is experiencing some problems. Data up to the year 2000 are of high accuracy, but at present, the instrument has calibration problems, and it is suggested that the data be used with caution (for more information see http://toms.gsfc.nasa.gov).

4.2 POAM

The Polar Ozone and Aerosol Measurement (POAM) III is a spaceborne instrument designed to measure the vertical profiles of ozone, water vapor, nitrogen dioxide, and aerosol extinction in the polar stratosphere and upper troposphere (*Lucke et al.*, 1999). POAM III provides data that in each hemisphere are restricted to a single latitude each day, with longitudinal spacing of 25.4° and a vertical resolution of 1–2 km. POAM III is operated by Remote Sensing Division of U.S. Naval Research Laboratory.

POAM III was launched on 23 March 1998, onboard the Satellite Pour l'Observation de la Terre (SPOT) 4, and is still operational. POAM III is the successor of the POAM II instrument (*Glaccum et al.*, 1996), launched in September 1993 and operational until November 1996. The basic POAM concept started with the POAM I instrument which failed immediately after launch in 1985.

In this section, brief descriptions of the POAM III instrument, the observations, and the retrieval algorithm are given.

4.2.1 Instrument Characteristics

POAM measurements are made by the solar occultation technique (*Mauldin et al.*, 1985; *Russell et al.*, 1993). POAM tracks the Sun as it rises and sets through the atmosphere, using a quad-cell sun tracker with a 1° square field of view. This tracker is supplemented with a sensor of a 10° square field to aid in initial acquisition of the Sun. Tracking begins (ends) when the light intensity rises (falls) to approximately 0.4% of unattenuated light.

An image of the Sun is formed with a fused silica plano-convex lens of a nominal focal length of 63 mm. The aspheric shape of the convex side of the lens eliminates spherical aberration. The vertical and horizontal field of view (defined as perpendicular and parallel to the Earth's horizon, respectively) are determined by the size of a horizontal slit in the focal plane of the lens. The height of the slit is 0.0138 mm, giving a geometric vertical field of view of 0.013°, and the length of the slit is 0.890 mm, giving a geometric horizontal field of view of 0.81°. The mask containing the slit has a reflective front surface and an absorptive back surface, allowing for minimal transmission of signals from parts of the Sun imaged outside the slit.

In the optical path behind the slit are narrow-band interference filters, used to isolate the appropriate parts of the spectrum. The central wavelengths and full width at half

maximum (FWHM) passbands of the filters are given in Table 4.2. Nitrogen dioxide,

Channel	Wavelength (nm)	Passband (nm)	Species
1	354.0	9.7	Rayleigh
2	439.6	2.1	NO_2 on
3	442.2	2.1	NO_2 off / aerosol
4	603.0	17.7	O_3
5	761.3	2.3	O_2 on
6	779.0	10.2	O_2 off / aerosol
7	922.4	2.6	H_2O off / aerosol
8	935.9	2.6	H_2O on
9	1018.0	11.6	aerosol

Table 4.2: POAM III wavelengths and measured species [from *Lumpe et al.* (2002)].

oxygen and water vapour are measured using a differential technique. The measurements for these gases are done in two narrow band channels closely spaced together, taking advantage of relative minima and maxima in the absorption spectra. At all of the POAM III wavelengths, aerosol and Rayleigh scattering continua are present. The aerosol extinction channels include the three differential "off" channels.

The detectors, directly behind the filters, are silicon photodiodes operated in photovoltaic mode. Signals from the detectors undergo analog and digital filtering which suppresses high-frequency noise. The signal-to-noise ratio for direct sunlight measurements is better than 10^4.

POAM III receives commands via the SPOT 4 uplink. Data are stored on board, and transmitted to the U.S. Air Force Space and Missile Command/Test and Evaluation Operations and Testing facility, usually twice a day.

The altitude resolution with which the measurements are made, is determined by the angular resolution of the sensor and the distance to the tangent point. The angular resolution of the sensor, i.e. the FWHM of the sensor's point spread function in the vertical direction, is $0.013° \pm 0.001°$. The tangent point is the point along the line of sight that is closest to the Earth's surface. At the 833 km altitude of SPOT 4, the distance to the tangent point is ~ 3400 km, so the vertical resolution is 0.77 km at the tangent altitude (*Lucke et al.*, 1999).

4.2.2 Observations

The SPOT 4 satellite's orbit is Sun-synchronous, with an altitude of 833 km, an inclination of 98.7° and a period of 101.5 min; the descending node is crossed at 10:30 local time. As seen from the satellite, the Sun rises in the north polar region and sets in the south polar region 14.2 times a day. Orbital sunsets (sunrises) have a latitude range of 63°–88° S

(54°–71° N). The latitude coverage changes slowly with the season, and is exactly periodic from year to year. During one orbital period, the Earth rotates 25.4° in longitude, so the observation point moves westward by 100–1300 km for orbital sunsets and 900–1700 km for orbital sunrises.

During each sunrise and sunset, POAM collects 100 seconds of data. At the end of a sunrise event, and before the beginning of a sunset event, a vertical Sun scan is executed. The purpose of a Sun scan is to measure unattenuated intensities for all possible slit positions on the Sun, and thus determine the reference intensity for the calculations of atmospheric attenuation as a function of tangent height.

The minimum height at which POAM can obtain useful data is determined by the lowest cloud-free line of sight. In especially clear conditions, POAM tracks to altitudes as low as 2 km above the sea level. In the Southern Hemisphere, the average minimum height is below the tropopause. In austral autumn and winter, the presence of polar stratospheric clouds over the Antarctic causes the minimum height to be as high as 15 km.

4.2.3   Retrieval Algorithm

The basis of the POAM III measuring technique lies in comparison of the solar radiance which is absorbed and scattered by the atmospheric constituents, and the solar irradiance. The starting property for the POAM III retrieval is a normalized transmission, defined as the ratio of the measured signal (in each of the channels) and the corresponding unattenuated signal measured at the same location on the solar disk.

Output from the measurements consists of the universal time stamps, the measured signals in the nine channels, the measured unattenuated signal, and the elevation and azimuth potentiometer readouts. The satellite ephemeris is incorporated directly into the POAM III telemetry stream.

The POAM III retrieval algorithm (*Lumpe et al.*, 2002) consists of three steps – calculation of absolute pointing information and normalization of measured radiance data, spectral inversion and spatial inversion. In the algorithm, the atmosphere from the surface to 90 km is divided into 1-km thick concentric shells. The algorithm explicitly assumes spherical symmetry, and does not allow for diurnal gradients in the retrieved products.

In the first step, the information about the exact location of the track point on the Sun is needed for proper determination of unattenuated signal, and hence, for proper calculation of normalized transmissions. The exact position of the Sun is also needed for calculating altitudes. Normalized transmissions, at each wavelength, represent averaged (over the passband) atmospheric transmittance, which is a product of the transmittances due to each individual atmospheric extinction component. Measured total slant optical depth (which is a logarithm of normalized transmission) as a function of tangent altitude,

is an output from the first step of the retrieval algorithm.

In the spectral inversion step, total slant optical depth for each atmospheric path is separated into its various gas and aerosol components. The accuracy of the components' cross-sections used in this step is fundamental to the retrieval. The spectroscopic data set used represents a compilation of several spectroscopic studies.

In the final step, spatial, or limb, inversion, altitude profiles of gas density and aerosol extinction are calculated.

The vertical resolution of output data depends on retrieval species and altitude. For ozone, the altitude range of valid retrievals is between 5 km and 60 km, with a resolution of ∼1 km in the 15–50 km range (*Lumpe et al.*, 2002).

4.2.4   Data Uncertainties and Validation

In the POAM III retrieval, the errors consist of three components: the total random error, an aerosol feedback error due to PSC contamination, and a residual error due to occasional sunspot artifacts. The total random error arises from random pointing uncertainties, random errors in data time stamping, statistical noise in the measured signals and errors in detector dark count values. For ozone, the total random error is less than 5% for all altitudes between 13 km and 60 km. On the other hand, the ozone retrieval is relatively insensitive to both the PSC feedback errors and sunspot artifacts.

The POAM III ozone measurements during the Northern Hemisphere winter of 1999/2000 were compared to a number of instruments from different aircraft and balloon platforms (*Lumpe et al.*, 2003). In the altitude range of 14–30 km, the POAM III ozone data agree with other measurements to 7–10%. These differences were within the combined errors of POAM III and the other measurement techniques used. Other POAM III product data have also been validated. For example, *Nedoluha et al.* (2002) validated the water vapour data in the lower stratosphere and upper troposphere, and *Randall et al.* (2001) validated the aerosol data with other satellite instruments.

4.3   Ozone Depletion in the Antarctic vortex

Data for the ozone depletion in the Antarctic vortex used in this work were calculated by *Hoppel et al.* (2003). The method used employs the POAM III ozone measurements and a vortex averaged descent method (*Hoppel et al.*, 2002), where the vortex boundary is defined by the middle vortex edge according to the algorithm of *Nash et al.* (1996) (see also Section 6.1). In this section, a description of the method, and the results for the years 1998, 1999 and 2000, which are of interest for the work presented here, are given.

The vortex averaged descent method of inferring ozone depletion is based on a number of assumptions. First, it is assumed that the dominant dynamical contributor to ozone

change inside the vortex is diabatic descent (Section 2.2.1). Other dynamical processes, such as mixing across the vortex edge, are neglected (Section 2.2.1). Second, the vortex is assumed to be homogeneous, and averaged ozone and averaged descent are assumed to accurately represent the whole vortex region.

Under the above assumptions, the ozone loss can be derived through the following steps. A vortex averaged vertical profile of ozone on an initial day, chosen to be prior to the commencement of the chemical destruction of ozone, is inferred from the ozone POAM III measurements. For each day after the initial day, this profile is vertically adjusted corresponding to averaged descent. Finally, on some day, when it is assumed that ozone depletion no longer takes place, the adjusted profile is compared to the measured profile of ozone. The difference between those two profiles is taken as the vertical profile of ozone depletion.

Hoppel et al. (2003) calculated ozone depletion in the Antarctic vortex using the heating rates of *Rosenfield et al.* (1994) (Section 3.4). Trajectory calculations were performed for an ensemble of air parcels distributed uniformly throughout the vortex, using the Met Office wind field analyses (Section 3.2). The results for the years 1998, 1999 and 2000, with the initial day being 1 July, and the final day being 10 October, are given in Figure 4.1. As discussed in Section 2.2.2, the ozone destruction processes start when sunlight
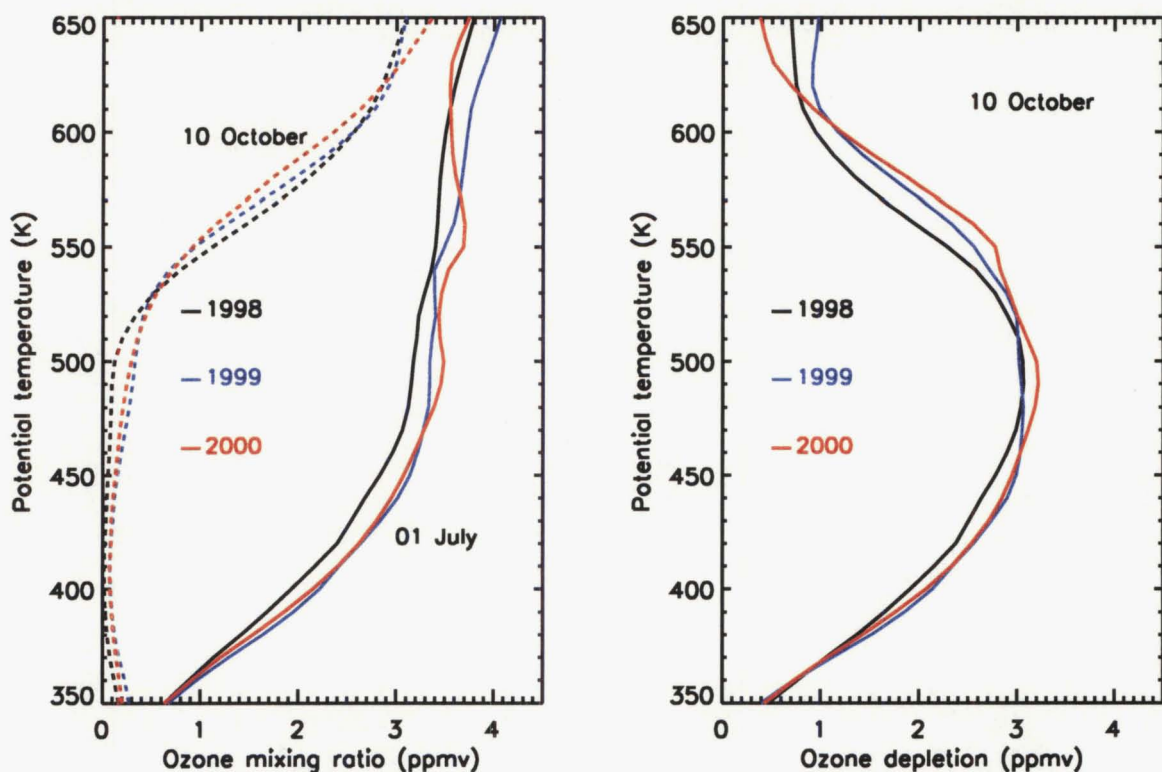
Figure 4.1: Vortex averaged vertical profile of ozone, vertically adjusted for descent, on initial day, 1 July (full line), and final day, 10 October (dashed line), for the years 1998, 1999 and 2000 (left). Vertical profile of depleted ozone, derived by subtracting the final profile from the initial profile (right).

returns to the polar vortex region, and usually cease in late September or early October. Hence, over the period 1 July – 10 October, most of the chemical ozone depletion is captured in the calculations.

Figure 4.1 shows that even though ozone depletion maximized around the potential temperature surface of 500 K, ozone destruction was almost complete between 400 K and 450 K. In 2000, the depletion was most severe, but in 1998, the region between 370 K and 490 K was nearly devoid of ozone. In all of the years, the calculated ozone depletion above 600 K is somewhat greater than expected (Karl Hoppel, private communication). In this region, PSCs occur infrequently (*Fromm et al.*, 1997), so it is unlikely that the depletion was caused by heterogeneous chemistry. The observed loss may be due to non-PSC related photochemical ozone destruction, or it may be an artifact from errors in the descent rates or the initial ozone profile.

The vortex averaged descent method, as described here, is prone to the POAM III vortex sampling biases. Since the POAM III measurement technique (Section 4.2) requires sunlight, its sampling is biased towards the sunlit part of the vortex, where ozone loss is larger than in the rest of the vortex. Hence, the derived ozone destruction could overestimate the true vortex average (*Hoppel et al.*, 2002).

Chapter 5

Case Study

A case study of the influence of the Antarctic vortex breakdown on the ozone levels above New Zealand in 1998 is presented here. The cause of an anomalous vertical profile of ozone over the National Institute of Water and Atmospheric Research (NIWA) site in Lauder (45.0° S, 169.7° E) is examined using reverse domain filling calculations combined with a PV/O_3 fitting technique applied to the POAM III ozone measurements. A method for determining the Antarctic vortex breakdown dates is briefly described, and the results for the years 1991–2000 are presented. In addition, a technique for generating high-resolution ozone maps for an isentropic surface, used here to illustrate the evolution of the stratosphere during and after breakdown of the vortex, is introduced.

5.1 Introduction

The dilution of ozone-poor air that takes place after breakdown of the polar vortices has an important effect on midlatitude ozone levels. Evidence for vortex filaments reaching midlatitudes in both hemispheres has been given in a number of studies (e.g. *Bowman,* 1993; *Waugh et al.,* 1997). In northern midlatitudes, *Knudsen et al.* (1998a) found that the dilution of chemically depleted ozone air from the Arctic vortex plays a significant role in spring- and summertime ozone decline. *Atkinson et al.* (1989) showed that atypically low total ozone values over New Zealand and Australia in December 1987 resulted from transport of ozone-poor Antarctic air into southern midlatitudes. In that event, a significant contribution of ozone hole dilution into midlatitudes was reported by *Atkinson and Plumb* (1997). Model results of *Eckman et al.* (1996) showed that after breakdown, ozone-depleted air from the Antarctic vortex reaches latitudes of ~20° S and that before the onset of the next ozone depletion cycle, the ozone levels do not reach the levels from the previous year. The severity of Antarctic ozone depletion has steadily increased over the past two decades (*Bodeker et al.,* 2002). Furthermore, the negative ozone trends observed over the NIWA site in Lauder are greater in summer than in any other season (*WMO,* 1999). Therefore, the dilution processes might be the most important cause of the ozone decreases over New Zealand in summer.

5.2   Data and Analysis

Ozonesonde profiles have been measured at the NIWA site in Lauder from August 1986 to the present (*Bodeker et al.*, 1998). The profiles for 14 and 24 December 1998 are shown in Figure 5.1. The two profiles differ considerably. While the profile for 14 December
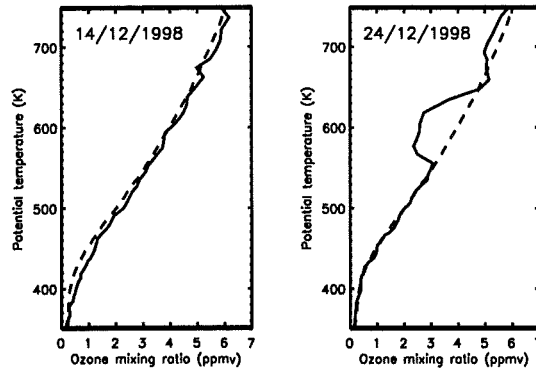
Figure 5.1: Vertical profiles of ozone (between potential temperature surfaces of 350 and 750 K) for 14 and 24 December 1998, over Lauder, New Zealand (full line). The ozonesonde climatology for the month of December (1986–2001) is plotted for comparison (dashed line).

resembles a typical midlatitude December ozone profile, ozone on 24 December was less abundant in the whole region between the potential temperature surfaces of 350 K and 750 K, with two conspicuous reductions, between 550 K and 650 K, and 680 K and 740 K.

The total column ozone dropped from 311 DU on 14 December to 253 DU on 24 December. This difference was caused solely by the changes in the ozone profile between 350 K and 750 K. The layer between 550 K and 650 K contributed ∼32 DU to the decrease. The reduction in the ozone mixing ratio between the 350 K and 450 K isentropes, contributed another ∼22 DU, and the reduction in the 100 K-layers centred around 500 K and 700 K added ∼5 DU to the decrease in the total column ozone.

The aim here is to examine the origin of the feature between the isentropes of 550 K and 650 K (hereafter referred to as "the notch"), seen in the ozone profiles on 24 December and 31 December 1998 (not shown). On 24 December, the ozone mixing ratio on the 600 K isentrope, was ∼40 % less than on 14 December. In the subsequent ozonesonde flight, on 31 December 1998, the notch was much smaller, spanning between the isentropes of ∼570 K and ∼590 K.

To explain the notch, we investigated its origin by first evaluating the ozone distribution over a more global area derived from satellite measurements. The ozone data used were from the Polar Ozone and Aerosol Measurement (POAM) III instrument (Section 4.2). Since POAM is a solar occultation instrument, the measurements in each hemisphere are restricted to a single latitude each day. One of the methods for calculating ozone mixing ratios over a much wider range of geographic locations than were actually observed

is by advecting the measurements forward or backward in time, thus filling in some of the gaps in data (*Pierce et al.*, 1994; *Morris et al.*, 1995). On the other hand, the same goal can be achieved by using well-established PV/O_3 mapping techniques (*Butchart and Remsberg*, 1986; *Schoeberl et al.*, 1989). The mapping assumes that PV is a conserved quantity during adiabatic transport, and can thus be used as a tracer of atmospheric motions. Under this assumption, any dynamically controlled trace species in the stratosphere should exhibit a single, well-defined relationship that defines its correlation with PV anywhere on a given potential temperature surface at any given point in time (e.g. *Leovy et al.*, 1985; *Allaart et al.*, 1993). While the validation of such a mapping technique in a dynamically quiescent period (the Northern Hemisphere winter of 1999-2000), using POAM III ozone measurements, was done by *Randall et al.* (2002), in this paper the use of that same mapping method in a dynamically active period (during the Antarctic vortex breakdown) is discussed.

Proxy ozone mixing ratios over middle and high southern latitudes in December 1998 were calculated according to the method of *Randall et al.* (2002). At that time the POAM measurement locations were about 20° poleward of Lauder. Briefly, the POAM data from a seven-day period centered around the day of interest were used to derive daily quadratic fits of ozone and PV (where the PV values at the POAM measurement locations were determined from a bilinear interpolation of the PV field obtained from the United Kingdom Meteorological Office (Met Office) analyses (*Swinbank and O'Neill*, 1994)). Examples of the POAM data on the potential temperature surface of 600 K for 7 and 24 December 1998, plotted against PV, are shown in Figure 5.2, along with the quadratic fits to the data. On 7 December, the fit matches the data reasonably well. The
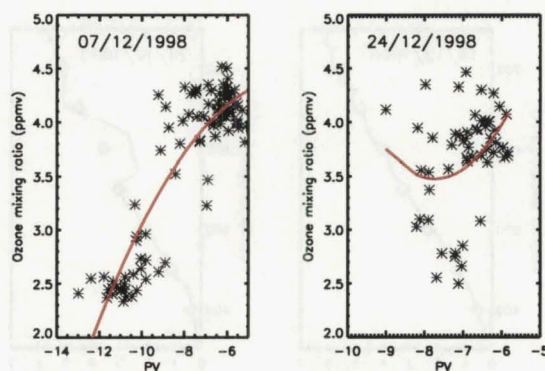
Figure 5.2: Ozone mixing ratio (in ppmv) and PV (in $10^{-5}\mathrm{K\,kg^{-1}\,m^2\,s^{-1}}$) for the Southern Hemisphere POAM III measurements on the 600 K isentropic surface, for two days, 7 December (left) and 24 December (right) 1998.

lowest ozone mixing ratio values correspond to the lowest PV values, and vice versa, which is consistent with the fact that on this day and on this isentropic surface, the Antarctic vortex still existed (Section 5.3). On the other hand, this is not true for the fit for 24

December. Furthermore, there is substantial scatter in the data for 24 December, which
is suggestive of the presence of significant small-scale structure in the ozone distribution;
this is discussed in more detail below. Daily fits such as those depicted in Figure 5.2
were used to derive proxy ozone throughout the southern middle and high latitudes. In
the regions where PV values were outside the PV range of the POAM measurements,
the proxy ozone values were calculated by extrapolating the PV/O_3 fit. An example of
the PV and proxy ozone maps for 24 December 1998, on the 600 K isentrope, is given in
Figure 5.3.
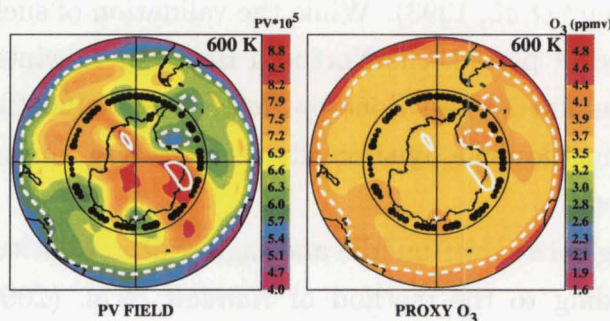
Figure 5.3: Polar stereographic (30–90° S) low-resolution absolute PV (in $10^{-5} \cdot K\,kg^{-1}\,m^2\,s^{-1}$) and
ozone fields on the 600 K isentropic surface, on 24 December 1998. Black dots represent the actual
POAM measurement locations. The overplotted contours border the regions where PV was higher (solid)
and lower (dashed) than that sampled by POAM.

The proxy ozone derived in such a manner was compared with Lauder ozonesonde data
for 14 and 24 December 1998. The ozone values at Lauder were bilinearly interpolated
from the proxy ozone field, and the results are shown in Figure 5.4. The agreement is
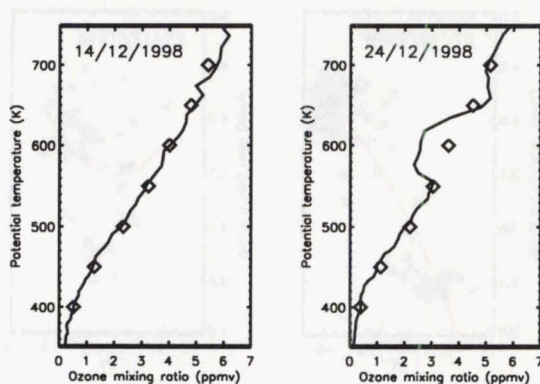
Figure 5.4: Lauder ozonesonde (full line) and POAM proxy ozone (diamonds) comparison for seven
isentropic surfaces (400–700 K) on 14 and 24 December 1998.

very good, except on the 600 K surface on 24 December. The proxy ozone map in Figure
5.3 therefore does not reproduce the low ozone values on 24 December 1998, at 600 K over

Lauder. The ozone mixing ratio derived from the PV/O_3 fit is approximately 1 ppmv greater than what the ozonesonde measured (Figure 5.4).

As mentioned above, however, the POAM ozone data from which the 24 December proxy was determined were only poorly represented by the quadratic PV/O_3 relation (Figure 5.2). The double-valued nature of the PV/O_3 correlation (i.e., two very different values of ozone for the same value of PV) has two implications. First, small-scale features in the PV field, including any possible vortex remnants, are not adequately represented, probably because the Met Office data have relatively low horizontal resolution (2.5° in latitude, 3.75° in longitude). Second, over this dynamically active period (seven days centred around 24 December), the change in the PV values associated with vortex remnants might lead to decorrelation of PV and ozone.

Furthermore, even if the resolution of the PV field can be improved and assuming that PV and ozone are correlated, the quadratic PV/O_3 fit may not be sufficient to define the observed structure in the PV/O_3 correlation on this particular day. In principle, the PV/O_3 fitting can incorporate numerical functions or higher-order analytic functions to more accurately represent small-scale structure in the ozone distributions. Drawbacks to this include the inability to extrapolate beyond the measured range of PV values if numerical functions are used, and the introduction of spurious structure with higher-order analytic functions.

In this work, the insufficient resolution of the PV field is addressed, whilst retaining the quadratic fitting procedure validated (in more quiescent conditions) by *Randall et al.* (2002). To improve the geographic resolution of the ozone field at the time the notch was observed, reverse domain filling (RDF) analyses (*Sutton et al.*, 1994) were performed. Air parcels initialized over the New Zealand region (34–48° S, 162–178° E on a 1° latitude by 1° longitude grid) from 23–26 December 1998 were traced back to their point of origin on 7 December 1998 (the choice of this date is discussed in Section 5.3). Isentropic trajectories at two potential temperature surfaces within the notch, 550 and 600 K, were examined. In theory, assuming no photochemical change and negligible vertical motion and mixing, the high-resolution ozone field on 23–26 December can be computed by using the ozone distribution on 7 December, and simply carrying it forward in time along the computed trajectories.

The RDF code uses winds interpolated from the original Met Office grid onto a 5°×5° horizontal grid, and a vertical grid ranging from 2 km to 60 km in 2-km increments. A fourth order Runge-Kutta method is used to integrate advection equations, and bilinear interpolation to calculate winds at parcel positions. The coordinate system of the code is spherical, apart from a polar cap of 25° radius where it is polar-stereographic. The time-step for calculations was two hours.

5.3   Vortex Breakdown Dates

A procedure used to determine the vortex breakdown dates was based on the work of *Nash et al.* (1996), whereby the product of the first derivative of the PV versus equivalent latitude and mean wind speed along PV isolines is representative of vortex strength. For the years 1991–2000, and seven isentropes of 400–700 K, with 50 K difference, the daily maxima of the product were calculated. For each calendar day, the median of the daily maxima during this ten-year period was then calculated, producing a reference climatology of the product maximum for the years 1991–2000. The reference climatology on the 500 K isentrope is given in Figure 5.5.
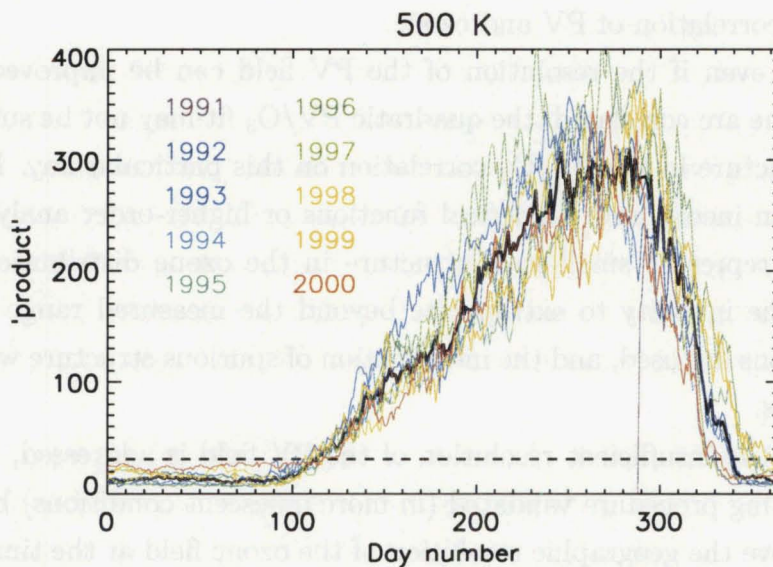
Figure 5.5: Daily maxima of the product of the derivative of PV vs equivalent latitude and the average wind speed along PV isolines (in $K\,kg^{-1}\,m^3\,s^{-2}\,deg^{-1}$) for the years 1991–2000. The thick black line represents the median of the daily maxima, and the dashed black line represents 10 % of the maximum value of the reference climatology. Note that the Met Office analysis started in October 1991.

For each year, the date when the daily maximum fell below 10 % of the maximum value of the reference climatology on a given isentrope, was taken as the breakdown date. The exception to this rule was the 400 K potential temperature surface, where the limit was taken as 30 % of the maximum value of the climatology. The reason for this is that the otherwise obtained dates were unrealistically late in the spring-summer season. The need to treat the 400 K level differently probably arises from the fact that the vortex is not as well isolated around this isentrope (Section 2.2.1). The calculated vortex breakdown dates for the years 1991–2000 are given in Figure 5.6.

The calculated dates for the 500 K isentrope are in good agreement with the dates determined by *Waugh and Randel* (1999), and consistent with the analysis of *Waugh et al.* (1999).
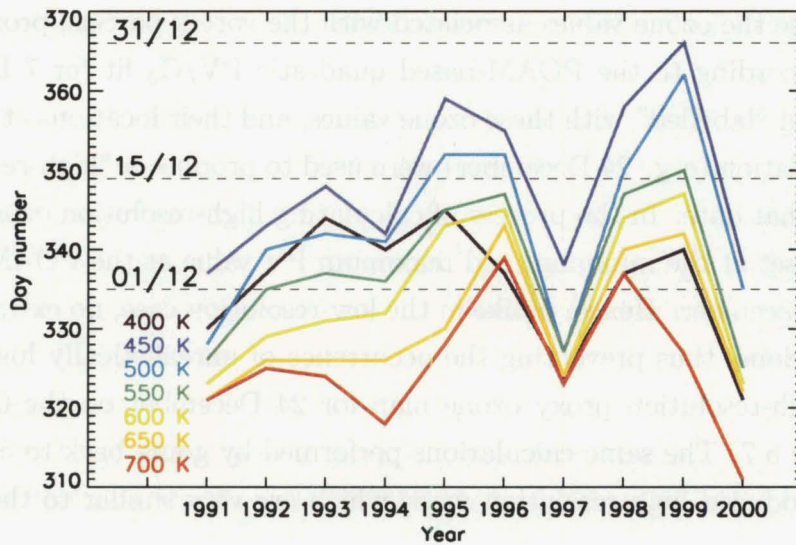
Figure 5.6: Antarctic vortex breakdown dates on seven isentropes, for the years 1991–2000.

7 December 1998 was chosen as the initial day for our analysis for two reasons. The fact that it is ~10 days before the determined breakdown dates for 550 and 600 K, ensures that the analysis was done for the period when the Antarctic vortex was still intact and the vortex properties were well defined (e. g., PV value of the vortex edge). On the other hand, by choosing 7 December, as opposed to some earlier date, the RDF trajectories were not run for longer than 19 days. Nevertheless, as a test of sensitivity to the initial date, all the calculations were additionally performed by using 5 December and 9 December as the initial days.

5.4 Results

Parcels originating within the vortex on 7 December were identified by comparing their PV values with the PV values defining the vortex edge according to the method of *Nash et al.* (1996). On 23 December, on the 550 and 600 K surfaces, no vortex parcels were present above the New Zealand region. On 24 December, ~10 % and ~25 % of the total number of parcels over the New Zealand region, on the 550 K and 600 K potential surfaces, respectively, originated within the vortex. On 25 December there were more than 50 % of vortex parcels on both isentropes (the South Island of New Zealand was completely covered by the vortex air at 600 K). On 26 December, at 550 K, the number of vortex parcels was more than 80 %, and at 600 K it dropped down to ~45 %. The number of parcels for all four days examined and for both of the isentropes, obtained by using 5 December and 9 December as the initial days, did not differ from the above results by more than 4 %.

To investigate the ozone values associated with the vortex parcels, proxy ozone values were derived according to the POAM-based quadratic PV/O_3 fit for 7 December. The parcels were then "labelled" with these ozone values, and their locations at the start of the trajectory calculation (e. g. 24 December) were used to produce a "high-resolution" proxy ozone map for that date. In the process of calculating high-resolution ozone values, "cut-off" levels were set at the minimum and maximum PV value at the POAM measurement locations on 7 December. Hence, unlike in the low-resolution case, no extrapolation of the PV/O_3 fit was done, thus preventing the occurrence of unrealistically high or low ozone values. The high-resolution proxy ozone map for 24 December on the 600 K surface is shown in Figure 5.7. The same calculations performed by going back to 5 December and 9 December, produced high-resolution maps which are very similar to the one in Figure 5.7.
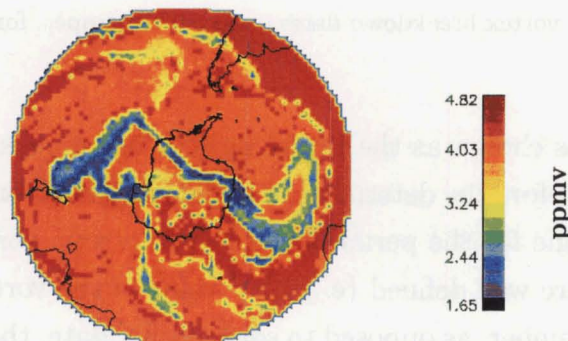
Figure 5.7: Polar stereographic (30–90° S) high-resolution ozone map on the 600 K surface, on 24 December 1998.

Figure 5.7 shows a filament of ozone-poor air situated above the South Island. It also reveals the fine details in the stratosphere after the Antarctic vortex broke down. None of this is evident in the low-resolution proxy ozone map (Figure 5.3). It is clear that the discrepancy between the ozonesonde and low-resolution PV/O_3 proxy ozone values for 24 December (Figure 5.4) is due to small-scale horizontal variations in the ozone field on 24 December that the PV/O_3 fitting technique does not accurately model.

This result illustrates the value of combining PV/O_3 mapping with the RDF calculations. The mapping as applied here gives excellent results when the PV field is relatively smooth and lacking in fine-scale horizontal structure, but works less well during dynamically active times such as vortex breakdown, when the presence of filaments can lead to a much more highly structured ozone field. In conjunction with the PV/O_3 proxy fields calculated during less active times, the RDF calculations enable the reconstruction of ozone fields even in the presence of a highly structured PV field.

Finally, to examine whether the air contained in the notch was chemically depleted, the vertical motion of vortex air parcels between 1 October, the time around which deple-

tion reaches maximum, and 7 December 1998, was analyzed. Diabatic RDF calculations (Section 3.4) were performed for the parcels that were inside the Antarctic vortex on 7 December 1998.

The results for 600 K showed that over this period, most of the air parcels descended from higher altitudes, where ozone-depleting heterogeneous chemical reactions do not take place (*Collins et al.*, 1993). Smaller ozone mixing ratios inside the vortex, compared to the surrounding air, were caused by two dynamical effects. First, horizontal mixing of midlatitude ozone-rich air, from which the vortex air is isolated, leads to accumulation of ozone outside the vortex (*Randall et al.*, 1995). Second, diabatic descent of vortex air above the ozone mixing ratio peak, reduces ozone levels at those altitudes (*Bevilacqua et al.*, 1997)). The results for 550 K showed that a significant number of air parcels originated between 500 K and 600 K, in the region of the ozone hole.

5.5 Discussion

In this section we discuss combining the PV/O_3 mapping and RDF calculations to illustrate the evolution of high-resolution ozone reconstructions during December. Figure 5.8 shows a selection of high-resolution proxy ozone maps for December 1998 on the 500 K potential temperature surface. Vertical motion calculation showed that the air at this isentrope mostly ascended from lower altitudes, where ozone depletion is most severe. Hence, the 500 K potential temperature surface was chosen to illustrate the evolution of the Antarctic vortex ozone-depleted air.

The calculations of the proxy ozone mixing ratios consisted of two steps. In the first step, high-resolution PV values were derived from isentropic RDF calculations run for five days back from the day of interest. The averaged heating rates for the month of December 1998, on the 500 K isentrope, for the region poleward of 60° S, were approximately -0.4 K/day, and for midlatitudes (30°–60° S) were ~ 0.3 K/day. Therefore, the errors in the calculations arising from the assumption of two-dimensional flow, are negligible. In the second step, the quadratic PV/O_3 fit on the initial day was used to derive ozone at the trajectory end-points. In this manner, the advantages of both of the methods were used. Even though the RDF technique explicitly neglects mixing between parcels, the process of mixing is implicitly represented in the daily POAM measurements, and thus only the last five days of mixing are neglected in the high-resolution proxy ozone maps.

The first plot (5 December) in Figure 5.8 shows ozone-depleted air well confined within the vortex and relatively high ozone values in midlatitudes. The following three plots show a highly distorted vortex and filaments peeling off from the edge of the vortex and reaching midlatitudes. At the same time, the midlatitude ozone levels steadily decreased. The last five plots show the period 21–27 December, in which an evolution of one of the vortex
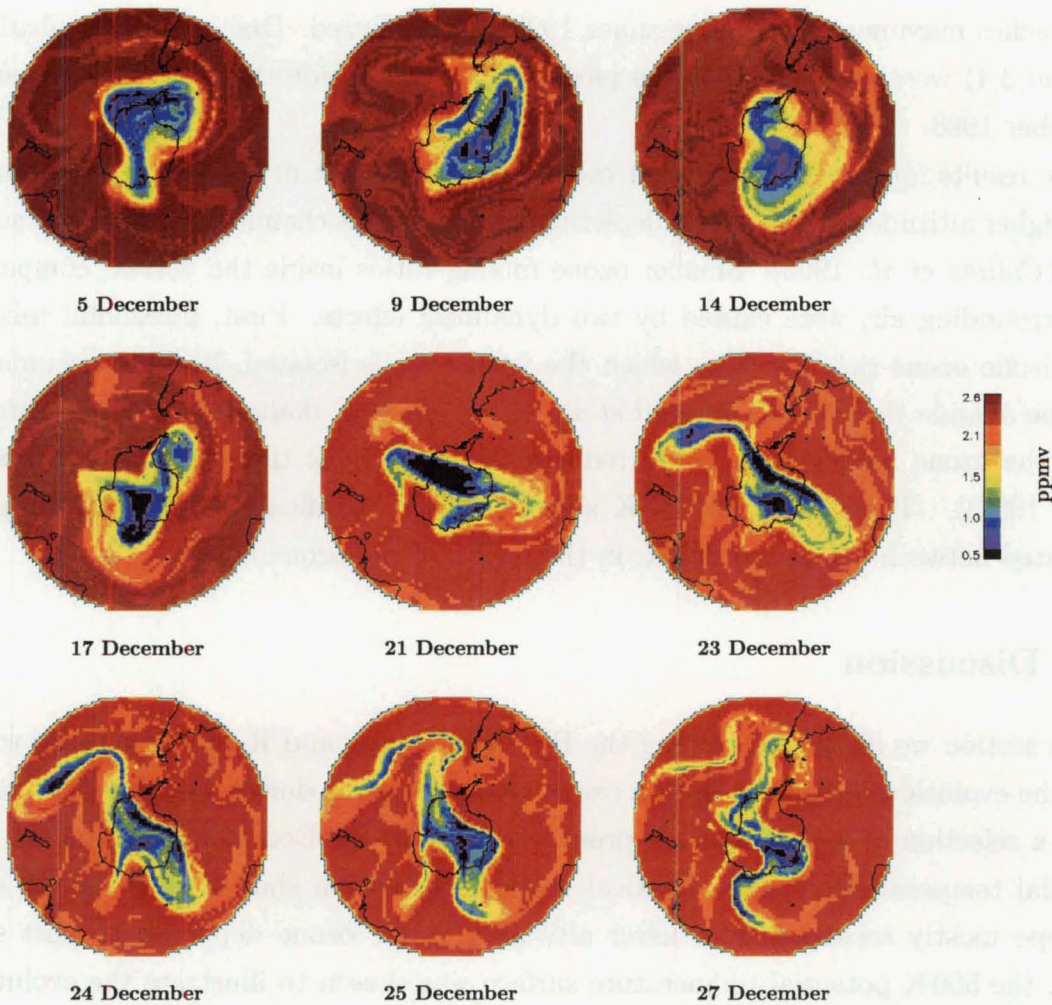
Figure 5.8: Polar stereographic (30–90° S) high-resolution ozone maps on the 500 K surface for nine selected days in December 1998.

filaments can be examined. On 21 December, during the process of vortex breakdown, the filament started forming south-east of New Zealand. Over the period of seven days it can be seen how the shape and the size of the filament changed. On 24 December, the filament is in the vicinity of New Zealand, but not reaching it. In fact, this filament is a part of the same vortex remnant as the filament at 600 K, situated above New Zealand on this day. Different positioning of these two filaments is a consequence of vertical misalignment (*Waugh et al.*, 1997). After 24 December, the ozone amounts inside the filament increased, while the width of the filament decreased. By 27 December this filament had a noticeably smaller area, with the lowest ozone values approximately three times greater than on 24 December.

Three PV/O$_3$ fits (along with the data) used to generate the high-resolution proxy ozone maps on 9, 17 and 25 December are shown in Figure 5.9. From these illustrative plots, the evolution of PV and ozone values sampled by POAM, as well as the evolution
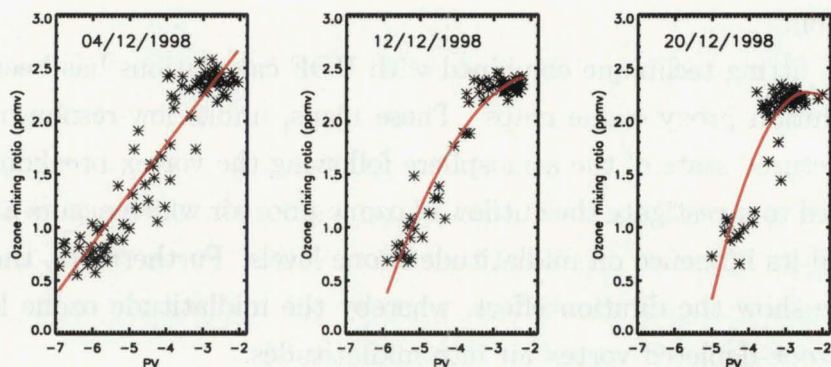
Figure 5.9: Ozone mixing ratio (in ppmv) and PV (in $10^{-5}\mathrm{K\,kg^{-1}\,m^2\,s^{-1}}$) for the Southern Hemisphere POAM III measurements on the 500 K isentropic surface, for three days, 4, 12 and 20 December 1998. The red line represents the quadratic fits.

of the $\mathrm{PV/O_3}$ fit, can be observed. The minimum PV values changed more rapidly than the sampled minimum ozone values. On the other hand, the maximum PV values were almost constant, while there was a slight decrease in the ozone values corresponding to those maximum PV values. Hence, the high-resolution proxy ozone maps in Figure 5.8, showing the decrease in midlatitude ozone values, are consistent with the POAM measurements.

The temporal evolution of the high-resolution ozone field illustrated in Figure 5.8, shows that throughout the month of December 1998, the vortex air was continually transported into midlatitudes. This suggests that the overall decrease in the midlatitude ozone mixing ratios seen at the end of December was at least partly due to the dilution of the ozone-depleted vortex air. This conclusion also offers a possible explanation for the decrease observed in the ozone mixing ratios on 500 K, between 14 and 24 December (Figure 5.1).

It is interesting to note that during the vortex breakdown, large parts of the ozone hole were northwards of the 60° S parallel (Figure 5.8). Hence, the total column ozone in midlatitudes was expected to decrease even before the calculated vortex breakdown date (Figure 5.6).

5.6 Conclusion

An analysis of the causes of the anomalous ozone profile on 24 December 1998 over Lauder has been performed using ozonesonde data, RDF calculations and POAM III ozone measurements. The analysis shows that in the period 24–26 December, after the Antarctic vortex breakdown, a vortex remnant on the 550 K and 600 K isentropes, was situated above New Zealand. The 600 K vortex remnant air originated from higher altitudes and was not subjected to ozone-depleting chemical reactions, while the 550 K air ascended from the

ozone hole region.

The PV/O$_3$ fitting technique combined with RDF calculations has been used to produce high-resolution proxy ozone maps. These maps, unlike low-resolution maps, show the highly structured state of the atmosphere following the vortex breakdown. They can therefore be used to investigate the outflow of ozone-poor air which occurs after the vortex breakdown, and its influence on midlatitude ozone levels. Furthermore, the maps on the 500 K isentrope show the dilution effect, whereby the midlatitude ozone levels decrease by mixing of ozone-depleted vortex air into midlatitudes.

Chapter 6

Calculations of Ozone Depletion

In this chapter, a method for calculating ozone depletion over a region, caused by the presence of Antarctic vortex air parcels, is presented. The method consists of three major steps:

1. advecting the parcels on a given grid backwards in time, from a given day of interest back to a chosen initial day,

2. recognizing the parcels that originate inside the vortex, and labelling them with the volume mixing ratio of depleted ozone, and

3. calculating ozone reduction in the chosen region.

A technique for recognizing air parcels with origin inside the vortex is given in Section 6.1. A method for calculating ozone reduction caused by the presence of vortex parcels, along with the concept of depleted ozone, is presented in Section 6.2. In that section, some of the disadvantages of the method are briefly addressed. Choice of the model domain and its properties are discussed in Section 6.3. The volume mixing ratio of depleted ozone assigned to air parcels originating in two different regions of the vortex, the core and the edge region, is examined in Section 6.4. Finally, the number of potential temperature surfaces within the domain, selected as the initial isentropes of advected air parcels, is discussed in Section 6.5. This section also gives the uncertainties in the calculations of ozone depletion arising from the uncertainties in temperatures used. A short summary of the algorithm is presented in Section 6.6.

6.1 Vortex Parcels

Back-trajectory calculations allow us to determine the point of origin of parcels which, on a chosen day of interest, are in a chosen geographical region. To quantify the influence of the Antarctic ozone hole on the ozone levels above the chosen region, we need to be able to recognize parcels that originate in the vortex. The method used here is based on the algorithm for vortex edge calculations of *Nash et al.* (1996).

According to the algorithm, the vortex edge on an isentropic surface is the location of the highest gradient of PV vs equivalent latitude, constrained by the proximity of a

strong jet. In other words, the vortex edge PV value corresponds to the maximum of the product of the derivative of PV vs equivalent latitude and the average wind speed along PV isolines. Hereafter, this vortex edge is referred to as the middle vortex edge (Figure 6.1). The local maximum convex and concave curvature in the PV curve surrounding the vortex edge are used to define another two boundaries of the vortex (*Nash et al.*, 1996), the equatorward and the poleward vortex edge (Figure 6.1). Hereafter, the vortex region poleward of the poleward vortex edge is referred to as the vortex core, and the region between the poleward and equatorward vortex edges, as the vortex edge region.

In this work, the PV values of the vortex core and edge, and the corresponding equivalent latitudes, on the isentropes of 350, 400, 450, 500, 550, 600, 650, 700 and 800 K from *Bodeker et al.* (2002), are used. Example profiles of the PV curve and the curve of the product of the derivative of PV vs equivalent latitude and the average wind speed along PV isolines, for the 500 K isentrope, on 10 October 1998, are presented in Figure 6.1.
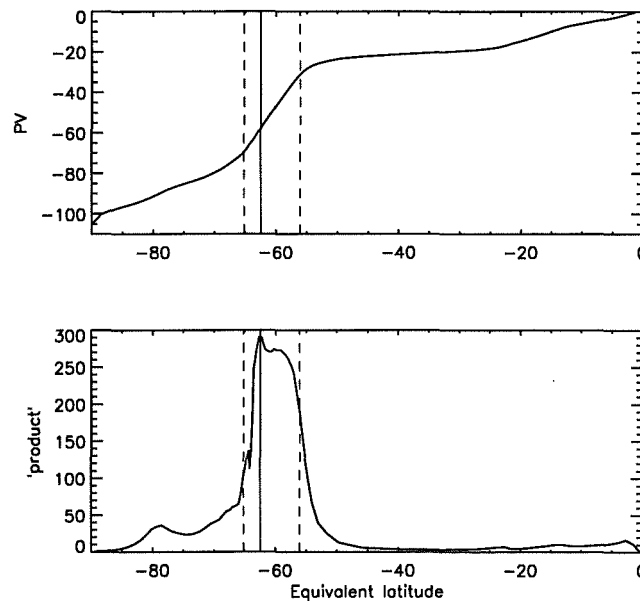
Figure 6.1: PV (in 10^{-5}K kg^{-1} m^2 s^{-1}; top) and product of the derivative of PV vs equivalent latitude and the average wind speed along PV isolines (in K kg^{-1} m^3 s^{-2} deg^{-1}; bottom) versus equivalent latitude (in degrees) on the 500 K isentrope on 10 October 1998. The dashed lines represent the equatorward and the poleward vortex edge, the full line represents the middle vortex edge.

Parcels originating within the vortex are recognized by comparing their PV value on the initial day with the PV values marking the vortex edges. The initial PV values of parcels are calculated through bilinear interpolation of the low-resolution Met Office PV field. In the case of isentropic RDF calculations performed on the isentropes for which the vortex edge PV values are available, comparison of the advected parcel's PV value with the PV values of the vortex edges determines whether the parcel originated in the vortex. The vortex parcels are classed into two sets:

1. core parcels, if their PV value is less or equal than the PV value marking the vortex core (poleward vortex edge), and

2. edge region parcels if their PV value is less or equal than the PV value of the equatorward vortex edge, and greater than the PV value of the poleward vortex edge.

Throughout this work, the above criteria are referred to as "the PV criterion".

A disadvantage of this method is that all features small enough not to be captured in the low-resolution PV field on the initial day, are neglected in the calculations. For example, if there is a filament peeling off the vortex on the initial day, air parcels associated with the filament will not be recognized as vortex parcels, and the final result of the calculations will underestimate the true result. This issue is addressed further in Section 7.3.2.

6.1.1 Diabatic Case

In the case of diabatic trajectories, advected parcels do not remain on the initial isentrope, and can originate at any given potential temperature surface between the lower and upper limit of the examined domain. Hence, an additional step in recognizing vortex parcels needs to be performed – interpolation of the PV values of the vortex edges.

Potential vorticity is a function of potential temperature, and for an isothermal atmosphere, it varies as $\theta^{9/2}$ (*Lait*, 1994). *Lait* (1994) introduced an alternative form of potential vorticity, the so called "modified potential vorticity", MPV, defined as

$$\text{MPV} = \text{PV} \left(\frac{\theta}{\theta_0} \right)^{-9/2}, \tag{6.1}$$

with θ_0 being an arbitrary constant. The scaling factor, $(\theta/\theta_0)^{-9/2}$, reduces the strong altitude dependance of PV, as can be seen in Figure 6.2. In this work, MPV is used in interpolation of the vortex edge PV.

Interpolation of the vortex edge PV for potential temperatures that do not coincide with the isentropes on which the data are available, is done through linear interpolation of MPV. The following test was performed to determine uncertainties associated with this method of interpolation. For a number of days, MPV (for all three vortex edges) was calculated, with $\theta_0 = 420\,\text{K}$, on the isentropes for which the data are available. A hundred and one days in each of the three years, 1998–2000, starting from 19 July (18 July in 2000) and ending on 27 October (26 October 2000) were chosen for the test. In this period (austral winter and early spring time), the Antarctic vortex was well defined. Two sets of linear interpolation were performed. First, the interpolation was done for
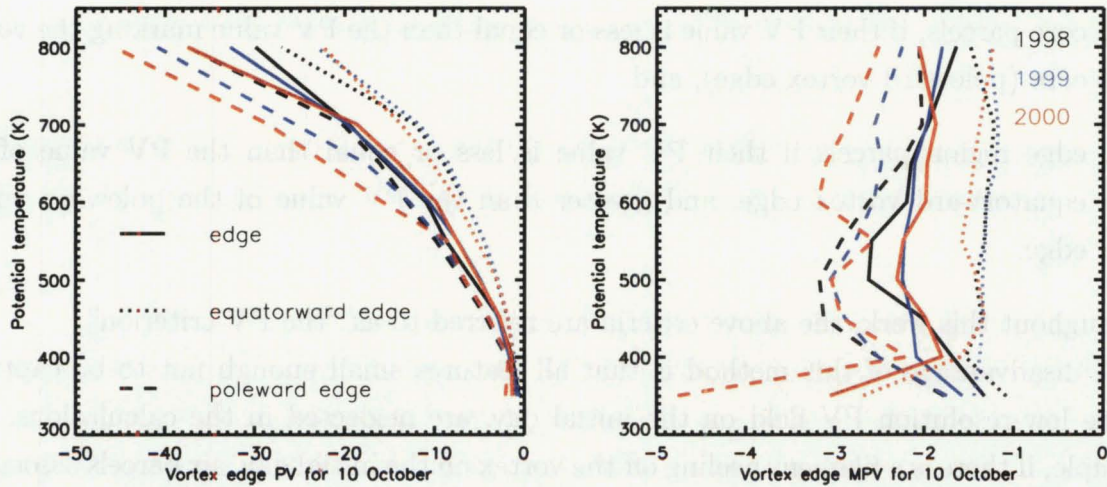
Figure 6.2: PV and MPV (in $10^{-5} \mathrm{K\,kg^{-1}\,m^2\,s^{-1}}$) of the three vortex edges, equatorward vortex edge (dotted line), vortex edge (full line) and poleward vortex edge (dashed line), as a function of potential temperature, on 10 October of the years 1998 (black), 1999 (blue) and 2000 (red). MPV was calculated using $\theta_0 = 420 \, \mathrm{K}$.

400 K, 500 K and 600 K, using the data on the rest of the isentropes. Similarly, the second interpolation was done for 450 K, 550 K and 650 K. The interpolated values of MPV were then compared to the initial values of MPV for the examined isentropes. The results of this test are shown in Figure 6.3.
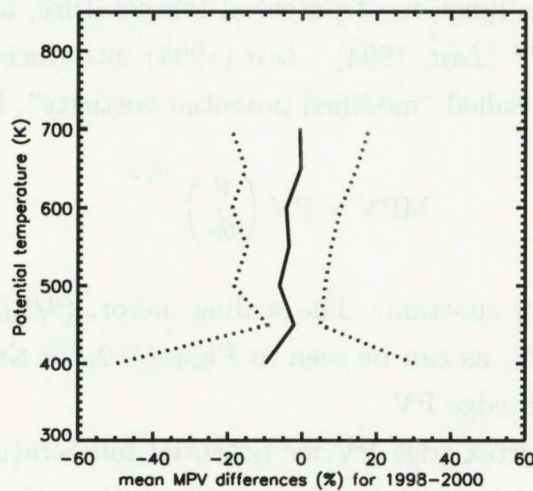
Figure 6.3: Mean (solid line) and standard deviation (dotted line) of percent differences arising from linear interpolation of the vortex edges' MPV.

The mean values of the percent differences range between $-10\,\%$ and $-0.4\,\%$. Hence, on average, the interpolated MPV values were less than the original MPV values. As a consequence, PV values marking the vortex edges, that are calculated from the interpolated MPV values, are less than the original values. Therefore, the interpolation of

PV leads to a somewhat smaller vortex. This implies that when PV values of the examined parcels are compared to the interpolated PV of the vortex edges, fewer parcels are recognized as vortex parcels.

As in the isentropic case, after comparing parcels' PV values with the PV values marking the vortex edges, the parcels were classed as either core parcels, or edge region parcels.

6.2 Ozone Depletion Integration

Once parcels that originate in the vortex core or in the vortex edge region are recognized, they are labelled with the volume mixing ratio of depleted ozone (Figure 4.1). It is assumed that the volume mixing ratio of depleted ozone is a constant along the trajectory of the parcel. In other words, in the region where the calculations are performed the ozone photochemical life-time is long, and ozone destroyed inside the vortex is not expected to recover over a period of a few months. Effectively, advecting the volume mixing ratio of depleted ozone is equivalent to advecting the observed and undepleted ozone and taking the difference (*Knudsen et al.*, 1998a; *Knudsen and Grooß*, 2000).

Even though RDF calculations advect only a point in space (i.e., a parcel), it is assumed that the volume surrounding that point, no matter how small, is representative of the spatial box defined by the grid on which parcels are arranged. Implications of this assumption are discussed in this chapter, as well as in Chapter 7.

The basis for the calculation of ozone reduction caused by the presence of Antarctic vortex parcels that underwent chemical ozone depletion inside the vortex (also referred to as ozone depletion, for simplicity, even though that term might be somewhat misleading), above some geographical region is presented here. First, the equations for calculating the number of depleted ozone molecules in the spatial box surrounding one parcel are given. Second, the equations for deriving ozone depletion in any given geographical region are presented.

Let the parcel be characterized by its longitude λ, latitude ϕ, potential temperature θ, pressure p_θ and temperature T_θ. The spatial box surrounding this parcel, with length $\Delta\lambda$ and width $\Delta\phi$, has two horizontal bases characterized by points $(\theta - \Delta\theta/2,\ p_{\theta-\Delta\theta/2},\ T_{\theta-\Delta\theta/2})$ and $(\theta + \Delta\theta/2,\ p_{\theta+\Delta\theta/2},\ T_{\theta+\Delta\theta/2})$, where $\Delta\theta$ is the thickness (in units of potential temperature) of the chosen box. The volume of the box is V, and the area of its base is A.

The volume mixing ratio of depleted ozone, vmr, is a function of potential temperature (Figure 2.2), and is defined as

$$vmr = \frac{N_{depleted\,ozone}}{N_{dry\,air}} \cdot 10^6, \tag{6.2}$$

where $N_{depleted\,ozone}$ and $N_{dry\,air}$ are the number concentrations (in molecules/cm^3) of depleted ozone and dry air, respectively, and the factor 10^6 arises from the chosen unit for volume mixing ratio – parts per million by volume (ppmv). The number concentration of dry air in the chosen box is given by

$$N_{dry\,air} = \frac{p_\theta}{k_B T_\theta}, \tag{6.3}$$

where k_B is Boltzmann's constant. The number of depleted ozone molecules, **N**, in the box of volume V is

$$\mathbf{N} = N_{depleted\,ozone}V. \tag{6.4}$$

The volume of the box of base A and the height which corresponds to the distance between two points, $(\theta - \Delta\theta/2,\ p_{\theta-\Delta\theta/2},\ T_{\theta-\Delta\theta/2})$ and $(\theta + \Delta\theta/2,\ p_{\theta+\Delta\theta/2},\ T_{\theta+\Delta\theta/2})$, is given by

$$V = AH \ln \frac{p_{\theta-\Delta\theta/2}}{p_{\theta+\Delta\theta/2}}, \tag{6.5}$$

where H is the scale height. Combining the above equation with the defining equation for potential temperature

$$\theta = T_\theta \left(\frac{p_S}{p_\theta}\right)^{R/c_P}, \tag{6.6}$$

where p_S is standard pressure, R is the gas constant for dry air and c_P is the specific heat of dry air at constant pressure, leads to

$$V = \frac{c_P}{R} AH \ln \frac{T_{\theta-\Delta\theta/2}(\theta + \Delta\theta/2)}{T_{\theta+\Delta\theta/2}(\theta - \Delta\theta/2)}. \tag{6.7}$$

The base area A of the chosen box is

$$A = R_E^2(\sin[\phi + \Delta\phi/2] - \sin[\phi - \Delta\phi/2])\Delta\lambda, \tag{6.8}$$

where R_E is the Earth's radius (note that the distance of the potential temperature surface from the surface of the Earth is negligible).

The number of depleted ozone molecules in the box of volume V (Equations 6.8, 6.7, 6.4, 6.3 and 6.2) is

$$
\begin{aligned}
\mathbf{N} &= 10^{-6} R_E^2 H \frac{c_P}{R} \frac{p_S}{k_B} \frac{T_\theta^{c_P/R-1}}{\theta^{c_P/R}} vmr \\
&\quad \cdot (\sin[\phi + \Delta\phi/2] - \sin[\phi - \Delta\phi/2])\Delta\lambda \\
&\quad \cdot \ln \frac{T_{\theta-\Delta\theta/2}(\theta + \Delta\theta/2)}{T_{\theta+\Delta\theta/2}(\theta - \Delta\theta/2)}.
\end{aligned} \tag{6.9}
$$

In the calculations performed in this work, parcels were arranged on a 1° longitude

by $1°$ latitude grid. The base area of the spatial box surrounding each parcel (with $\Delta\lambda = \Delta\phi = 1°$ in Equation 6.8) is

$$A_{1°.1°} = R_E^2(\sin[\phi + 0.5°] - \sin[\phi - 0.5°]). \tag{6.10}$$

Now, let the geographical region of interest be characterized by the range of longitudes between $\lambda - \Delta\lambda$ and $\lambda + \Delta\lambda$ and the range of latitudes between $\phi - \Delta\phi$ and $\phi + \Delta\phi$. The base area, A, of the region is given by Equation 6.8.

The total number of depleted ozone molecules above this geographical region, $\mathbf{N}_{total}$, between potential temperature surfaces $\theta - \Delta\theta$ and $\theta + \Delta\theta$, is equal to the sum of the total number of depleted ozone molecules in the $1°$ longitude by $1°$ latitude boxes surrounding vortex parcels (counted by i)

$$\mathbf{N}_{total} = \sum_i \mathbf{N}_i. \tag{6.11}$$

Ozone depletion in the region of interest is expressed in Dobson units. A Dobson unit, DU, is the thickness, measured in units of hundredths of a millimetre, that the ozone column would occupy at standard temperature, T_S, and standard pressure, p_S. Ozone depletion, D, in Dobson units, over the geographical region A, is

$$D = k_B \frac{T_S}{p_S} \frac{\mathbf{N}_{total}}{A} 10^5, \tag{6.12}$$

where the factor 10^5 arises from the fact that the thickness is expressed as 10^{-5} m.

Parcels originating in two different regions of the Antarctic vortex, the core and the edge, carry different ozone depletion, hence the calculations were performed separately for those two classes of parcels. Combining Equations 6.11, 6.8, 6.10, and 6.9 with Equation 6.12 yields

$$
\begin{aligned}
D_\theta =\ & 10^{-6} 10^5 H \frac{c_P}{R} \frac{T_S}{\theta^{c_P/R}} \\
& \cdot \frac{1}{\Delta\lambda} \frac{1}{\sin[\phi + \Delta\phi/2] - \sin[\phi - \Delta\phi/2]} \\
& \cdot \sum_{i'=1}^{2} \sum_{i=1}^{n(i')} vmr_{\theta_{init},i} T_{\theta,i}^{c_P/R-1} \ln \frac{T_{\theta - \Delta\theta/2,i}(\theta + \Delta\theta/2)}{T_{\theta + \Delta\theta/2,i}(\theta - \Delta\theta/2)} \\
& \cdot (\sin[\phi_i + 0.5°] - \sin[\phi_i - 0.5°]), \tag{6.13}
\end{aligned}
$$

where D_θ is ozone depletion centred around a given potential temperature surface, over the geographical region A. Core and edge region parcels are counted by i', whereas parcels within those two classes are counted by i. Note that the volume mixing ratio of depleted ozone is a function of parcel's potential temperature on the initial day inside the vortex

(θ_{init}).

Finally, total depletion, D, over the geographical region represents the sum of individual depletions centred around the chosen isentropic surfaces $(\theta_1, \theta_2, ...,\theta_n)$

$$D = \sum_{\theta=\theta_1}^{\theta_n} D_\theta. \tag{6.14}$$

Throughout this work, the values of the constants were taken as follows: $c_P/R = 3.497$, $H = 6.950\,\text{km}$ and $T_S = 298\,\text{K}$. The value of the combined constant, α,

$$\alpha = 10^{-6}10^5 H\frac{c_P}{R}T_S \tag{6.15}$$

is $\alpha = 724263.67$ (in hundredths of a millimetre). Combining equations 6.14 and 6.13 yields

$$D = \alpha \ \frac{1}{\Delta\lambda}\frac{1}{\sin[\phi + \Delta\,\phi/2] - \sin[\phi - \Delta\,\phi/2]}$$
$$\cdot\sum_{\theta=\theta_1}^{\theta_n}\frac{1}{\theta^{3.497}}\sum_{i'=1}^{2}\sum_{i=1}^{n(i')}vmr_{\theta_{init},i}T_{\theta,i}^{2.497}\ln\frac{T_{\theta-\Delta\theta/2,i}(\theta + \Delta\theta/2)}{T_{\theta+\Delta\theta/2,i}(\theta - \Delta\theta/2)}$$
$$\cdot(\sin[\phi_i + 0.5°] - \sin[\phi_i - 0.5°]) \quad [\text{DU}]. \tag{6.16}$$

Temperatures $T_{\theta,i}$ at the parcels' positions were bilinearly interpolated from the Met Office temperature fields.

Equation 6.16 is the basis of the results obtained in this work. Let us discuss some of the drawbacks arising from it.

First, let us examine how depletion depends on the latitudes of vortex parcels. Consider an air parcel coming out of the vortex, and reaching the latitude of $59.5°$ S on some day. The base area of the associated box, $A_{1°.1°}$, is proportional to $(\sin 60° - \sin 59°)$. If on a later day, this parcel's latitude is $30.5°$, then $A_{1°.1°} \propto (\sin 31° - \sin 30°)$. The base area of the box surrounding the same parcel, is ~1.7 times larger in the latter case, leading to a greater number of depleted ozone molecules in the box (all other variables being constant).

The vertical motion of vortex air parcels also influences the results. Consider a parcel that on some day is on the $700\,\text{K}$ isentrope, and on the $550\,\text{K}$ isentrope on some later day. The height of the corresponding box is less in the former case, hence there are fewer depleted ozone molecules (all other variables being constant).

The given examples point out the fact that the mass associated with the same parcel depends on the position of the parcel. This discrepancy is inherent in Lagrangian models, and the additional constraints introduced to force mass conservation are discussed in

Section 7.1.1.

6.3 Model Domain

As discussed in Section 4.3, chemical depletion of ozone inside the Antarctic vortex occurs between the potential temperature surfaces of 350 K and 700 K. In other words, the vortex air in this region at the beginning of October can be labelled with a non-zero volume mixing ratio of depleted ozone. The aim of RDF calculations performed here was to track as many of those air parcels as possible, in order to get a complete picture of dilution of ozone-depleted air.
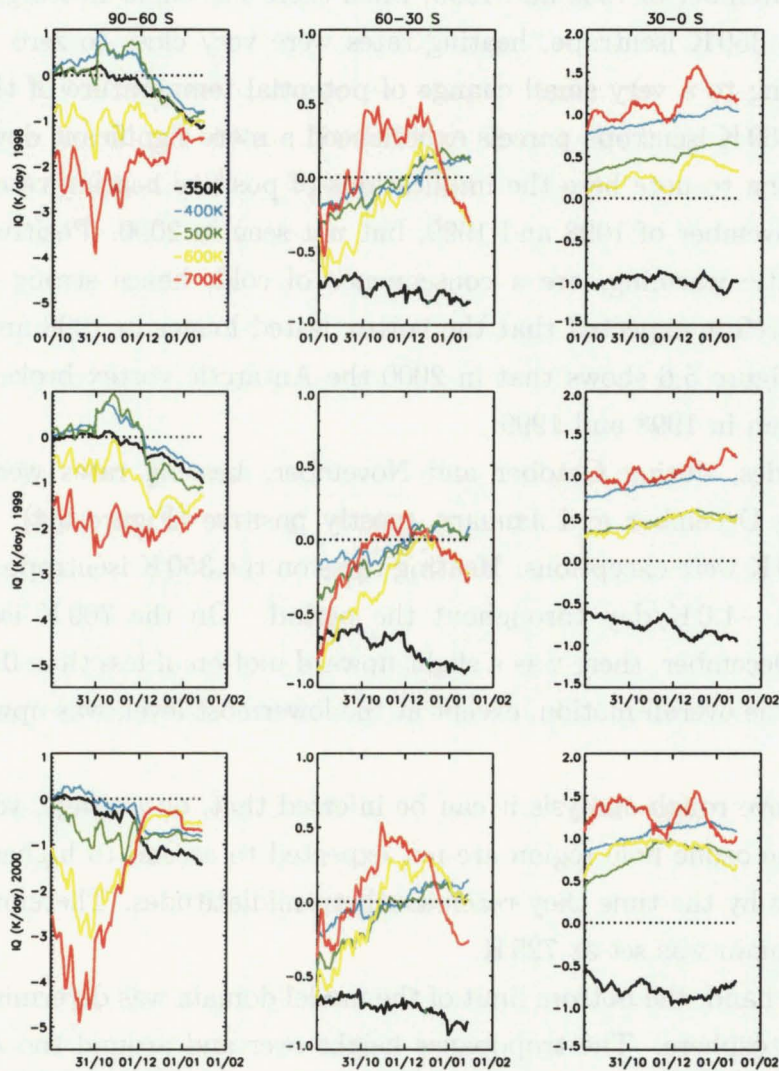

Figure 6.4: Heating rates on five isentropes, for the months of October, November, December and the first half of January, of the years 1998, 1999, and 2000, averaged for the latitudes south of 60°S (left), between 60°S and 30°S (middle), and between 30°S and 0°S (right).

To set the vertical limits for RDF calculations, heating rates (Section 3.4) in the months of October, November, December and the following January, of the years 1998, 1999 and 2000, were first examined. Figure 6.4 shows the mean heating rates for three regions, poleward of 60°S (polar region), between 60°S and 30°S (midlatitudes), and between 30°S and 0°S (tropical region), for five isentropes of 350, 400, 500, 600, and 700 K.

In the polar region, heating rates were mostly negative. In other words, most of air parcels were descending throughout the examined period (see discussion in Section 3.4 about the vertical motion of air parcels in the coordinate system with potential temperature as the vertical coordinate). The exception were air parcels on the 400 K and 500 K isentropes, in November of 1998 and 1999, when there was slight heating, i.e. an upward motion. On the 350 K isentrope, heating rates were very close to zero in October and November, leading to a very small change of potential temperature of these parcels. In December, the 350 K isentrope parcels experienced a more significant downward motion.

It is interesting to note here the implications of positive heating rates seen at 400 K and 500 K in November of 1998 and 1999, but not seen in 2000. Positive heating rates, indicating diabatic warming, are a consequence of cold, hence strong (Section 2.2.1), vortex. It is therefore expected that the vortex lasted longer in 1998 and 1999, than in 2000. Indeed, Figure 5.6 shows that in 2000 the Antarctic vortex broke down almost a month earlier than in 1998 and 1999.

In midlatitudes, during October and November, heating rates were mostly negative, and during December and January, mostly positive (Figure 6.4). The isentropes of 350 K and 700 K were exceptions. Heating rates on the 350 K isentrope ranged between −0.5 K/day and −1.0 K/day throughout the period. On the 700 K isentrope, during November and December, there was a slight upward motion of less than 0.5 K/day. In the tropical region, the overall motion, except at the lowermost level, was upward throughout the period.

From the above rough analysis it can be inferred that, on average, vortex air parcels originating in the ozone hole region are not expected to ascend to higher potential temperature surfaces by the time they reach southern midlatitudes. Therefore, the top limit of the model domain was set at 725 K.

On the other hand, the bottom limit of the model domain was determined by the lower limit of the stratosphere. The tropopause height over and around the Antarctic in the August–October period is approximately 305 K (*Tuck and Proffitt*, 1997), but it increases in midlatitudes and tropical region. In the tropics, the annual mean tropopause height is ∼380 K, and ∼350 K at 30°S (*Holton et al.*, 1995). Hence, the bottom limit of the model domain was set at 375 K.

Although vortex air descends to the troposphere (*Li et al.*, 2002; *Öllers et al.*, 2002),

causing a reduction in the tropospheric ozone column (*Prather et al.*, 1990), the troposphere was excluded from the analysis. The primary reason for this is that the inaccuracies in trajectory calculations associated with a complex tropospheric flow are much larger than in the stratosphere. Furthermore, the impact of ozone reduction in the troposphere was expected to be lower than in the stratosphere. *Prather et al.* (1990) reported a reduction of $\sim$10 % in the tropospheric column ozone due to the dilution of the Antarctic ozone hole. Considering low amounts of ozone in the troposphere (5–10 % of the total column ozone, see Section 2.1), the impact of ozone reduction in the troposphere was not expected to be higher than $\sim$1 % of the total column ozone. The exclusion of the troposphere is discussed further in Section 7.6.4.

With the vertical model domain between the potential temperature surfaces of 375 K and 725 K, any air parcels descending to the isentropes lower than 375 K, or ascending to the isentropes higher than 725 K, at any point in their trajectories, were not included in the ozone depletion calculations. As already discussed, on average, the parcels originating in the vortex were not expected to leave the domain by crossing the top limit. In contrast, the downward motion was expected to lead to "leakage" through the bottom limit of the domain.

It is also worth noting here that Figure 6.4 will often be referred to in the following chapter. An assumption that the polar region coincides with the Antarctic vortex will be made, and not explicitly stated. The validity of this assumption arises from two facts. First, the vortex is nearly circular on any given potential temperature surface, and usually centred over the south pole (e.g. *Schoeberl and Hartmann*, 1991; *Manney et al.*, 1995; *Waugh*, 1997). Second, the vortex boundary is close to the 60 $^\circ$ S parallel (*Bodeker et al.*, 2002). The assumption is valid only if the vortex is not highly disturbed.

As discussed in Section 3.4, the physical height of air parcels whose motion is viewed in the coordinate system with potential temperature as the vertical coordinate, can be neglected. In this sense, the domain set between 375 K and 725 K can be considered stationary. However, the change in the physical height of the domain affects the ozone depletion calculations (Equation 6.16). In other words, any change in the thickness (i.e. the volume) and the density of the domain directly influence the number of depleted ozone molecules in the domain. Therefore, those two properties are briefly examined here.

Figure 6.5 shows the change in the thickness and in the density of the 375–725 K layer in the Southern Hemisphere, over the period 1 October – 15 January of the years 1998, 1999, and 2000. The thickness of the domain represents the difference between the mean (averaged over the whole Southern Hemisphere) geopotential heights of the top (725 K) and the bottom (375 K) isentrope of the domain.

The thickness and the density of the domain increased between October and January. The increase in the thickness was caused by both descent of the 375 K isentrope and ascent
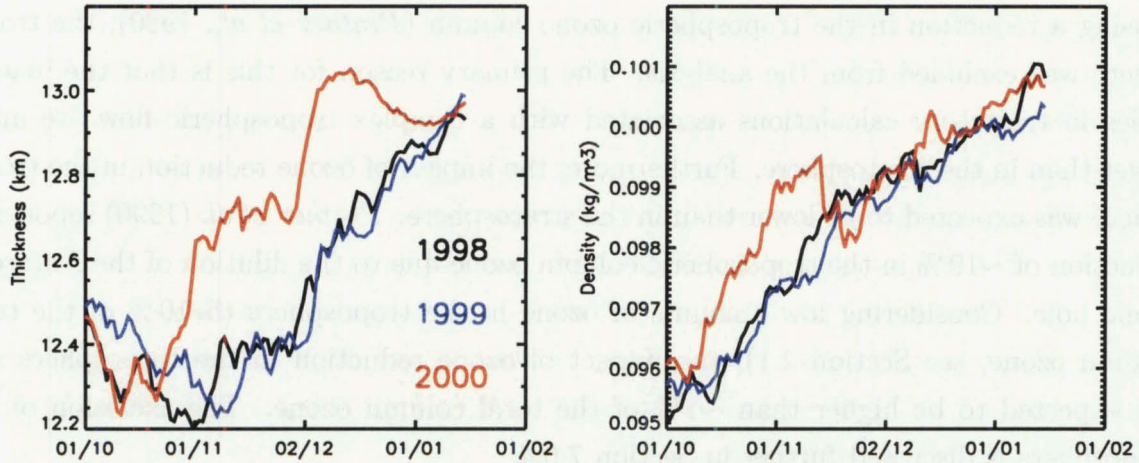
Figure 6.5: The thickness (left) and the density (right) of the 375–725 K layer in the SH, between 1 October and 15 January of the years 1998 (black), 1999 (blue) and 2000 (red).

of the 725 K isentrope (not shown). The outstanding difference in the domain thickness between the year 2000 on one hand, and the years 1998 and 1999, on the other hand, is a consequence of a faster descent (ascent) of the bottom (top) limit of the domain in 2000. The differences in the temporal evolution of the model density were pronounced only during October and November.

In the calculations of ozone depletion (Section 6.2), the first step is determining the number of depleted ozone molecules in the domain. According to Equations 6.2–6.4, the calculated number of depleted ozone molecules is directly proportional to the thickness and the density of the domain. The increase in the volume and the density of the domain therefore leads to an increased number of calculated depleted ozone molecules. In other words, even if depleted ozone molecules did not move inside the domain, mere day-to-day variations of the domain physical properties would give rise to spurious variations in the total number of depleted ozone molecules. This effect is different from the effect arising when depleted ozone molecules move inside the domain (discussed in Section 6.2). A scaling method, introduced in Section 7.1.1, which effectively preserves the total number of ozone depleted molecules in the domain, is used to correct the final results for the unrealistic increase in the number of depleted ozone molecules.

6.4 Ozone Depletion in the Vortex Core and Edge Region

As discussed earlier, ozone depletion occurring in the vortex core is different than the depletion occurring in the vortex edge region. In this work, ozone depletion in the vortex core was taken from the work of *Hoppel et al.* (2003), while ozone depletion inside the vortex edge region was calculated assuming that depletion is a linear function of PV.

In the ozone depletion calculations, vortex parcels originating in the vortex core be-

tween 700 K and 725 K, were assumed not to have undergone any chemical depletion. In the region between 600 K and 700 K, instead of using the volume mixing ratio of depleted ozone from *Hoppel et al.* (2003) (see discussion in Section 4.3), the depletion was linearly interpolated starting from the calculated value at 600 K, and going to zero at 700 K (as suggested by Karl Hoppel, private communication). The "corrected" depletion curves, spanning the vertical extent of the model domain (375–725 K) for the years 1998, 1999 and 2000, are shown in Figure 6.6.
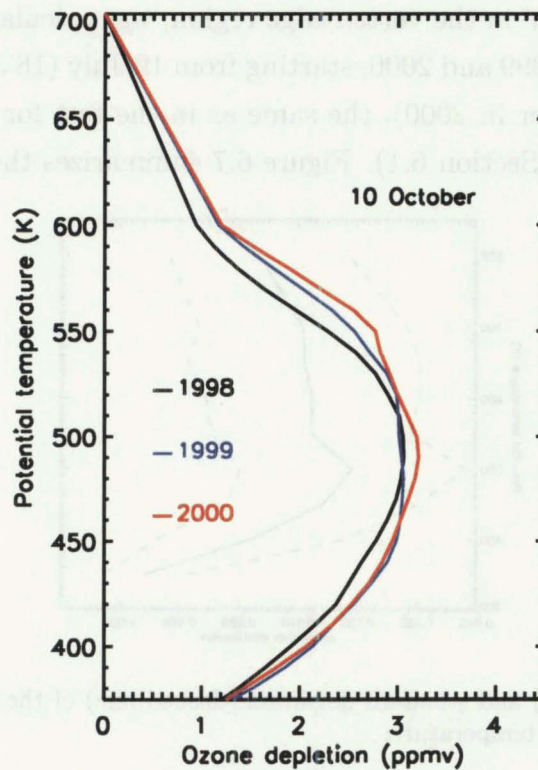
Figure 6.6: "Corrected" volume mixing ratio of depleted ozone in the Antarctic vortex core, for the years 1998, 1999 and 2000 (cf. Figure 4.1).

Model results of *Lee et al.* (2001) showed that the volume mixing ratio of depleted ozone in the vortex edge region, between 60°S and 65°S, decreases as (the absolute value of) equivalent latitude decreases. *Bodeker et al.* (2002) showed that in the vortex edge region, the zonal mean ozone decreases as (the absolute value of) equivalent latitude increases. Based on those results, in this work, it was assumed that inside the vortex edge region, the volume mixing ratio of depleted ozone is a linear function of equivalent latitude. If, in the vortex edge region, equivalent latitude is a linear function of PV, then the volume mixing ratio of depleted ozone in the vortex edge region is also a linear function of PV.

Results presented in the top plot of Figure 6.1 show that although equivalent latitude

is not a linear function of PV throughout the hemisphere, in the vortex edge region the relationship between equivalent latitude and PV is very close to linear. This hypothesis was tested using Pearson's correlation coefficient (*Press et al.*, 1989), r, defined as

$$r = \frac{\sum_i (x_i - \overline{x})(y_i - \overline{y})}{\sqrt{\sum_i (x_i - \overline{x})^2}\sqrt{\sum_i (y_i - \overline{y})^2}},\tag{6.17}$$

where (x_i, y_i), $i = 1, ..., N$ are pairs of quantities for which the correlation coefficient is calculated, and $\overline{x}$ and $\overline{y}$ are the means of the sets. Pearson's correlation coefficient for equivalent latitude and PV in the vortex edge region, was calculated for 101 days in each of the three years, 1998, 1999 and 2000, starting from 19 July (18 July in 2000) and ending on 27 October (26 October in 2000), the same as in the test for the linear interpolation of the vortex edge MPV (Section 6.1). Figure 6.7 summarizes the results.
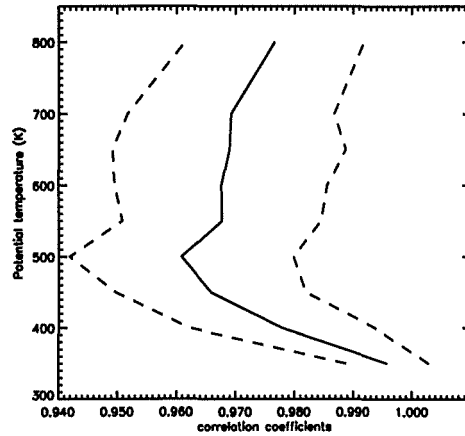
Figure 6.7: Mean (solid line) and standard deviation (dashed line) of the Pearson's correlation coefficients as function of potential temperature.

On all of the examined isentropes, the mean of the Pearson's correlation coefficient ranged between ∼0.961 and ∼0.996, with standard deviation between ∼0.007 and ∼0.020. From these results, it was concluded that in the vortex edge region, equivalent latitude can be represented as a linear function of PV.

6.5   Choice of Potential Temperature Surfaces

As discussed in Section 6.3, the potential temperature surfaces of 375 K and 725 K were chosen as the vertical limits of the model domain. The question of how many potential temperature surfaces in this region were chosen to initialize advected parcels on, and consequently, to integrate ozone depletion around, and why, is discussed here.

Two tests were performed to determine an optimal number of isentropes for calculations. In those tests, three cases of different isentropes, with different spacings between

them, were considered:

Case 1 Five isentropes centred on 400, 450, 500, 550, and 600 K ($\Delta\theta = 50\,K$),

Case 2 Eleven isentropes centred on 375, 400,..., 625 K ($\Delta\theta = 25\,K$),

Case 3 Twenty-five isentropes centred on 380, 390,..., 620 K ($\Delta\theta = 10\,K$).

For these three cases, the integration of depleted ozone volume mixing ratio was done in individual layers. Then, the results for Case 2 and Case 3 were summed into the layers defined in Case 1 to analyze the differences.

First, a simple integration of the depletion curve (Figure 6.6) was performed: for each potential temperature surface, a property D_s was calculated by

$$D_s = vmr_\theta \Delta\theta. \qquad (6.18)$$

The results for three years, 1998, 1999 and 2000, are presented in the left panel of Figure 6.8. Assuming that Case 3 gives most accurate results, the results of Case 1 and Case 2 were compared to the results of Case 3. The percent differences are shown in the right panel of Figure 6.8.
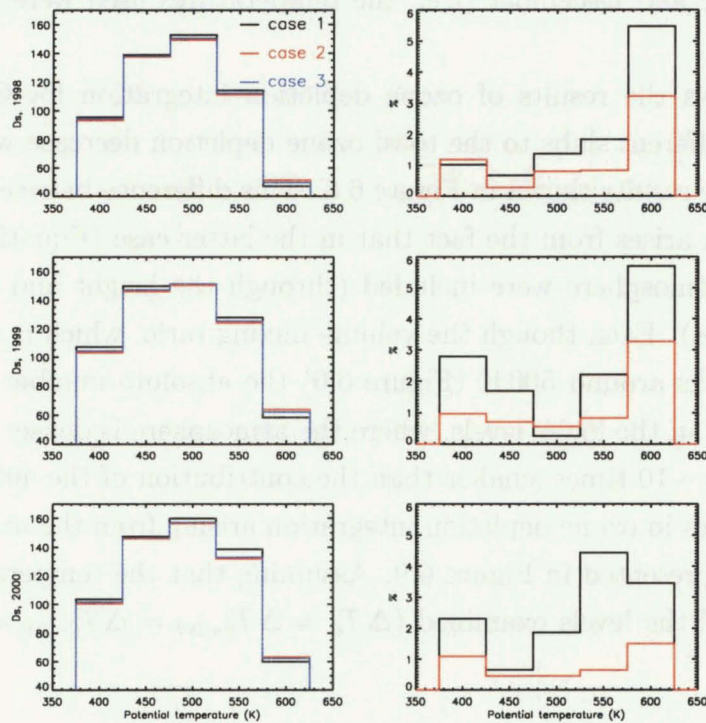
Figure 6.8: Results of simple integration of the depletion curve, for three different choices of isentropes, for the years 1998–2000 (left), and percent differences of the results in Case 1 (black line) and Case 2 (red line) compared to the results in Case 3 (right).

As expected, the differences between Case 2 and Case 3, maximizing around 3 %, are less than the differences between Case 1 and Case 3, reaching the values as high as 6 %. The differences are the least in the slabs where the depletion curve is either almost constant (e. g. 500 K in the year 1999) or the gradient of the curve is almost constant (e. g. 450 K in the years 1998 and 2000). On the other hand, the differences (larger than 3 %) are the greatest around 600 K for all three years and around 550 K in 2000, because the depletion curve gradient is considerably different for the surrounding lower and higher theta surfaces.

In the second test, it was assumed that at 45° S, in a box of 1° longitude by 1° latitude, on all of the isentropes defined in Cases 1, 2, 3, there was a parcel that originated in the Antarctic vortex core. The centre points of the bases of the spatial boxes surrounding the vortex core parcels were characterized by the mean temperature along the 45° S circle, on corresponding isentropes. Ozone depletion in each spatial box, on each isentrope, was calculated (from Equation 6.13 with $A = A_{1°.1°}$) using:

$$D_\theta = \alpha\, vmr_\theta \frac{T_\theta^{2.497}}{\theta^{3.497}} ln \frac{T_{\theta-\Delta\theta/2}(\theta + \Delta\theta/2)}{T_{\theta+\Delta\theta/2}(\theta - \Delta\theta/2)} \quad [\text{DU}]. \tag{6.19}$$

The calculations were performed for the years 1998, 1999 and 2000, and for the months of October, November and December (i. e., the temperatures used were both monthly and zonally averaged).

Figure 6.9 shows the results of ozone depletion integration for Cases 1, 2, and 3. Contributions of different slabs to the total ozone depletion decrease with potential temperature, unlike the results shown in Figure 6.8. This difference between simple and more realistic integration arises from the fact that in the latter case (Equation 6.19) the properties of the real atmosphere were included (through the height and the density of the chosen spatial boxes). Even though the volume mixing ratio, which is a relative property (Equation 6.2) peaks around 500 K (Figure 6.6) the absolute number of depleted ozone molecules is largest in the lower levels, where the atmosphere is denser. The contribution of the 600 K slab is ~10 times smaller than the contribution of the 400 K layer.

The uncertainties in ozone depletion integration arising from the uncertainties in temperatures are also presented in Figure 6.9. Assuming that the temperature uncertainties are the same for all the levels examined ($\Delta T_\theta = \Delta T_{\theta+\Delta\theta} = \Delta T_{\theta-\Delta\theta} = \Delta T$), the uncertainty in D_θ is:

$$\Delta D_\theta = \alpha\, vmr_\theta \frac{T_\theta^{1.497}}{\theta^{3.497}} [2.497 ln \frac{T_{\theta-\Delta\theta/2}(\theta + \Delta\theta/2)}{T_{\theta+\Delta\theta/2}(\theta - \Delta\theta/2)} + T_\theta(\frac{1}{T_{\theta+\Delta\theta/2}} + \frac{1}{T_{\theta-\Delta\theta/2}})]\Delta T. \tag{6.20}$$

The uncertainties calculated for Case 1, with ΔT=1 K (*Swinbank and O'Neill*, 1994), are also plotted in Figure 6.9.
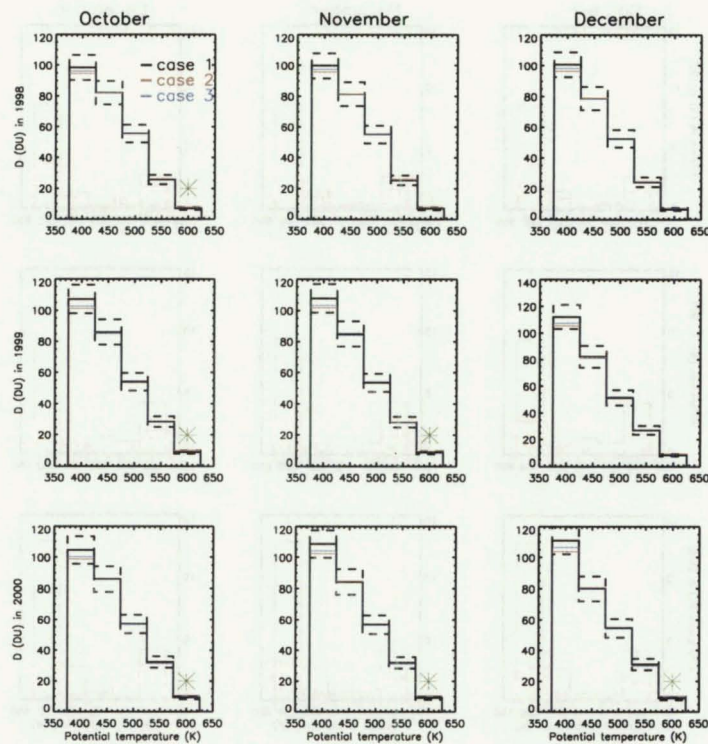
Figure 6.9: The results of integrated depleted ozone volume mixing ratios for Cases 1, 2, 3. The dashed black line represents uncertainties calculated for Case 1. The green asterisk symbols indicate slabs in which the results of either Case 2 or Case 3 are not within the uncertainties of Case 1.

The relative uncertainties, $\Delta D_\theta / D_\theta$, for Case 1, range between 8 % (in the 400 K layer) and 14 % (in the 600 K layer). The relative uncertainty, $\Delta D/D$, where $D = \sum_{\theta=400\,\mathrm{K}}^{600\,\mathrm{K}} D_\theta$, averaged over three years and three months, is 4.9 %. In Figure 6.9, green asterisks indicate when the results of Case 2 and Case 3 are not within the temperature uncertainties of Case 1.

Figure 6.10 shows relative differences for Case 1 and Case 2 compared to the results of Case 3. With the exception of the 600 K slab, the differences are better than 4 %. For the 600 K layer, the differences for Case 1 are as high as ~13 %. Considering that this layer contributes only ~10 DU to the total depletion of ~270 DU, the 13 % difference in this slab corresponds to ~0.5 % of the total depletion.

The tests performed show that differences arising from different choice of isentropes were:

1. not greater than 4 % with the exception of the 600 K slab, where the absolute contribution to the depletion is small enough it can be neglected, and

2. in almost all of the cases they were masked by the uncertainties in depletion arising from the uncertainties in temperatures.
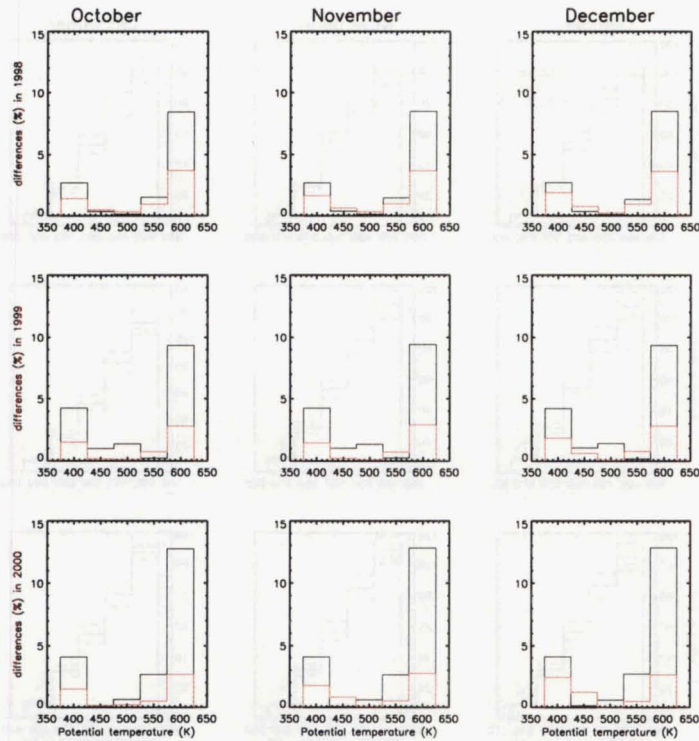
Figure 6.10: Relative differences for Case 1 (black line) and Case 2 (red line) compared to Case 3.

Hence, in this work, RDF calculations were performed for the potential temperature surfaces as defined in Case 1, with two additional isentropes, centred around 650 K and 700 K. These isentropes were included to complete the vertical region where ozone destruction occurs, although the contribution of these levels is not expected to be large (relatively small volume mixing ratios of depleted ozone, in the stratospheric region where density is also relatively small).

6.6   Summary of the Method

A method for calculating ozone reduction on a given day, over a geographical area, caused by the presence of Antarctic vortex parcels that underwent chemical ozone depletion inside the vortex has been presented in this chapter. In the first step, parcels arranged on a given grid above the geographical area, on the day of interest, are advected backwards in time, to a chosen initial day. On this day, the parcels' PV values are calculated through bilinear interpolation of the Met Office PV field. The PV values thus obtained are compared to the PV values marking the poleward and equatorward Antarctic vortex edge. If a parcel's PV value is less or equal than the PV value of the poleward vortex edge, the parcel is classed as vortex core parcel. On the other hand, if the parcel's PV value is greater than the PV value of the poleward vortex edge, and at the same time, less or equal than the PV

value of the equatorward vortex edge, the parcel is classed as vortex edge region parcel.

Parcels classed as vortex parcels are labelled with depleted ozone volume mixing ratio. In the case of core parcels, the depleted ozone volume mixing ratio is taken from the calculations of *Hoppel et al.* (2003), with slight modifications in the region between 600 K and 700 K. In the case of edge region parcels, the volume mixing ratio of depleted ozone is linearly interpolated for the parcels' PV value. The interpolation is done between the values of the volume mixing ratio of depleted ozone inside the vortex core and zero, which indicates that outside the vortex no ozone depletion processes occur.

Under the assumption that the volume mixing ratio of depleted ozone is constant along the trajectories of the advected parcels, it is brought forward unchanged, and depletion over a geographical region is calculated. RDF calculations are performed for parcels initialized on seven potential temperature surfaces, 400 K,..., 700 K, with $\Delta\theta$=50 K. Integration of ozone depletion is performed for seven layers of 50 K thickness (in potential temperature units) centred around the initial isentropes.

Chapter 7

Influence of the Antarctic Ozone Hole

In this chapter, the results for ozone reduction in southern midlatitudes caused by the presence of the Antarctic ozone hole parcels, for the years 1998, 1999, and 2000, are presented. The method for obtaining the results was described in detail in Chapter 6.

Diabatic RDF calculations are performed for southern midlatitudes, i.e. for parcels initialized on a $1°$ longitude by $1°$ latitude grid for the latitudes between $59.5°$S and $30.5°$S. The total range of latitudes analyzed is between $60°$S and $30°$S, with spatial boxes of $1°$ longitude and $1°$ latitude corresponding to each initialized parcel. The period examined in all of the years is 15 October through to 15 January of the following year. The initial day to which RDF calculations are run is 10 October. This day was chosen as the last day for the calculations of ozone depletion inside the vortex core (discussed in Section 4.3). Hence, by taking this day as the day to which trajectories are brought backward in time, the influence of ozone depletion within the vortex on midlatitude ozone levels during spring- and summertime, can be examined. Note that the first day of the period is chosen to be five days after the initial day, allowing for small-scale features to be captured.

In Section 7.1 the results for the year 1998 are presented. In Section 7.1.1, the problem of mass conservation is studied in detail for 1998. A method for scaling the ozone depletion results, the need for which arises from non-conservation of mass inherent in the calculations, is introduced. The scaling method is applied to all subsequent depletion calculations. In Section 7.2, ozone depletion in four regions in southern midlatitudes (spanning longitude regions of $90°$, starting from $0°$) in 1998, is analyzed.

The sensitivity of the results to the perturbations in the winds, and the initial conditions, for the year 1998, is examined in Section 7.3. The results of the sensitivity tests are combined with the depletion uncertainties arising from the uncertainties in temperatures (Section 6.5) to yield the absolute and relative uncertainties in the results for 1998.

In Section 7.4, the results for the years 1998, 1999 and 2000, both for midlatitudes and subregions, are presented. The similarities and differences between the years are addressed.

The ozone depletion results for 1998–2000 are discussed in the context of the total column ozone in Section 7.5. The calculated ozone depletion is first compared to the total

column ozone measured by TOMS, to quantify the relative influence of the dilution effect. Then, ozone depletion is compared to the change in the total column ozone since 1979, to infer how much of the observed change can be attributed to the dilution effect.

In Section 7.6, the errors associated with the method employed in this work are summarized. The limitations of the method, and their influence on the results, are also discussed in that section. Section 7.7 offers conclusions.

7.1 Depletion in Midlatitudes: Year 1998

The results depend directly on the Antarctic vortex "state" on the initial day. Therefore, the size and the position of the vortex on 10 October 1998 are discussed first.

Figure 7.1 shows the vertical profile of the Antarctic vortex on 10 October 1998. On all of the isentropes the vortex was well isolated (as far as can be concluded from the low-resolution PV field), but slightly elongated along the $0°$–$180°$ longitude line. As a consequence, parts of the vortex were situated equatorwards of $60°$ S.
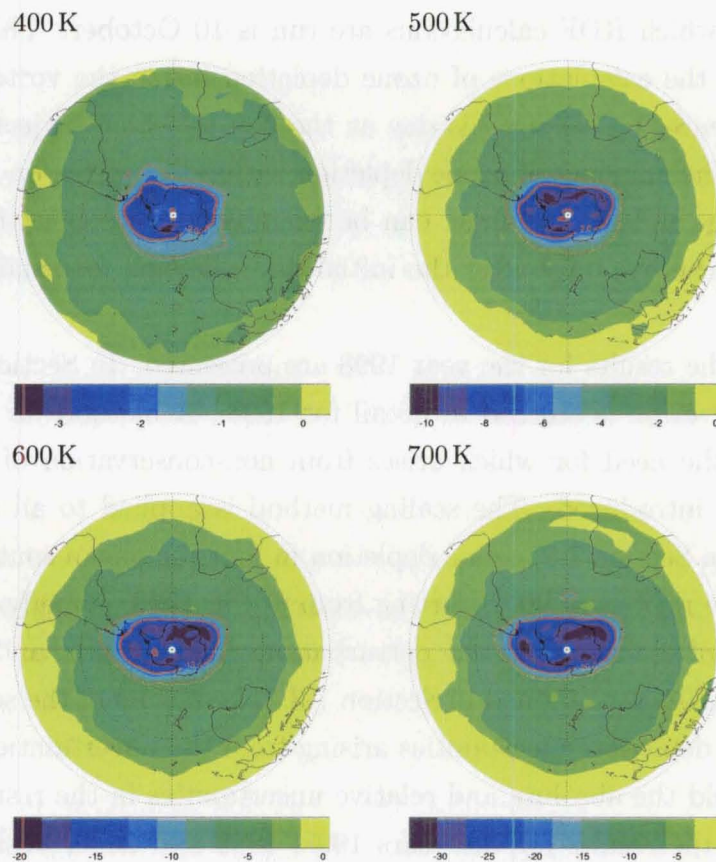
Figure 7.1: Polar-stereographic view ($0°$–$90°$ S) of low-resolution PV fields (in 10^{-5} K kg^{-1} m^2 s^{-1}) on the 400 K, 500 K, 600 K and 700 K isentropes, on 10 October 1998. The full (dotted) red line indicates the PV value of the poleward (equatorward) vortex edge.

The equivalent latitudes of the poleward and equatorward vortex edge on this day are given in Figure 7.2. Studies of *Chen* (1994) and *Haynes and Shuckburgh* (2000b) showed
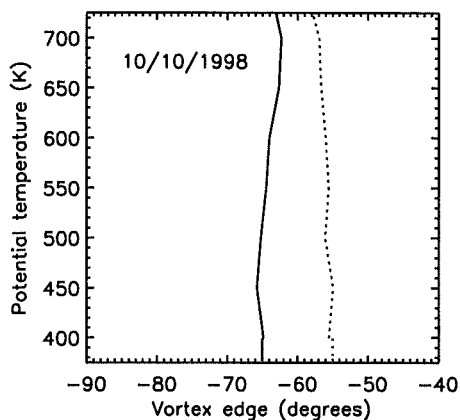
Figure 7.2: Equivalent latitude of the poleward (full black line) and equatorward (dotted black line) vortex edge on 10 October 1998. The full (dotted) red line indicates the values of the poleward (equatorward) vortex edge between 375 K and 400 K.

that below 400 K the vortex is not well isolated from the surrounding air. The isentrope at which the transition from complete isolation of vortex air to mixing of vortex air with midlatitude air occurs is around 375–380 K. As shown by *Chen* (1994), at 350 K, vortex air can be eroded to as far as 30 ° S, and midlatitude air can intrude into the polar region. For these reasons, an extra criterion for parcels originating in the vortex below 400 K was introduced.

Parcels originating from the 375–400 K layer need to satisfy the PV criterion (Section 6.1) as well as to have a latitude of origin of less than 65 ° S, or between 65 ° S and 55 ° S, to be recognized as core, or edge region vortex parcels, respectively (as indicated by the red lines in Figure 7.2). Thus, it was assumed that ozone depletion inside the vortex on those isentropes occurred in polar and near-polar regions. The latitude criterion was applied to all of the calculations performed.

As the first step in the analysis, the number of vortex parcels reaching midlatitudes between 15 October 1998 and 15 January 1999 was examined. The left panel in Figure 7.3 shows the number of vortex parcels as a percent of the total number of initialized parcels (on each isentrope), for seven examined isentropes.

At the very beginning of the period, there were both core and vortex edge parcels present in midlatitudes. The number of core parcels was relatively small, ~5 %, while number of the vortex edge parcels was approximately 10–20 %. This is a consequence of the fact that the vortex protruded into southern midlatitudes (discussed in more detail in Section 7.2). During the three months under examination, the total number of vortex parcels increased, with more parcels from the core and fewer parcels from the edge region

Year 1998/1999
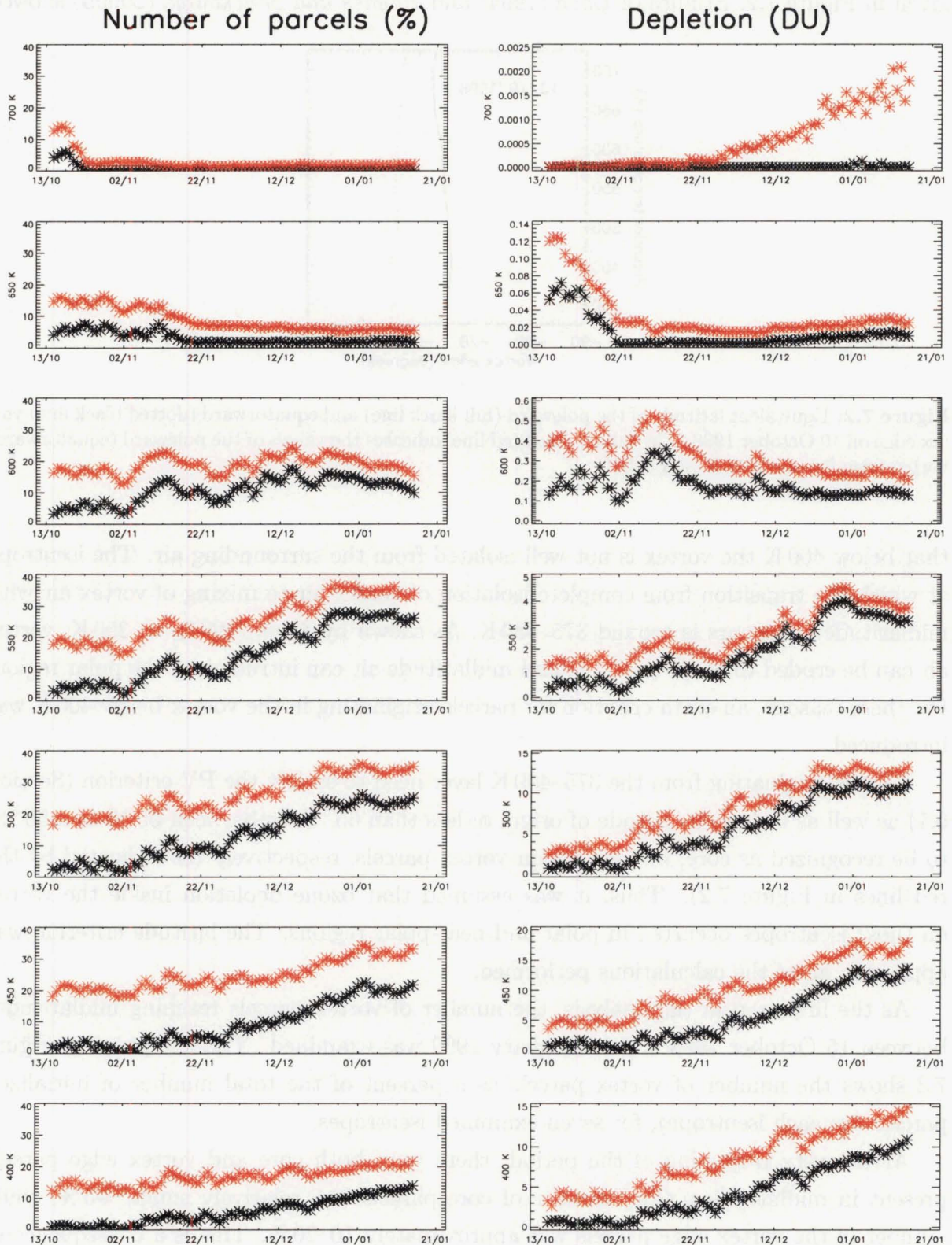
Figure 7.3: Left: The number of vortex parcels reaching southern midlatitudes between 15 October 1998 and 15 January 1999, as a percent of the total number of parcels initialized on seven isentropes. Right: Ozone depletion (in DU) caused by the presence of vortex parcels. The black asterisks show vortex core parcels (depletion caused by vortex core parcels), the red asterisks show the sum of core and vortex edge parcels (the sum of ozone depletion caused by core and vortex edge parcels).

reaching midlatitudes. The exceptions were the two topmost levels, where, due to descent, the number of parcels decreased.

The right panel in Figure 7.3 shows ozone depletion in midlatitudes caused by the presence of the vortex parcels. In the slabs centred around 600 K, 650 K and 700 K, depletion was less than 1 DU. In the lower layers, depletion was significant, reaching $\sim$20 DU in the 450 K slab.

The depletion differences seen in different layers cannot be explained solely by the number of vortex parcels. For example, the total number of vortex parcels on 600 K was similar to the total number of vortex parcels on 400 K, yet the maximum depletion in these two slabs differed by a factor of $\sim$30. The potential temperature surface on which vortex parcels originated determines the volume mixing ratio of depleted ozone assigned to the parcels. Therefore, the isentropes from which the vortex parcels originated need to be examined.

Figure 7.4 shows the height distribution of vortex parcels present in midlatitudes. On each potential temperature surface, the heights (in units of potential temperature) on which vortex parcels originated are examined. The heights of the point of origin were binned into layers of 50 K, centred around the seven isentropes. The numbers are given as a percent of the total number of vortex parcels present on each isentrope. The analyses were done separately for core and edge region parcels.

The vertical motion of vortex parcels was not one-directional. For example, parcels originating in the 450 K slab were present in both the 500 K and the 400 K layer. Furthermore, the vertical motion of core and edge region parcels was somewhat different. The subsidence of core parcels above 550 K was larger, with some of the parcels from the 700 K slab descending to the 550 K layer in January. On the other hand, the descent at and below 500 K was stronger for edge region parcels.

The results for depletion in midlatitudes can be explained having in mind the results of the tests performed in Section 6.5, the volume mixing ratio of depleted ozone in the vortex core presented in Figure 6.6, and the results presented in Figures 7.3–7.4. Generally speaking, in the higher levels of the domain, a box of unit volume contains fewer depleted ozone molecules than the same box at a lower level. Hence the total column of the depleted ozone molecules (in DU) is less than lower down.

The original isentrope of the parcels also influences the amount of depletion caused. For example, in the 600 K slab, depletion at the end of December was less than depletion in mid-October, even though the number of vortex core parcels increased. At the end of December, most of core parcels present in this slab originated in the 700 K layer, where the volume mixing ratio of depleted ozone was small. In mid-October, all of the parcels in the 600 K slab originated from that layer, with a volume mixing ratio of

Year 1998/1999
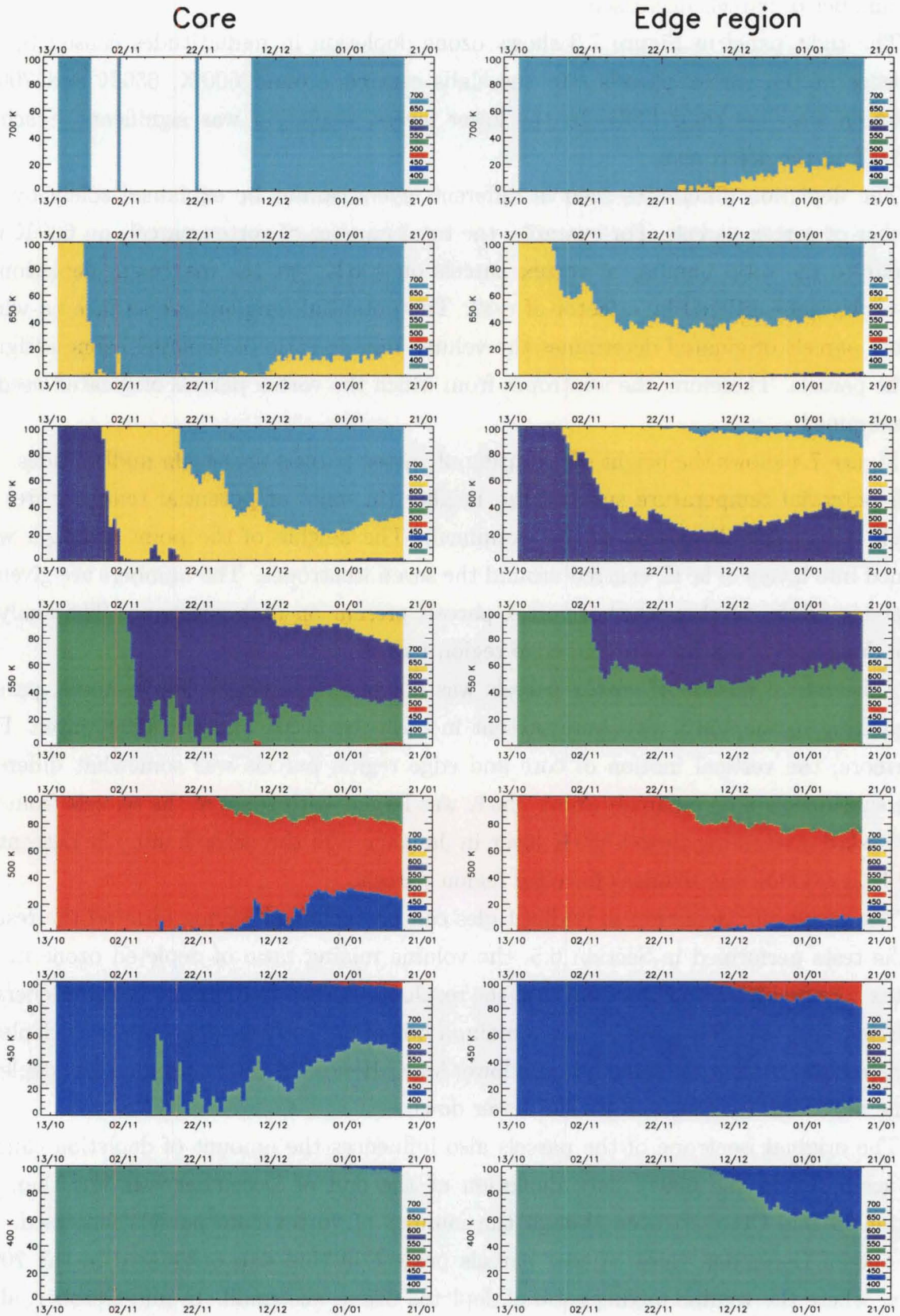
Core

Edge region

Figure 7.4: The height distribution of vortex core (left) and edge region parcels (right), as a percent of the total number of core (edge region) parcels present on seven isentropes in midlatitudes.

depleted ozone of ~1 ppmv. This same argument explains why depletion in the 550 K slab decreased from the end of December, while the number of vortex parcels was almost constant – the presence of parcels from the 650 K and 700 K layers decreased the depletion over this period.

Depletion maximized in the region below 550 K as a consequence of the combination of denser air, greater volume mixing ratio of depleted ozone that vortex parcels carried, and the vertical motion of vortex parcels.

The bottom panel in Figure 7.5 shows the total number of vortex parcels present in midlatitudes between the potential temperature surfaces of 375 K and 725 K. The numbers are given as a percent of the total number of parcels initialized on each examined day, on all of isentropes. The number of core parcels increased with time, unlike the number
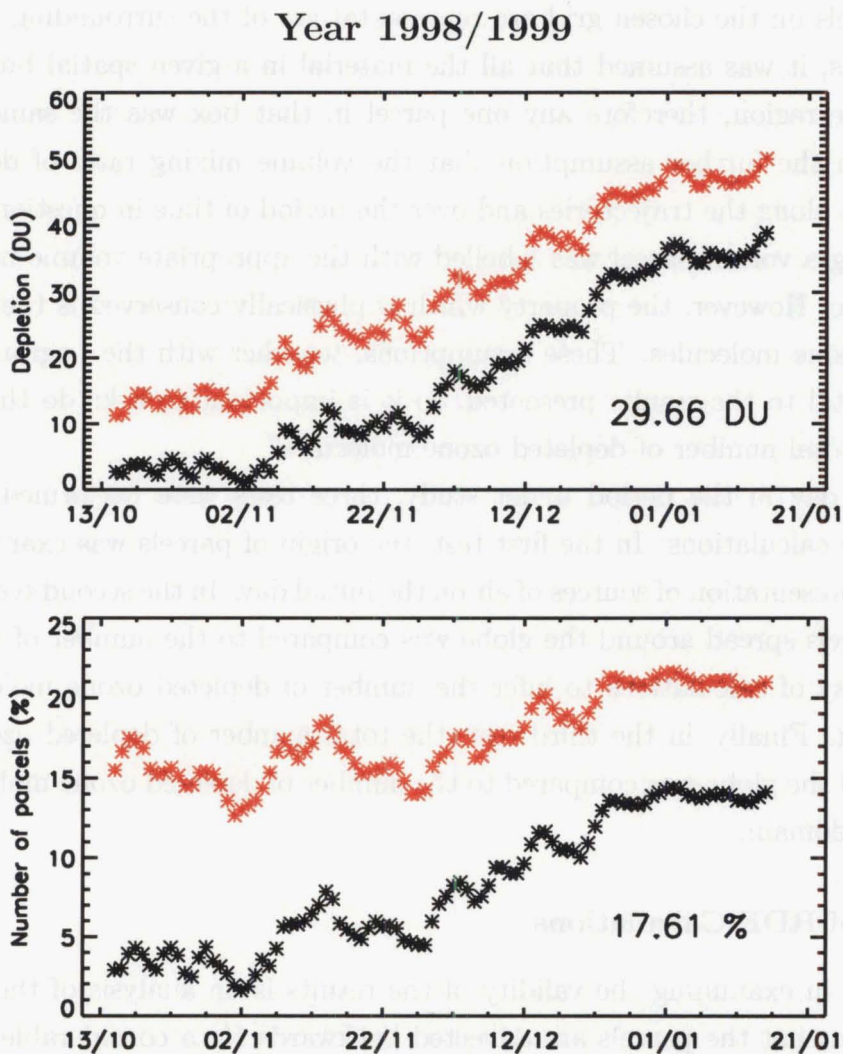
Figure 7.5: Total number of vortex parcels (bottom) and total depletion (top) in southern midlatitudes, in the 375–725 K layer, in 1998 (colour code as in Figure 7.3). The mean values (over the whole period) are indicated on the lower right.

of edge region parcels. As a result, the total number of vortex parcels ranged between

~12 % and ~22 %. From around the middle of December until the end of the period, the change in the number of parcels was relatively small. The mean number of parcels (from the core and the edge region) was 17.61 %, as indicated on the lower right of the plot.

The corresponding total depletion in midlatitudes, in the 375–725 K layer, is presented in the top panel of Figure 7.5. Over the whole period, the depletion increased, reaching ~50 DU on 15 January. The mean depletion over the examined period was 29.66 DU, as indicated on the lower right of the plot. The validity of this result is examined in the following section.

7.1.1   Validation of the Method

In the calculations of ozone depletion as presented in this work, the key assumption was that the parcels on the chosen grid are representatives of the surrounding spatial boxes. In other words, it was assumed that all the material in a given spatial box was coming from the same region, therefore any one parcel in that box was the same as all other parcels. With the further assumption that the volume mixing ratio of depleted ozone was conserved along the trajectories and over the period of time in question, each spatial box containing a vortex parcel was labelled with the appropriate volume mixing ratio of depleted ozone. However, the property which is physically conserved is the total number of depleted ozone molecules. These assumptions, together with the Lagrangian method, are fundamental to the results presented, so it is important to ask: do the calculations conserve the total number of depleted ozone molecules?

For every day in the period under study, three tests were performed to check the validity of the calculations. In the first test, the origin of parcels was examined to check the spatial representation of sources of air on the initial day. In the second test, the number of vortex parcels spread around the globe was compared to the number of vortex parcels on the first day of calculations to infer the number of depleted ozone molecules present in the domain. Finally, in the third test, the total number of depleted ozone molecules spread around the globe was compared to the number of depleted ozone molecules present in the model domain.

Validation of RDF Calculations

The first step in examining the validity of the results is an analysis of the origin of the parcels. Given that the parcels are advected backwards for a considerable time to their initial positions, the possibility exists that those initial positions could be an unreasonable spatial sample of the initial day. To assess this, RDF calculations were performed for parcels on a 1° longitude by 1° latitude grid, spread over the whole globe, on seven isentropes, 400–700 K. Parcels were advected backward in time to 10 October 1998. Figure

7.6 shows the number density of the initial positions as a function of potential temperature, longitude and latitude, for parcels in the Southern Hemisphere, for each day the calculations were performed.

Year 1998/1999
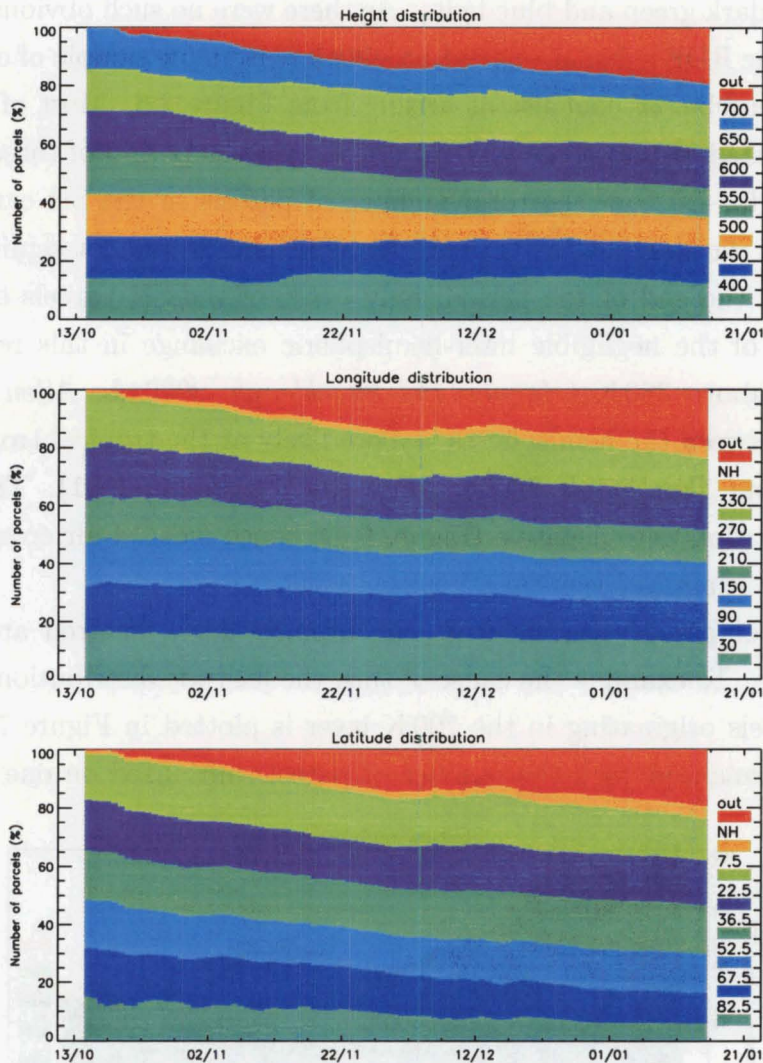
Figure 7.6: Height, longitude and latitude distribution of the Southern Hemisphere parcels initialized on seven isentropes, between 400 K and 700 K, for each day between 15 October 1998 – 15 January 1999.

The potential temperatures of origin were binned into slabs of 50 K, centred around 400–700 K. The parcels with potential temperature at origin below 375 K or above 725 K, were classed as "out". The longitudes of origin were binned into slabs of 60°, centred around 30°–330°, and the parcels with origin in the Northern Hemisphere were classed as "NH". Finally, the latitudes of origin were binned into belts of 15° centred around 82.5°–7.5°S. The numbers are given as a percent of all the initialized parcels.

The main purpose of this analysis is to determine whether there were any regions

which were unrealistic sources of parcels, or any regions which were not well sampled. If either of these were true, then Figure 7.6 would show "bulging" of some of the examined belts. For example, if on 1 January 1999, all the air in the SH came from a region of potential temperatures between 375 K and 475 K, with longitudes between 0° and 120° and latitudes between 90°S and 60°S, then on this day, the distributions would contain only the dark green and blue belts. As there were no such obvious cases, it can be concluded that the RDF calculations did provide a reasonable sample of origin air masses.

There are a number of conclusions arising from Figure 7.6. Most of SH air between 375–725 K originated in that same vertical region over the period of three months (at the end of the period, ~20 % of the total number of parcels in the SH came from outside this region). The exchange of air between the hemispheres was not significant over those three months (at the end of the period, only ~4 % of the SH parcels originated in the NH). The cause of the negligible inter-hemispheric exchange in this region is a strong tropical barrier above 380 K (*Haynes and Shuckburgh*, 2000a,b; *Allen and Nakamura*, 2001). Mixing between the hemispheres is more likely at the tropical tropopause, around 350 K (*Haynes and Shuckburgh*, 2000b; *Allen and Nakamura*, 2001). The mean heating rates at this isentrope were negative (Figure 6.4), hence most of air crossing into the SH did not reach the examined vertical domain.

The number of parcels coming from the topmost level, centred around 700 K, decreased with time. To examine the cause of this, the latitude distribution of the Southern Hemisphere parcels originating in the 700 K layer is plotted in Figure 7.7 (the numbers presented are normalized with the number of parcels initialized on one isentrope). The
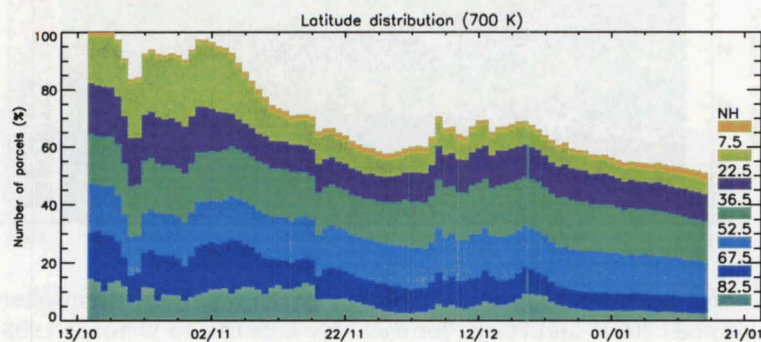
Figure 7.7: Latitude distribution of the Southern Hemisphere parcels originating in the 700 K layer, for each day between 15 October 1998 – 15 January 1999.

"shrinking" of the 700 K slab, seen in Figure 7.6, was caused by two effects – in this layer, fewer parcels originated in the tropics, between 0°S and 30°S, as well as in the polar region, between 60°S and 90°S. The former was due to the rising motion of air in the tropics (Figure 6.4), resulting in air crossing the top layer of the domain. In the tropics, the average heating rates on 700 K were ~1 K/day throughout the period, which

essentially means that parcels initialized on this isentrope crossed the 725 K surface after only ~25 days of backward advection.

A smaller number of air parcels originating in the polar region is also evident in Figure 7.6, where at the end of the three months, only ~17 % of the hemispheric parcels originated in the polar region, compared to ~31 % at the beginning of the period. To properly establish the problem of conservation of the number of depleted ozone molecules, it is essential to understand the causes of the decrease in the number of parcels originating in the polar region. Therefore, heating rates in the polar region are examined in more detail (than in Section 6.3).

Figure 6.4 shows that in the polar region on the 600 K and the 700 K isentropes the mean motion was downwards throughout the period. At the same time, the mean vertical motion on the isentropes of 400 K and 500 K, was upwards in October and November, but downwards later in the period. From these averaged heating rates the following picture of the vertical motion inside the polar region could be inferred. Parcels descending from the 700 K and 600 K, would start ascending once they reached the 500 K isentrope, and parcels rising from the 400 K and 500 K surfaces, would move back down once they reached the 600 K isentrope. Thus, in the polar region, parcels would actually oscillate around the isentrope of ~550 K during the months of October and November. Only in December, when heating rates in the lower region also became negative, would parcels leave the domain through the lower boundary. However, this averaged motion does not explain why the number of parcels with origin in the polar region decreased over the examined period.

A closer examination of heating rates inside the polar region, on the isentropes of 375 K, 400 K and 500 K, reveals relevant details of the vertical motion. Figure 7.8 shows the number of points (in the low-resolution heating rates field) in the polar region with negative heating rates. The daily mean values of those negative heating rates are also plotted.

During October and November, on all three isentropes there were regions in which air was descending. On 500 K, roughly 30% of the points had an average heating rate of less than -1 K/day. On 400 K and 375 K there were fewer air parcels which experienced cooling. Still, with the average cooling rate of about 1 K/day, some of the parcels on those isentropes must have descended and crossed the bottom boundary of the domain. This suggests that vortex air continuously left the set domain by crossing the lower boundary of 375 K.

The qualitative picture drawn from Figure 6.4 and Figure 7.8, showing that in the lower part of the vortex some regions experienced cooling, and some heating, agrees with the findings of Öllers et al. (2002).
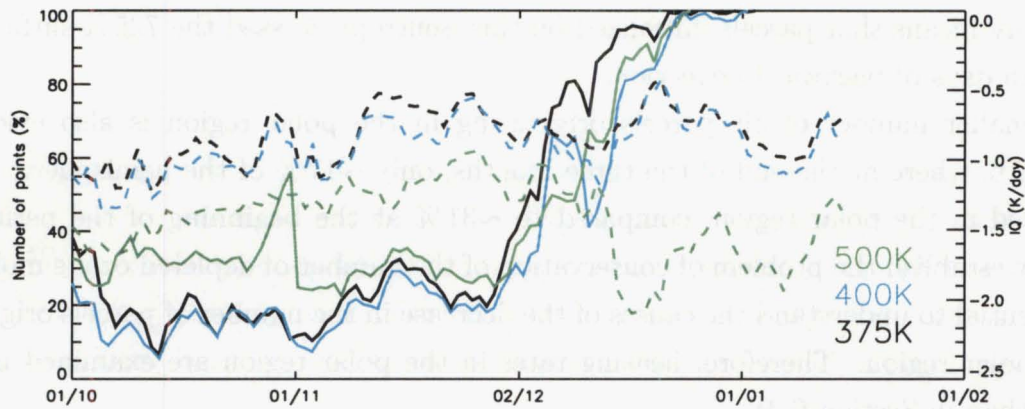
Figure 7.8: Number of points with negative heating rates (full lines) in the polar region (as a percent of the total number of points in the polar region, from the low-resolution heating rates field), on the 375 K (black), 400 K (blue), and 500 K (green), and the mean value of the heating rates on those points (dashed lines).

Mass Conservation - Refinement I

The above conclusion indicates that throughout the three examined months, vortex air was leaving the vertical domain of the model, causing the total number of depleted ozone molecules within the domain to decrease. On the other hand, as discussed in Sections 6.2–6.3, the motion of depleted ozone molecules within the domain, and the change in the volume and the density of the domain, present a source of a spurious variability in the total number of depleted ozone molecules. In this test, a method for inferring the number of depleted ozone molecules present in the domain is introduced. In the following test, the results of this method are used to constrain the unrealistic change in the total number of depleted ozone molecules.

The number of depleted ozone molecules in the model domain, on any given day, was calculated under the following three assumptions.

1. All of the vortex air between the isentropes of 375 K and 725 K, is present in the domain on the first day of calculations, i.e. 15 October 1998.

2. On any given day, the number of parcels originating in the vortex is directly proportional to the fraction of the vortex still in the domain on the given day. In other words, if on 15 October the number of parcels originating in the vortex is n_0, and n_n on some other day, then the fraction of the initial vortex still in the domain is n_n/n_0.

3. Assuming that the depleted ozone molecules are uniformly spread throughout the vortex, leads to n_n/n_0 being directly proportional to the number of depleted ozone molecules inside the domain. In other words, if N_0 is the total number of depleted

ozone molecules inside the vortex on 10 October 1998, then on the n-th day, the number of depleted ozone molecules in the domain, N_n, is $N_n = N_0 \cdot n_n/n_0$.

The results for n_n/n_0 are given in Figure 7.9. The parcels examined were the same as in the preceding test, i.e. globally distributed on a $1°$ longitude by $1°$ latitude grid. The calculations for core and edge region parcels were performed separately.

Year 1998/1999
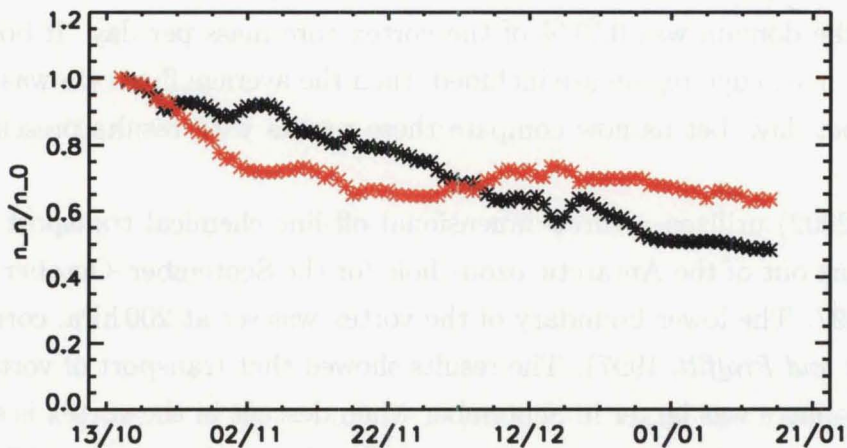
Figure 7.9: Total number of vortex parcels on the whole globe compared to the total number of vortex parcels on 15 October 1998 (black – core; red – edge region).

As expected, the results show that the number of vortex parcels inside the domain decreased with time. At the end of the period only $\sim 50\%$ and $\sim 65\%$ of core parcels and edge region parcels, respectively, were still present in the domain. The rate at which core and edge region parcels left the domain was different, indicating different regimes of vertical motion.

Under the third assumption, the ratios n_n/n_0 also represent the fraction of the initial number of depleted ozone molecules still inside the examined domain. However, this assumption is only a very coarse estimate. The number concentration of depleted ozone in the vortex varies with height, and the number of depleted ozone molecules that leave the vertical domain of the model depends on the original height of the parcels. Backward RDF calculations performed here only contain information about vortex parcels present in the domain, and, consequently, about the number of depleted ozone molecules associated with those parcels. The exact information about vortex parcels that leave the domain, and the associated depleted ozone molecules, could be obtained by initializing air parcels inside the vortex, and advecting them forward in time. To test the validity of the third assumption without performing forward RDF calculations, the n_n/n_0 ratios in a somewhat different interpretation were compared with some of the results presented in recent publications.

In the third assumption, the n_n/n_0 ratios represent the fraction of the number of depleted ozone molecules inside the domain. In a slightly more realistic interpretation, those ratios represent mass ratios, i.e. a fraction of the initial vortex mass inside the domain. The advantage of this interpretation is that it does not include the assumption of uniform distribution of depleted ozone molecules. However, mass non-uniformity in the vortex is still neglected. In this interpretation, the complement ratios, $(1 - n_n/n_0)$, represent "vortex mass leakage" from the domain. The results in Figure 7.9 then show that between 15 October and 31 October, the average rate at which the vortex core material left the domain was 0.71 % of the vortex core mass per day. If both the vortex core and the vortex edge region are included, then the average flow rate was 0.91 % of the vortex mass per day. Let us now compare these results with results presented in recent publications.

Li et al. (2002) utilized a three-dimensional off-line chemical transport model to examine transport out of the Antarctic ozone hole for the September–October period of the years 1993–1997. The lower boundary of the vortex was set at 200 hPa, corresponding to $\sim$305 K (*Tuck and Proffitt*, 1997). The results showed that transport of vortex air parcels into the troposphere was larger in September when descent in the vortex is stronger. The flow rate of vortex air into the troposphere, averaged over the months of September and October, for the years 1993–1997, was 0.98% of the vortex mass per day. Assuming that the Antarctic vortex defined in *Li et al.* (2002) and in our work (including the core and the edge region) encompass the same region, then our result for the mass flow rate of 0.91 %/day is slightly less than the result of *Li et al.* (2002).

Öllers et al. (2002) used three-dimensional forward trajectories to quantify transport of Antarctic vortex air, initialized on the 350 K, 450 K and 550 K isentropes, below the 340 K boundary. The "horizontal" region analyzed in that study can roughly be compared to our vortex core region. The results for the month of October 1998, showing mass exchange rate of 0.59 % per day, are less than in our analysis.

There are a number of differences between the studies that can explain the disagreement. Obviously, *Li et al.* (2002) analyzed different years (and noted an interannual variability in the transport). Next, the results of *Li et al.* (2002) present averaged results for the September–October period, and are higher than the results for the month of October. Finally, the vertical boundaries of the domains do not match and the meteorological data used in the studies are not identical. Nevertheless, the agreement of our result with those two different studies is encouraging, and gives confidence to the conclusions that are drawn from inference of the vortex leakage through the lower boundary of the domain.

Mass Conservation - Refinement II

Based on the results of the previous test, the mass conservation problem can be formulated as follows: The number of depleted ozone molecules (originating in the vortex) globally distributed between the isentropes of 375 K and 725 K must be equal to the total number of depleted ozone molecules contained in the fraction of the vortex present in the model domain. This restriction effectively removes the unrealistic change in the number of depleted ozone molecules that is otherwise present in the calculations (Sections 6.2–6.3).

The restriction was incorporated into the analysis through the following steps. First, the total number of depleted ozone molecules in the vortex, between the isentropes of 375 K and 725 K, on 10 October 1998, was calculated. The integration was done for the 5° longitude by 5° latitude spatial boxes, which satisfied the PV and latitude criteria. This number was then scaled with the results presented in Figure 7.9 to yield a number of depleted ozone molecules in the model domain on each examined day, N_n. Next, the total number of depleted ozone molecules, with origin in the vortex, spread all over the globe in the 375–725 K layer, N_{calc}, was calculated using equations from Section 6.2. The calculations for the vortex core and the vortex edge region were done separately. Finally, the ratios N_{calc}/N_n were used to apply mass-flux constraints to the analysis.

Figure 7.10 shows the ratios N_{calc}/N_n. On the first day of the period, 15 October, the

Year 1998/1999
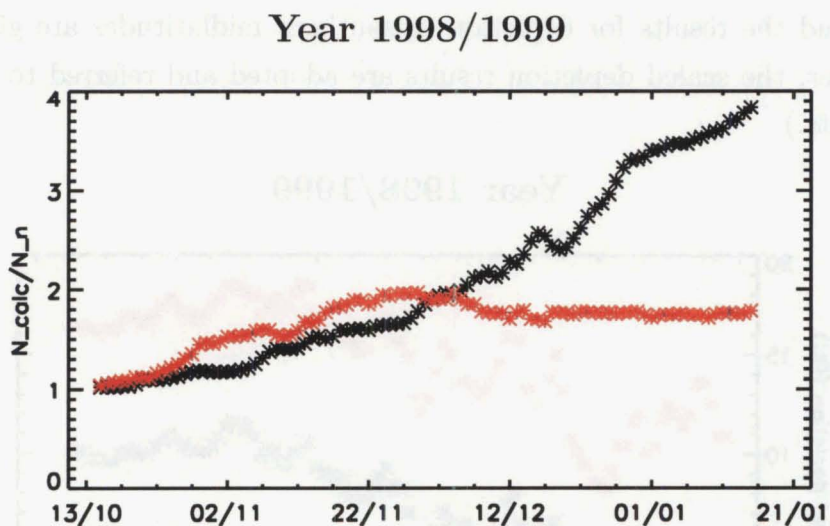
Figure 7.10: Total number of depleted ozone molecules on the whole globe compared to the number of depleted ozone molecules contained in the fraction of the vortex present in the model domain (black – core; red – edge region).

calculated mass ratios for the core and the edge, are 1.02 and 1.04, respectively, which essentially means that the total number of depleted ozone molecules on 10 October and 15 October was almost identical. In turn, this means that on 15 October all of the vortex between 375 K and 725 K was still in the domain, validating the first assumption made in

the previous test.

The calculated ratios for the core increased with time, implying that the calculations produced more and more depleted ozone molecules. This increase in the number of depleted ozone molecules was caused by the increase in the domain volume and density (Section 6.3), as well as by the northwards and downwards motion of advected vortex air parcels (Section 6.2).

The fact that the calculated ratios for the core increased rapidly throughout the period, indicates that the mean latitude of the core parcels' positions moved northwards, and that core parcels descended. On the other hand, the calculated ratios for the vortex edge remained almost constant from the end of November, suggesting that there was no significant change in the mean height and mean latitude of those parcels.

The inability to associate mass with advected parcels is a disadvantage of Lagrangian models. Parcels are no more than points in space, with dimensions equal to zero. Information about any arbitrary volume, no matter how small, initially associated with a parcel advected by Lagrangian models cannot be retrieved. It would be possible to initialize a much greater ensemble of parcels with many representative of each box, but this would lead to prohibitive computing expense, and might not actually improve matters significantly. Alternatively, the ratios in Figure 7.10 can be used to apply mass-flux constraints to the calculations. The results presented in Figure 7.5 were scaled with the ratios in Figure 7.10, and the results for depletion in southern midlatitudes are given in Figure 7.11. (Hereafter, the scaled depletion results are adopted and referred to simply as the depletion results.)
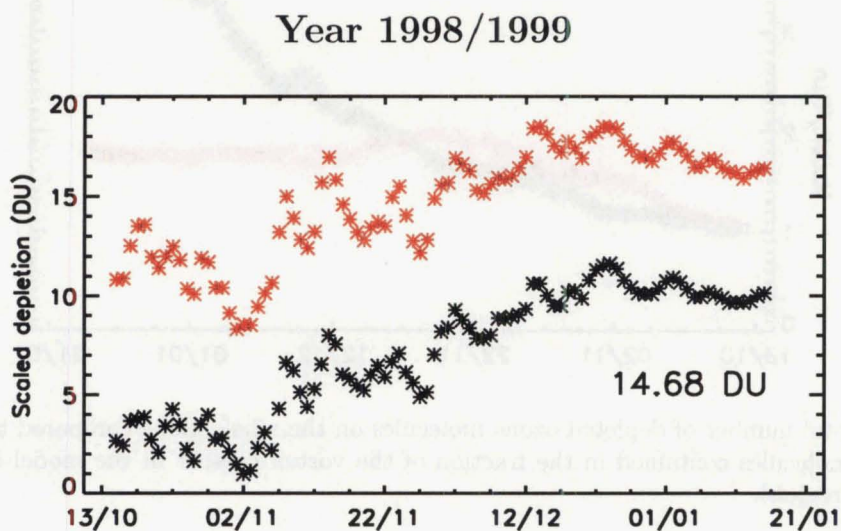
Figure 7.11: Scaled depletion in 375–725 K, 1998 (colour code as in Figure 7.3). The mean value over the examined period is indicated on the lower right.

Ozone depletion in southern midlatitudes caused by the presence of vortex core parcels, ranged between ∼1 DU (on 2 November 1998) and ∼12 DU (on 24 December 1998). On

average, depletion increased with time until 24 December 1998, after which date it slowly decreased. On the other hand, depletion caused by the presence of vortex edge parcels reached a maximum of ~10 DU on 18 October 1998, and a minimum of ~6 DU on 12 January 1999. The total depletion reached a maximum of ~18.5 DU on 23 December 1998. The mean depletion over the 15 October – 15 January period was 14.68 DU, as indicated in Figure 7.11. The uncertainties associated with this result are examined in Section 7.3, where sensitivity tests are presented.

7.2   Depletion in Different Regions: Year 1998

To examine the influence of the Antarctic ozone hole on different regions, southern mid-latitudes (30°–60°S) were divided into four regions: "Africa" with longitudes 0°–90°E, "Australia and New Zealand" with longitudes 90°–180°E, "Pacific" with longitudes 180°–270°E, and "South America" with longitudes 270°–360°E. The total number of vortex parcels (as a percent of the total number of initialized parcels in each region) and the corresponding depletion in those regions are given in Figure 7.12.

Year 1998/1999
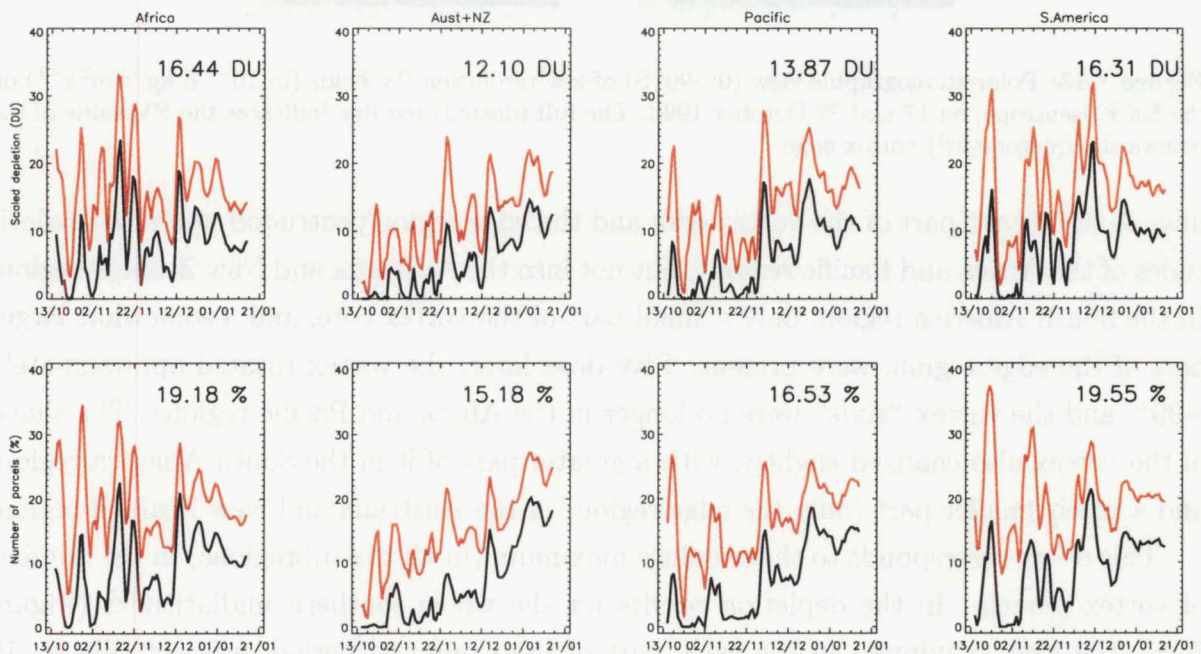
Figure 7.12: The total number of vortex parcels (bottom) and the corresponding ozone depletion (top), in the 375–725 K layer, in four regions in southern midlatitudes (colour code as in Figure 7.3). The mean values over the whole period are indicated on the upper right.

The details in Figure 7.12 can be understood by carefully examining the size, shape and positioning of the vortex, vortex filaments and vortex remnants (after the breakdown

of the vortex). In this analysis, emphasis is given to the overall results, and only two prominent events are discussed.

On 17 October, the number of vortex parcels in the Africa and Pacific regions was ~30 %, while in the South America region on that day, the number of vortex parcels had a local minimum. Five days later, on 22 October, the situation was reversed. In the Africa and Pacific regions the number of parcels reached a local minimum, while in the South America region, the number of parcels was extremely high (~37 %).

Figure 7.13 shows low-resolution PV fields on the 500 K isentrope on those two days. On 17 October, the vortex was asymmetrical and elongated along the 45°–225° longitude
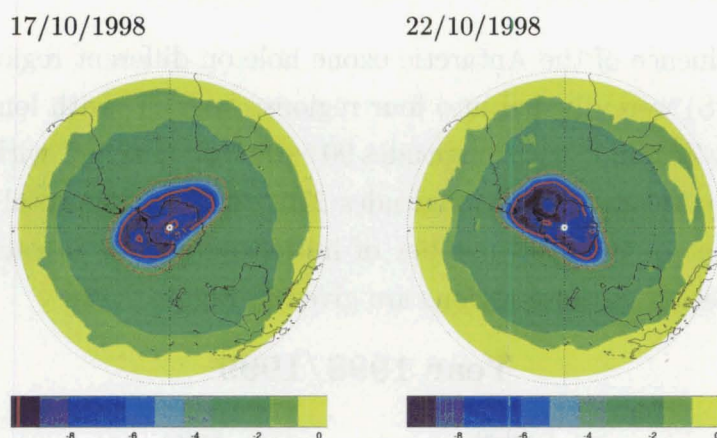
Figure 7.13: Polar-stereographic view (0°–90° S) of low-resolution PV fields (in $10^{-5}\,\mathrm{K\,kg^{-1}\,m^2\,s^{-1}}$) on the 500 K isentrope, on 17 and 22 October 1998. The full (dotted) red line indicates the PV value of the poleward (equatorward) vortex edge.

line. A significant part of the vortex core and the edge region protruded well into midlatitudes of the Africa and Pacific regions, but not into the Australia and New Zealand region. In the South America region, only a small part of the vortex core, and a somewhat larger part of the edge region, were present. Five days later, the vortex rotated approximately −90°, and the vortex "ends" were no longer in the Africa and Pacific regions. The shape of the vortex also changed slightly, with a greater part of it in the South America region, and a much smaller part (only the edge region) in the Australia and New Zealand region.

This event corresponds to the absolute maximum (in all the subregions) in the number of vortex parcels. In the depletion results for the whole southern midlatitudes (Figure 7.11), the local maximum in the early part of the examined period, was actually on 19 October.

As a contrast to the above event, on 2 November 1998, the vortex was more circular in shape, and the bulk of it was in the polar region (Figure 7.14). Only in the Australia and New Zealand region did a significant part of the vortex core reach midlatitudes (Figure 7.12). This event corresponds to the local minimum in ozone depletion in the early part of the period (Figure 7.11).

02/11/1998
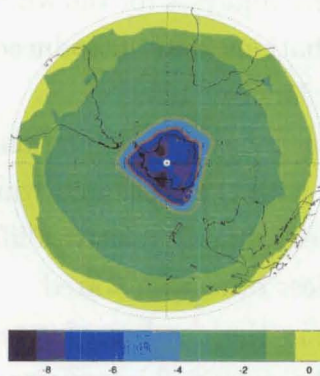
Figure 7.14: Polar-stereographic view (0°–90° S) of low-resolution PV fields (in $10^{-5}\,\mathrm{K\,kg^{-1}\,m^2\,s^{-1}}$) on the 500 K isentrope, on 2 November 1998. The full (dotted) red line indicates the PV value of the poleward (equatorward) vortex edge.

The analysis of these two prominent examples stresses the differences arising from the choice of examined regions. Many of the details in four subregions cannot be seen in the analysis for southern midlatitudes. Likewise, the importance of the prominent case for New Zealand, on 24–26 December 1998, studied in Chapter 5, is not reflected in the analysis for the Australia and New Zealand region. On the other hand, applying the results obtained for midlatitudes to subregions can lead to erroneous conclusions.

The mean values of the number of vortex parcels and ozone depletion in the four regions, shown in Figure 7.12, indicate that the influence of the Antarctic ozone hole was strongest in the Africa and South America regions, and weakest in the Australia and New Zealand region. However, starting in December, depletion was decreasing in both the Africa and South America regions, reaching values less than in the Australia and New Zealand region by the end of the period. This later period (close to solstice) is characterized by low noontime solar zenith angles, when ultra-violet radiation reaching the Earth's surface is largest, and ozone depletion has its greatest effect on UV.

7.3 Sensitivity of the Results: Year 1998

In this section, the sensitivity of the results to the perturbations in the winds, and to the choice of the initial day is examined. The results of these tests are used to infer the uncertainties in the overall results presented in Sections 7.1–7.2.

7.3.1 Perturbations in the Winds

An additional set of RDF calculations was obtained using zonal and meridional wind fields perturbed with normally distributed random numbers, with mean of 0 m/s and standard

deviation of 6 m/s. The value of standard deviation was chosen because the estimated standard deviation in the Met Office analyses for the wind components in the stratosphere is 6 m/s (Table 3.1). The perturbations were introduced over the examined period, i.e. between 10 October 1998 and 15 January 1999.

The differences between the "perturbed" (calculation runs with the perturbed winds) and "standard" (calculation runs with the measured winds) cases presented here are the mean (averaged over the examined period) relative differences, with the standard case results taken as the base line, unless otherwise stated.

Figure 7.15 shows differences in the number of core and vortex edge region parcels reaching midlatitudes on each of the examined isentropes, as well as in the 375–725 K layer. Between the isentropes of 400 K and 600 K, with the exception of the 450 K isentrope, the
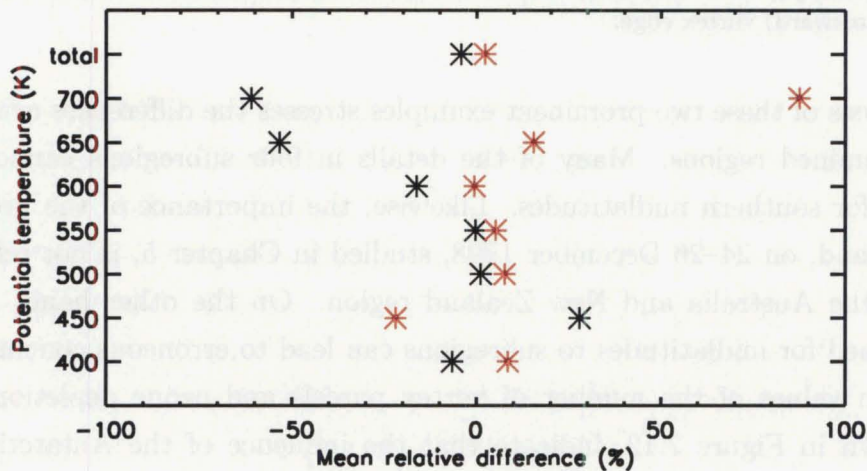
Figure 7.15: Mean relative differences in number of vortex parcels reaching midlatitudes, on seven examined isentropes, and in the 375–725 K layer (denominated as "total" on the y-axis). The differences for the core (edge region) parcels are given in black (red).

differences, both for core and edge region parcels, are between −20% and 20%. However, on the 450 K isentrope, where the number of vortex parcels, as well as depletion, peaks (Figure 7.3), the number of core parcels in the perturbed case is ∼30 % larger. The differences reach a maximum on the 650 K and 700 K potential temperature surfaces, where the absolute number of vortex parcels is relatively small, and depletion is negligible (Figure 7.3).

In the whole domain (375–725 K), in the perturbed case there were ∼4 % fewer parcels from the core and ∼2 % more parcels from the vortex edge region (Figure 7.15). This result indicates that the total number of vortex parcels reaching midlatitudes did not differ much between those two cases, as confirmed in Figure 7.16, discussed next.

The features of the temporal evolution in the standard and perturbed case match well (Figure 7.16). The mean number of parcels in the perturbed case is somewhat less than
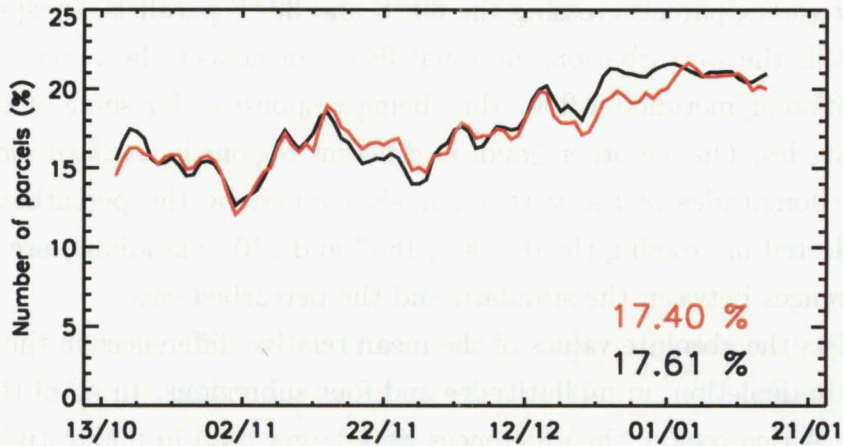
Figure 7.16: Total number of vortex parcels (in the 375–725 K layer) reaching midlatitudes, in the standard (black) and the perturbed (red) case. The averaged values over the examined period are given on the lower right.

in the standard case. The mean relative difference in the total number of parcels is only −0.9%.

The total depletion in midlatitudes, in the standard and perturbed cases, is given in Figure 7.17. The mean depletion in the perturbed case is somewhat larger than in the standard case, with a mean relative difference of 4.9% (corresponding to less than 1 DU in absolute difference). The maximum absolute difference between the cases is ∼3.3 DU.
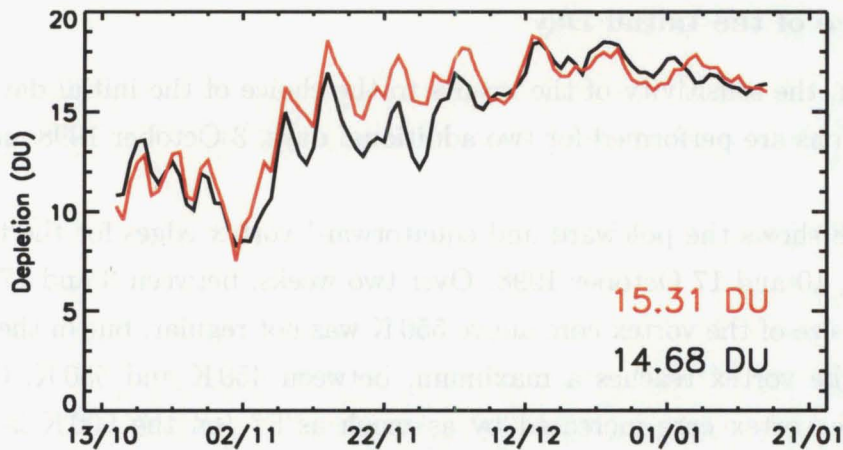
Figure 7.17: Total depletion (in the 375–725 K layer) in midlatitudes, in the standard (black) and the perturbed (red) case. The averaged values over the examined period are given on the lower right.

The differences between the standard and the perturbed cases in four subregions (Section 7.2) are expected to be somewhat higher than in midlatitudes as a whole. If the changes in vertical motion, caused by different advection using the perturbed zonal and meridional winds, are neglected, then the perturbations in meridional winds are mainly responsible for the differences seen in midlatitudes. The differences in midlatitudes are a

consequence of vortex parcels crossing the 60° S and 30° S parallels, irrespective of their longitudes. Still, the perturbations in zonal flow can advect the parcels to regions of significantly different meridional flow, thus being responsible for some of the differences seen in midlatitudes. On the other hand, in different regions in midlatitudes, day-to-day changes of the longitudes of the vortex parcels (caused by the perturbations in zonal winds, and reflected in crossing the 0°, 90°, 180° and 270° meridians) are an additional source of differences between the standard and the perturbed case.

Table 7.1 lists the absolute values of the mean relative differences in the total number of parcels and in depletion, in midlatitudes and four subregions. In all of the subregions, apart from the Africa region, the differences were larger than in midlatitudes.

	Relative difference (%)	
Region	**Number of parcels**	**Depletion**
SH midlatitudes	0.9	4.9
Africa	0.3	3.5
Aust+NZ	4.3	13.6
Pacific	4.6	11.7
S.America	2.7	6.0

Table 7.1: Absolute values of the mean relative differences (%) in the number of vortex parcels and depletion in different regions, between the standard and perturbed cases.

7.3.2   Choice of the Initial Day

In this section, the sensitivity of the results to the choice of the initial day is examined. RDF calculations are performed for two additional days, 3 October 1998 and 17 October 1998.

Figure 7.18 shows the poleward and equatorward vortex edges for the three different initial days, 3, 10 and 17 October 1998. Over two weeks, between 3 and 17 October, the change in the size of the vortex core above 550 K was not regular, but in the region where depletion in the vortex reaches a maximum, between 450 K and 550 K, the equivalent latitude of the vortex core increased by as much as 5° (on the 500 K isentrope). On the other hand, the equatorward edge of the vortex did not change significantly. As a consequence, the size of the vortex edge region below 550 K decreased between 3 and 17 October 1998.

A comparison of the results obtained with the initial day 3 and 10 October was done for the whole period 15 October – 15 January. The first examined day in the analysis with the initial day 17 October, was 22 October.

As an example, the number of vortex parcels in midlatitudes on the 550 K isentrope, obtained by running RDF calculations back to 3, 10 and 17 October is shown in Figure
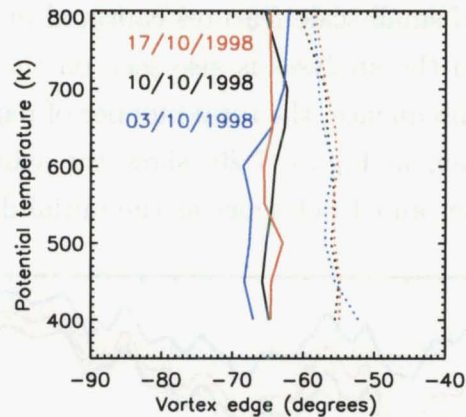
Figure 7.18: Equivalent latitude of the poleward (full line) and equatorward (dotted line) vortex edge on 3 (blue), 10 (black) and 17 (red) October 1998.

7.19. The agreement between the analyses is good. Although there are differences in the actual values (more pronounced in the number of edge region parcels), the features in the temporal evolution are very similar. The differences can be attributed to two factors. First, the different size of the core and of the edge region (Figure 7.18) is reflected in
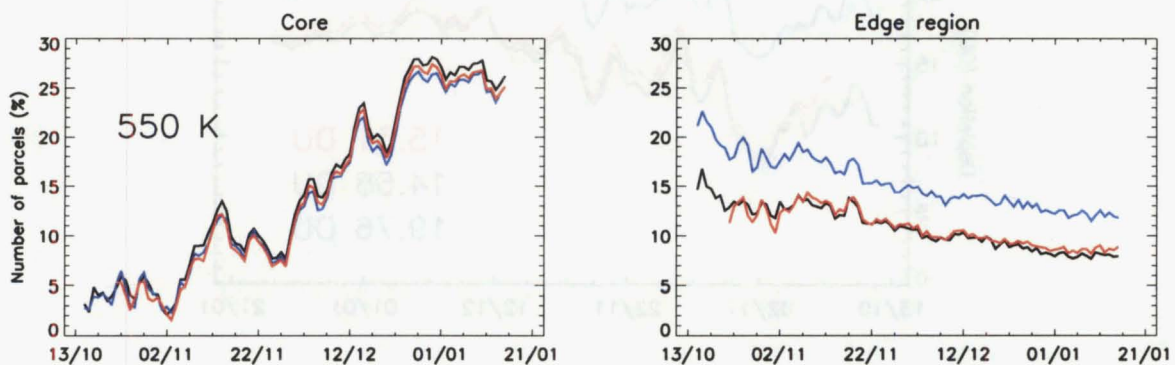
Figure 7.19: The number of the vortex core (left) and edge region (right) parcels reaching southern midlatitudes on the 550 K isentrope. The colour code is the same as in Figure 7.18.

the number of parcels with origin in those two regions. Second, between different initial days, small-scale filaments might develop. These features would not be included in the calculations, as the PV criterion for selecting vortex parcels relies on the low-resolution PV field on the initial day. Mass exchange rates between the Antarctic polar vortex and southern midlatitudes, calculated by *Öllers et al.* (2002) using three-dimensional forward trajectories, showed that on 550 K most of the exchange during October 1998 was due to filaments peeling off from the vortex edge. Indeed, Figure 6 in *Öllers et al.* (2002) shows a filament on the 550 K isentrope on 10 October 1998. Since the exchange rate of *Öllers et al.* (2002) represents a mass rate, it is somewhat difficult to use it to quantify the difference seen in the number of edge region parcels in our analyses performed for different initial days. Nevertheless, it is important to stress that the choice of the initial

day influences the number of small-scale features captured in the calculations.

Good agreement between the analyses is also seen on the rest of the examined isentropes (not shown). As a consequence, the total number of parcels in the 375–725 K layer and the total depletion, given in Figure 7.20, show the same properties. Overall, the differences between 3 October and 10 October as the initial day are largest.
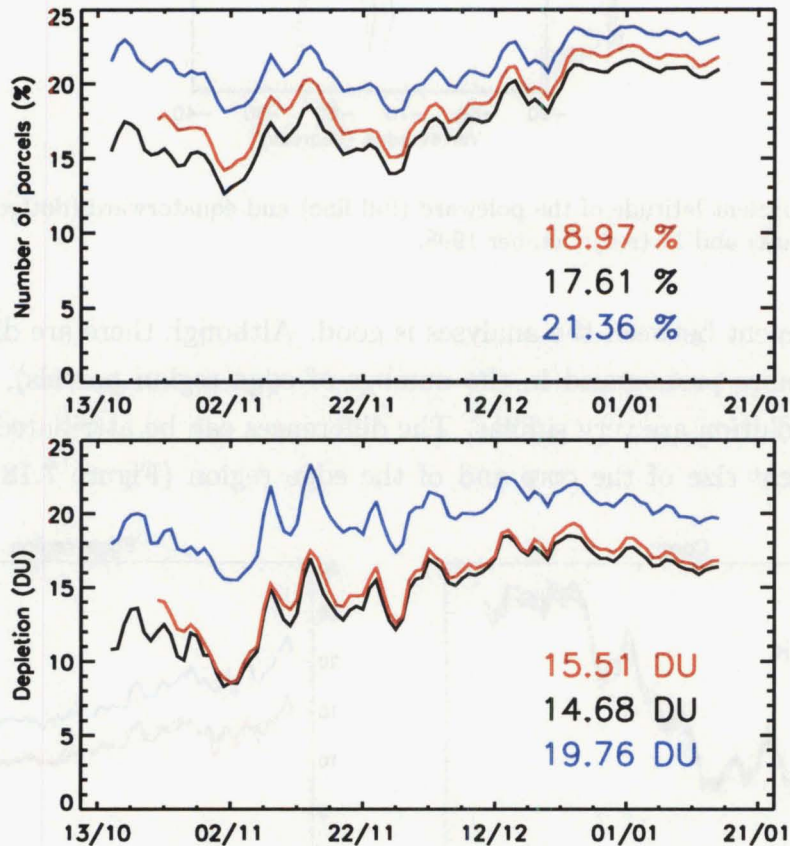
Figure 7.20: The total number of vortex parcels (top) and the total depletion (bottom), in southern midlatitudes, calculated with 3, 10 and 17 October 1998 as the initial day. The mean values over the examined period are indicated on the lower right. The colour code is the same as in Figure 7.18.

The same analysis performed for four subregions in southern midlatitudes (Section 7.2) shows essentially the same results. Table 7.2 lists the absolute values of the mean (averaged over the examined period) relative differences in the number of vortex parcels and depletion, in midlatitudes and four subregions. The differences listed are for the analyses with 3 and 10 October as the initial day (with the 10 October results taken as the base line).

7.3.3 Summary

Two tests were performed to analyze the sensitivity of the results presented in Section 7.1. In the first test, the zonal and meridional wind components were perturbed with

	Relative difference (%)	
Region	**Number of parcels**	**Depletion**
SH midlatitudes	22.6	37.9
Africa	22.9	36.6
Aust+NZ	39.5	65.2
Pacific	30.1	50.8
S.America	22.1	43.8

Table 7.2: Absolute values of the mean relative differences (%) in number of vortex parcels and depletion, in different regions, with 3 and 10 October 1998 as the initial day.

normally distributed random numbers with mean of $0\,m/s$ and standard deviation of $6\,m/s$. In the second test, two additional initial days were chosen. The results of the tests for midlatitudes and four subregions are given in Table 7.1 and Table 7.2.

In the first sensitivity test, the mean relative differences for the number of vortex parcels and depletion in midlatitudes, were $0.9\,\%$, and $4.9\,\%$, respectively. The relative difference for depletion corresponds to less than $1\,DU$ in absolute difference. In subregions, the differences were mostly larger, but still less than $5\,\%$ and $14\,\%$ for the number of parcels and depletion, respectively.

The second test showed that there is a strong dependance of the results on the choice of initial day, arising from the size of the vortex on the initial day, and from the amount of the vortex filamentation that occurs prior to the initial day. The mean relative differences for the number of vortex parcels and depletion in midlatitudes, were $22.6\,\%$, and $37.9\,\%$, respectively. In subregions, the differences peaked at $\sim40\,\%$ and $\sim65\,\%$ for the number of parcels and depletion, respectively.

The relative uncertainties in the number of parcels and depletion, estimated in those two tests, and the uncertainties in depletion arising from the uncertainties in temperatures (Section 6.5) are given in Table 7.3. The combined uncertainty, which presents the total uncertainty of the results, is also given.

The results for the mean number of parcels and depletion, over the 15 October 1998 – 15 January 1999 period, and the corresponding absolute uncertainties are given in Table 7.4.

7.4   Depletion in 1999 and 2000 compared to 1998

In this section, the results for the years 1999 and 2000 are presented and compared to the year 1998. The results are obtained using the same method described in detail in Sections 7.1–7.2.

The poleward and equatorward vortex edges on 10 October 1998, 1999 and 2000, are given in Figure 7.21. Below $550\,K$, the vortex core for all three years was almost the same,

Region	Wind perturbations	Initial day	Temperature	Combined
Relative uncertainties in the number of parcels(%)				
SH midlatitudes	0.9	22.6	N/A	23
Africa	0.3	22.9	N/A	23
Aust+NZ	4.3	39.5	N/A	40
Pacific	4.6	30.1	N/A	31
S.America	2.7	22.1	N/A	23
Relative uncertainties in depletion(%)				
SH midlatitudes	4.9	37.9	4.9	39
Africa	3.5	36.6	4.9	38
Aust+NZ	13.6	65.2	4.9	67
Pacific	11.7	50.8	4.9	53
S.America	6.0	43.8	4.9	45

Table 7.3: Relative uncertainties (%) in the number of parcels (top) and depletion (bottom) arising from the wind perturbations, the choice of the initial day, the uncertainties in temperatures (not applicable for the number of parcels), and the combined uncertainty.

Region	Number of parcels (%)	Depletion (DU)
SH midlatitudes	18±5	15±6
Africa	19±5	16±6
Aust+NZ	15±6	12±8
Pacific	17±6	14±8
S.America	20±5	16±8

Table 7.4: Mean number of parcels (%) and mean depletion (DU) with corresponding uncertainties, in midlatitudes and subregions, over the 15 October 1998 – 15 January 1999 period.

apart from the year 2000, when at 400 K, the equivalent latitude of the vortex core was larger by $\sim4°$. At the same time, the equatorward edge of the vortex was almost the same. In the region above 550 K, the vortex core in 2000 was significantly smaller than in 1998 and 1999.

The total number of vortex core and edge region parcels, on seven isentropes, reaching midlatitudes in 1998–2000 is given in Figure 7.22. Generally speaking, the features in the temporal evolution are the same for all the years. The number of core parcels in midlatitudes increased with time, apart from the two top-most isentropes, where, due to descent, the number of core parcels decreased with time. On the other hand, the number of the edge region parcels decreased with time.

A full understanding of the differences between the three years can be obtained by a detailed examination of the wind fields and the size and the position of the vortex. Some of the differences, though, can be explained by neglecting differences in the zonal and meridional flow, and concentrating only on the size of the vortex and heating rates.
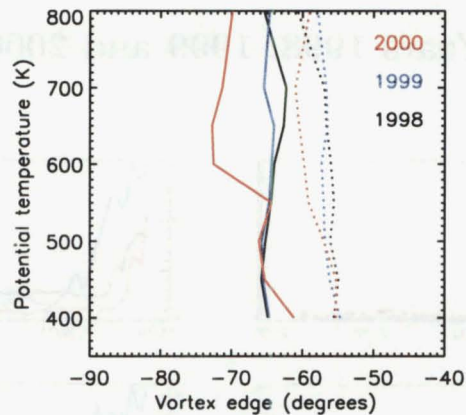
Figure 7.21: Equivalent latitude of the poleward (full line) and equatorward (dotted line) vortex edge on 10 October of 1998 (black), 1999 (blue) and 2000 (red).

On the 700 K isentrope, the vortex core was largest in 1998, hence the largest number of core parcels in midlatitudes was present in that year. The vortex edge region on this isentrope was larger in 1999 than in 1998, hence there were more vortex edge region parcels in midlatitudes. In contrast, the vortex core was smallest in 2000, leading to fewer vortex core parcels present in midlatitudes. On the other hand, the sharp drop in the number of core parcels on the 700 K isentrope happened earlier in 2000 than in 1998 and 1999. This was caused by the strongest descent inside the vortex in 2000 (Figure 6.4). In 1999, when heating rates were least negative, the presence of the vortex edge region parcels lasted longer.

Examination of the height distribution plots (see Figure 7.4) for 1999 and 2000 (not shown) shows that the strong descent rates in 2000 partly explain the different features between the years on the 550 K isentrope (another contributing factor is discussed below). Around 10 December 2000, the number of core parcels on this isentrope levelled off, unlike in the previous years when the numbers continued to increase. This was in part caused by the descent of the 650 K core parcels, which by 10 December 2000 descended to the 550 K isentrope. As, in 2000, the vortex core was significantly smaller at 650 K, this was reflected in the levelling off in the number of parcels. At the same time, the vortex edge region parcels from 650 K descended to the 550 K isentrope. As the vortex edge region was larger in 2000 than in 1998 or 1999 (Figure 7.21), the total number of edge region parcels increased on the 550 K isentrope, from around 10 December 2000.

In the year 2000, at the lower-most level, the vortex core was the largest, and the vortex edge region the smallest, causing the presence of more core parcels, and fewer edge region parcels on the 400 K isentrope.

Another conspicuous difference between the years 1998 and 1999, on one hand, and the year 2000, on the other hand, is the decrease in the number of core parcels on the isentropes of 450 K and 500 K, from around 10 December 2000. To examine this, the

Years 1998, 1999 and 2000
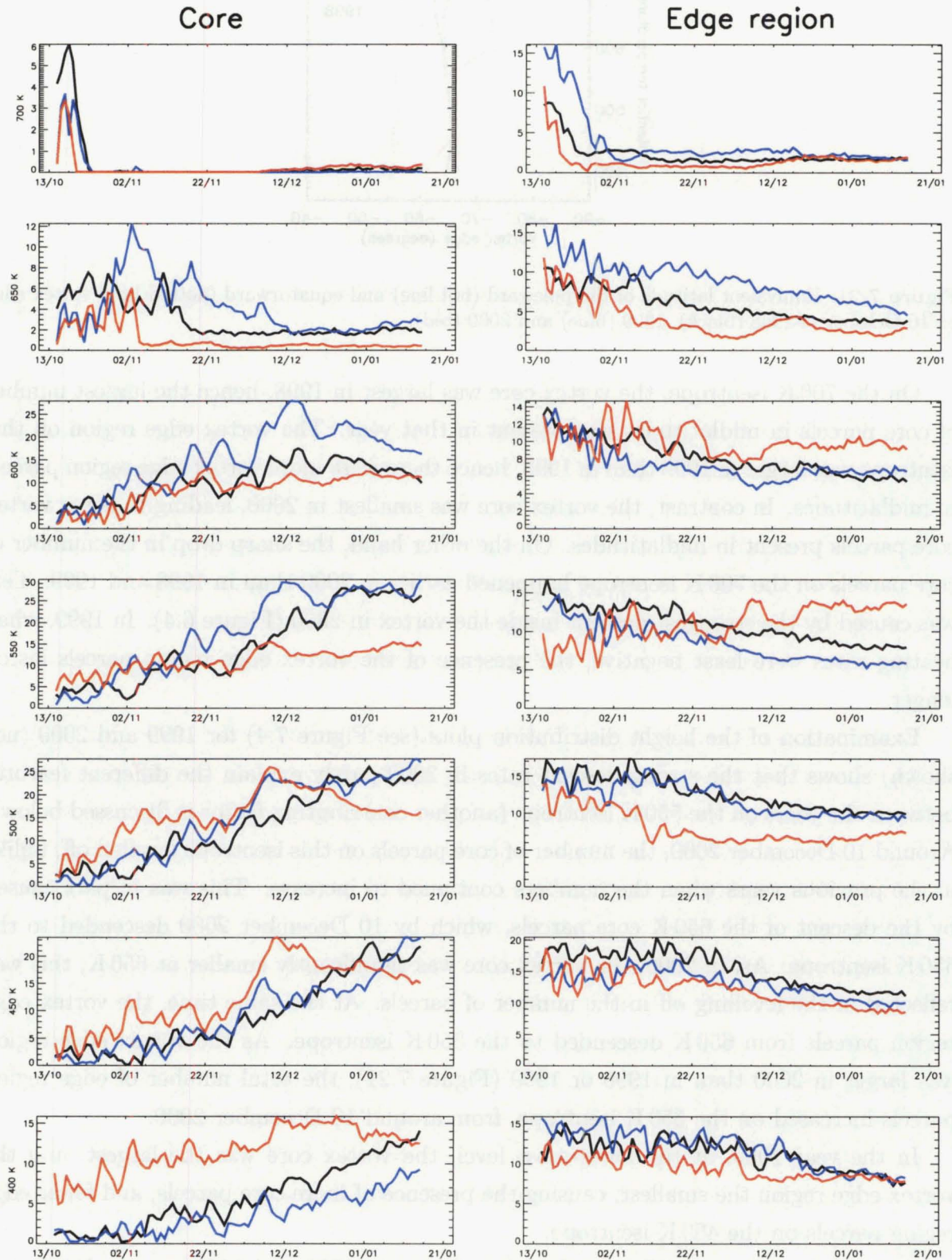
Core   ## Edge region

Figure 7.22: The number of vortex core (left) and edge region (right) parcels reaching southern midlatitudes in 1998, 1999 and 2000. The colour code is the same as in Figure 7.21.

number of vortex core parcels in the region north of 30°S was analyzed (by identical calculations as those for midlatitudes). The temporal evolution of the number of core parcels showed a pronounced increase between 7 and 12 December 2000, on the 450 K, 500 K and 550 K isentropes. This essentially means that the vortex remnants partly moved from midlatitudes into the tropics. One of the possible reasons why the same feature was not seen in 1998 and 1999 is that in 2000 the vortex broke down almost a month earlier (Figure 5.6).

The total number of vortex parcels (the sum of core and edge region parcels) and the total depletion (caused by the presence of vortex core and edge region parcels) in southern midlatitudes in 1998, 1999 and 2000 are presented in Figure 7.23. The mean values in
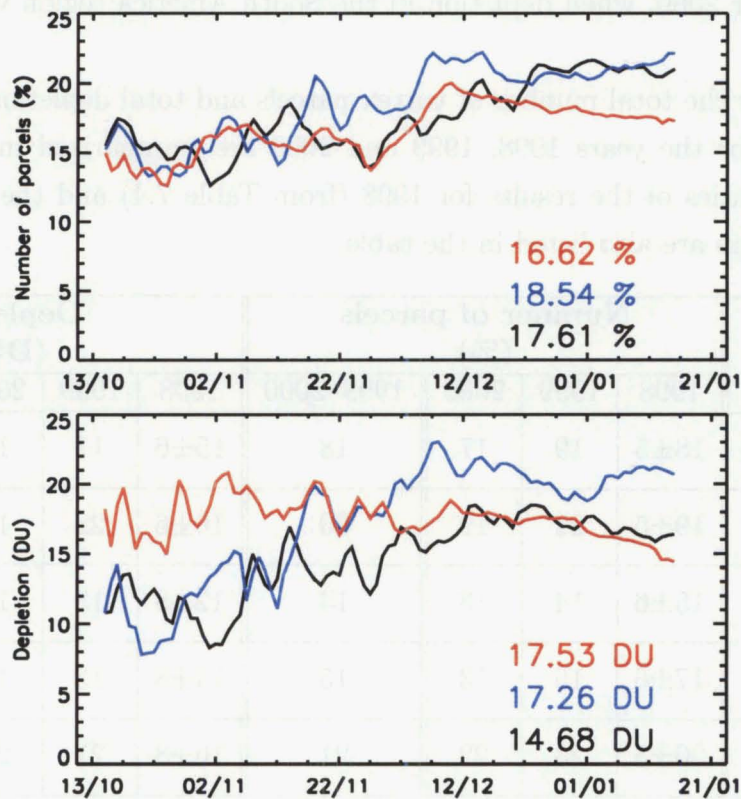
Figure 7.23: The total number of vortex parcels (top) and the total depletion (bottom) in southern midlatitudes, in 1998, 1999 and 2000. The mean values over the examined period are indicated on the lower right. The colour code is the same as in Figure 7.21.

the number of parcels and depletion did not differ much (~2 %, and ~3 DU, respectively) between the years. Although the mean number of parcels in the year 2000 was the smallest, the mean depletion was the largest, caused mostly by two factors. First, the depletion inside the vortex was most severe in 2000 (Figure 6.6). Second, a relatively high number of vortex core parcels was present in midlatitudes on the 400 K isentrope (Figure 7.22), where air is most dense and the contribution to the total depletion is highest.

7.4.1   Depletion in Different Regions

The results for four subregions in midlatitudes (Section 7.2) are given in Figure 7.24 for all the years. The results indicate that the Australia and New Zealand region was most quiescent. The events in which either vortex filaments or vortex remnants reached this region were not as pronounced as in the other subregions. The depletion in mid-October was less than 5 DU for all the years, and the variations in depletion were rarely ever of an order of 20 DU.

In contrast, the occurrences of the Antarctic vortex air over the Africa and South America regions were more frequent as well as more intense. The days in which the depletion was more than 20 DU were numerous. A prominent case was middle October to early November 2000, when depletion in the South America region was mostly above 30 DU.

The results for the total number of vortex parcels and total depletion in midlatitudes and subregions, for the years 1998, 1999 and 2000 are summarized in Table 7.5. The absolute uncertainties of the results for 1998 (from Table 7.4) and the results averaged over all of the years are also listed in the table.

Region	Number of parcels (%)				Depletion (DU)			
	1998	1999	2000	1998–2000	1998	1999	2000	1998–2000
SH midlatitudes	18±5	19	17	18	15±6	17	18	16
Africa	19±5	22	19	20	16±6	22	19	19
Aust+NZ	15±6	14	13	14	12±8	13	14	13
Pacific	17±6	15	13	15	14±8	13	14	14
S.America	20±5	23	22	21	16±8	21	23	20

Table 7.5: Mean total number of parcels (%) and mean total depletion (DU) in midlatitudes and the subregions, in the years 1998, 1999 and 2000, and mean over the three years.

As can be seen from Table 7.5, the interannual variability of the number of vortex parcels and depletion in midlatitudes and subregions is within the uncertainties of the results for 1998.

Years 1998, 1999, 2000
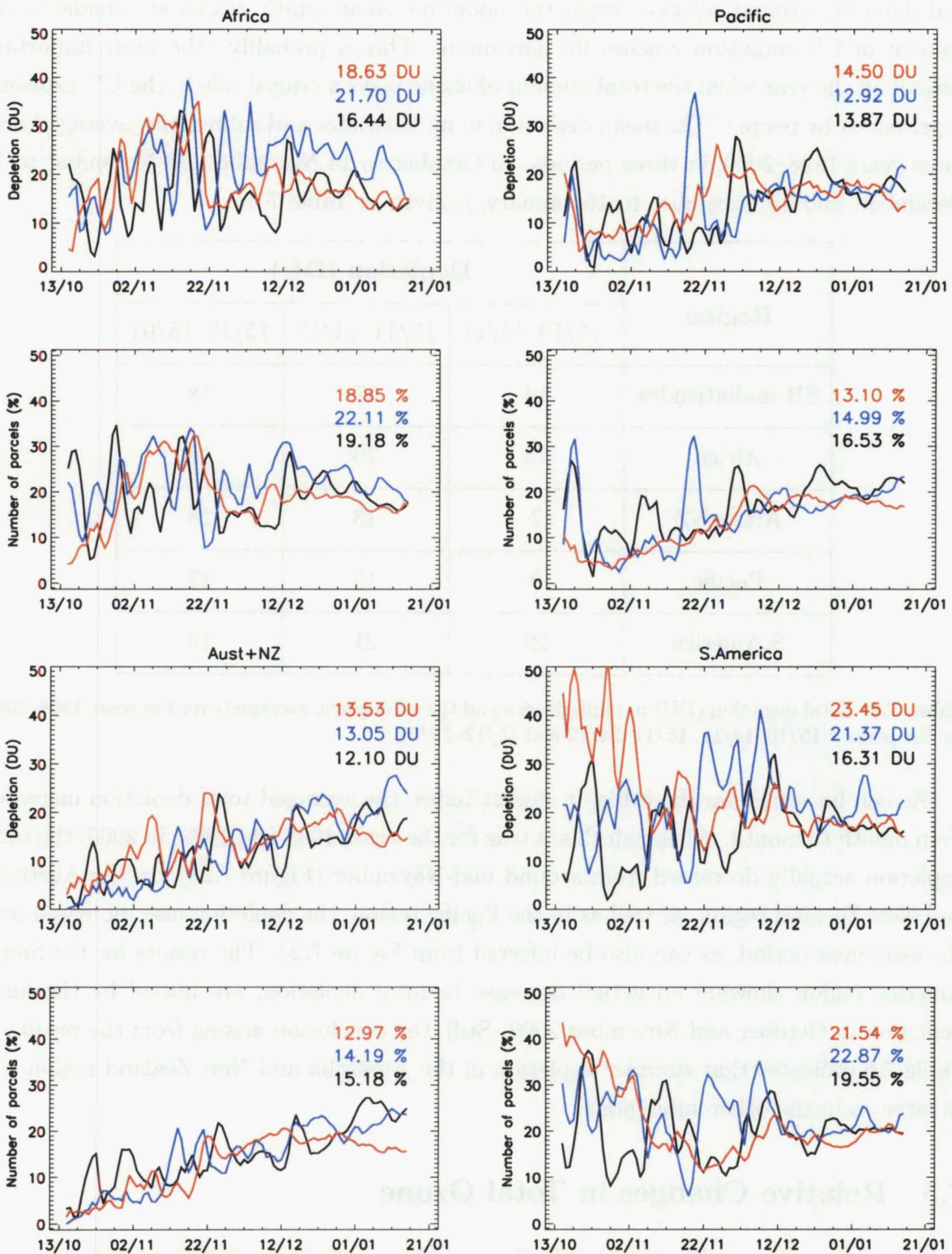
Figure 7.24: The total number of vortex parcels and the corresponding ozone depletion, in the 375–725 K layer, in four regions in southern midlatitudes (colour code as in Figure 7.21). The mean values over the examined period are indicated on the upper right.

It is interesting to see how the influence changed from month to month. The amount of UV radiation reaching the Earth's surface depends on the solar zenith angle. In December and January, around solstice, when the noontime solar zenith angles are smallest, the amount of UV radiation reaches its maximum. This is probably "the most important period" in the year when the total amount of ozone plays a crucial role in the UV exposure experienced by people. The mean depletion in midlatitudes and subregions, averaged over three years 1998–2000, in three periods, 15 October to 14 November, 15 November to 14 December, and 15 December to 15 January, is given in Table 7.6.

Region	Depletion (DU)		
	15/10–14/11	15/11–14/12	15/12–15/01
SH midlatitudes	14	17	18
Africa	18	20	18
Aust+NZ	7	13	18
Pacific	9	15	17
S.America	22	21	18

Table 7.6: Total depletion (DU) in midlatitudes and the subregions, averaged over the years 1998–2000, for the periods 15/10–14/11, 15/11–14/12 and 15/12–15/01.

As can be seen from the table, in midlatitudes, the averaged total depletion increased from month to month. Although this is true for the years 1998 and 1999, in 2000, the total depletion actually decreased from around mid-November (Figure 7.23). In the Australia and New Zealand region, as well as in the Pacific region, the depletion also increased over the examined period, as can also be inferred from Figure 7.24. The results for the South America region showing an actual decrease in total depletion, are biased by the large depletion in October and November 2000. Still, the conclusion arising from the results in Table 7.6 indicates that summer depletion in the Australia and New Zealand region was as large as in the other subregions.

7.5   Relative Changes in Total Ozone

In this section, the results presented in the preceding sections are discussed in the context of the total column ozone. TOMS total column ozone data (Section 4.1) are used here to determine what the ozone levels in southern midlatitudes would have been without the influence of the Antarctic ozone hole, and to quantify how much of the change in the

total column ozone that occurred since 1979, was caused by depletion inside the Antarctic ozone hole.

TOMS total column ozone in southern midlatitudes, over the period 15 October to 15 January, for the years 1998, 1999 and 2000, and for the year 1979, for comparison, is plotted in Figure 7.25. The sum of the actual measured total column ozone and the calculated depletion in the 375–725 K layer, is also plotted. The days when TOMS data were either incomplete (17 and 18 November in 1998 and 1999) or when TOMS was not operational (13 December 1998 to 3 January 1999), are excluded from the analysis.
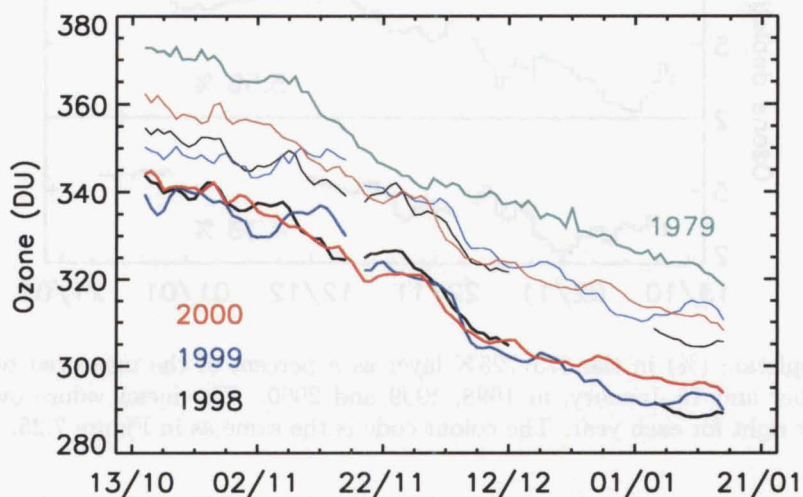
Figure 7.25: TOMS total column ozone in midlatitudes (thick lines), for the years 1979 (green), 1998 (black), 1999 (blue) and 2000 (red), and the sum of TOMS ozone and the calculated depletion in the 375–725 K layer (thin lines).

The difference in the total column ozone between 1979 and the years 1998, 1999 and 2000, is ~30 DU both in the early and the later part of the period. The difference is at minimum around the end of November. In 1979, approximately three weeks before this date were characterized by a fast drop in the total column ozone, suggesting that the Antarctic vortex was in the process of breaking down (the analysis of *Waugh et al.* (1999) showed that in 1979 the breakdown was around 20 November). As shown in Section 5.5, the vortex is highly distorted prior to breakdown, and large masses of vortex air can reach latitudes north of 60° S. On the other hand, the sharpest decrease in total ozone in 1998, 1999 and 2000, happened between the end of November and the beginning of December (somewhat earlier than the calculated breakdown dates presented in Figure 5.6). This result indicates that in those years the breakdown of the vortex was delayed by about three weeks compared to 1979 (this is in agreement with the findings of *Waugh et al.* (1999) and *Zhou et al.* (2000)). As a consequence, the minimum difference in the total ozone at the end of November reflects the fact that the comparison is done for the period when ozone-poor air from the vortex was prevalent in 1979, but only partially present in 1998, 1999 and 2000.

The sum of TOMS total column ozone and the calculated depletion (thin lines in Figure 7.25) essentially gives what the total ozone would have been had the ozone depleting processes inside the vortex not occurred. Figure 7.26 shows the calculated depletion in the 375–725 K layer as a percent of the measured total ozone in midlatitudes. In 1998 and
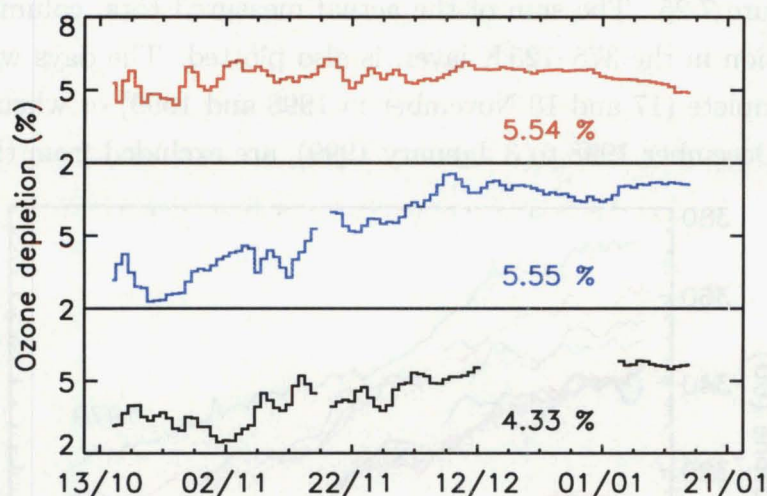
Figure 7.26: Depletion (%) in the 375–725 K layer as a percent of the measured total column ozone between 15 October and 15 January, in 1998, 1999 and 2000. The mean values over the period are indicated on lower right for each year. The colour code is the same as in Figure 7.25.

1999, the percent depletion increased until about the middle of December, corresponding to the increase in depletion (Figure 7.23) and decrease in the total column ozone (Figure 7.25). In contrast, in 2000, there was not much change in percent depletion, due to very high depletion in October and November (Figure 7.23).

Although a direct comparison of these results with model studies of *Prather et al.* (1990), *Mahlman et al.* (1994), *Eckman et al.* (1996) and *Chipperfield* (1999) is not possible, it is worth mentioning that all of them showed a decrease of 2–5 % in total ozone, either in southern midlatitudes or in a midlatitude subregion, as a consequence of dilution. The mean results in Figure 7.26 are higher than those model results, especially in December–January for the year 1999, when they reached values of around 7–8 %.

Table 7.7 summarizes the results for percent depletion in midlatitudes and subregions, for 1998, 1999 and 2000. On average, in midlatitudes there would have been ∼5 % more ozone without the influence of the Antarctic ozone hole. In subregions, the impact was least pronounced in the Australia and New Zealand region (∼4 % more ozone) and most pronounced in the South America region (∼7 % more ozone).

It is interesting to note that depletion results, expressed as a percent of undepleted ozone, rather than observed ozone, can be used to estimate an increase in erythemal UV radiation. Each 1 % decrease in ozone corresponds to 1.2 % increase in erythemal UV (*McKenzie et al.* (1999) and references therein). From our results, it can be concluded that

Region	Depletion (%)			
	1998	1999	2000	1998–2000
SH midlatitudes	4.33	5.55	5.54	5.14
Africa	5.00	6.97	5.99	5.99
Aust+NZ	3.42	4.18	4.26	3.95
Pacific	4.00	4.09	4.64	4.24
S.America	5.13	7.20	7.70	6.68

Table 7.7: Mean total depletion (%) in midlatitudes and the subregions, in the years 1998, 1999 and 2000, as a percent of the actual total column ozone measured by TOMS. The mean values (averaged for all three years) are also presented.

on average, in midlatitudes, there was ∼6 % increase in erythemal UV as a consequence of dilution.

The calculated depletion in the 375–725 K layer expressed as a percent of the change in the total ozone from 1979 is plotted in Figure 7.27. On average, 50–60% of the change in column ozone can be attributed to the dilution of the Antarctic vortex ozone-depleted air. The maxima seen around the end of November in all three years, reaching values of more than 80 %, are a consequence of the shift in the vortex breakdown date (as discussed earlier).
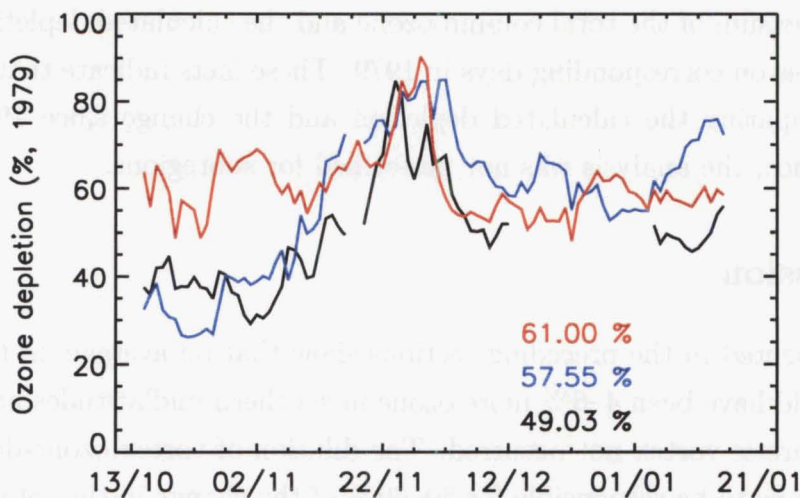
Figure 7.27: Depletion (%) in the 375–725 K layer as a percent of the change in the total column ozone compared to 1979, in 1998, 1999 and 2000. The mean values over the examined period are indicated on lower right. The colour code is the same as in Figure 7.25.

It is important to stress here that the above analysis is somewhat simplistic. The comparison between the years 1998, 1999 and 2000 with the year 1979 does not take into

account any other factors that influence ozone levels (Section 2.1.2).

The study performed for midlatitudes masks the fact that in subregions, where scatter in the data was more substantial, the situation was significantly different. For example, Figure 7.28 shows TOMS total column ozone for the Australia and New Zealand region, in 1979, 1998, 1999 and 2000. Over a few days in late October 1979, the total column
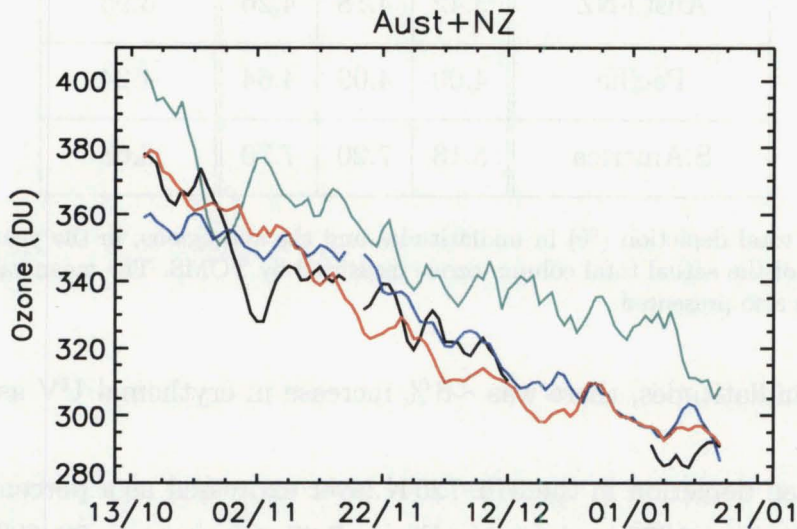
Figure 7.28: TOMS total column ozone in the Australia and New Zealand region in 1979, 1998, 1999 and 2000. The colour code is the same as in Figure 7.25.

ozone was less than in some (or even all) of the later years, which means that the change from 1979 to any given year has an opposite sign to the rest of the period. Furthermore, on a few days the sum of the total column ozone and the calculated depletion exceeds the total ozone values on corresponding days in 1979. These facts indicate that this simplistic method for comparing the calculated depletion and the change since 1979 has serious limitations. Hence, the analysis was not performed for subregions.

7.6   Discussion

The results presented in the preceding sections show that on average, in the years 1998–2000, there would have been 4–6 % more ozone in southern midlatitudes had ozone depletion in the Antarctic vortex not occurred. The dilution of vortex ozone-depleted air into midlatitudes seems to be responsible for 50–60 % of the change in the total column ozone since 1979. In this section, some of the critical steps in the method for obtaining these results are discussed. The critical steps are divided roughly into three areas: the "state" of the Antarctic vortex, the advection, and the numerical calculations. Processes which were neglected in the method are discussed at the end of this section.

7.6.1 "State" of the Antarctic Vortex

First, the steps that include the recognition of vortex parcels, the size and the filamentation of the vortex on the initial day, and the volume mixing ratio of depleted ozone inside the vortex are examined.

The recognition of vortex parcels as well as the size of the vortex (in equivalent latitude) directly depend on the calculations of the PV values of the vortex edges. The area of the vortex on a given isentrope, is directly proportional to $(1 - \sin \varphi)$, where φ is the equivalent latitude of the vortex edge. As a consequence, the relative changes in the vortex size are larger around the poleward vortex edge than around the equatorward vortex edge. For example, let's assume that the real vortex poleward (equatorward) edge is at $65\,^\circ$S ($60\,^\circ$S), while the calculations give the results of $62\,^\circ$S ($57\,^\circ$S). The area of the core (vortex edge region) would be 25 % (10 %) larger than in reality, which, under the assumption of ideal parcel tracking possibilities by the RDF calculations, would lead to as many more parcels being recognized as vortex core (edge region) parcels. Hence, the uncertainties in the number of vortex core parcels are larger.

Furthermore, recognition of vortex parcels is limited by the low-resolution PV field on a chosen initial day, in which many fine-scale features are not distinguished. This affects vortex edge region parcels more than core parcels, as the filaments peeling off the vortex usually originate in the edge region.

The sensitivity of the results to the size of the vortex, and the filamentation, was effectively, but not independently, tested in the runs performed for different initial days (Section 7.3.2). Therefore, only the combined contribution of those two effects can be derived, and it ranges between 37–65 % for calculated depletion in midlatitudes (Table 7.2).

Another step that influences the number of vortex parcels is the interpolation of the vortex edge PV values in the vertical. The test performed in Section 6.1.1, showed that on average, interpolated PV values are less than the original values (≤ 10 %), possibly causing fewer parcels to be recognized as vortex parcels.

The volume mixing ratios of depleted ozone assigned to vortex parcels also directly influence the results. As mentioned in Section 4.3, there is a possibility that the technique used to derive ozone depletion inside the vortex overestimates the true depletion. This overestimate is to a degree alleviated in the calculations as the results of *Hoppel et al.* (2003) were applied to a smaller vortex area. Specifically, *Hoppel et al.* (2003) used the middle edge of the vortex as a vortex boundary, while in our calculations, only parcels coming out of the vortex core (poleward of the poleward vortex edge, hence a smaller area than in the calculations of *Hoppel et al.* (2003)) were labelled with the calculated volume mixing ratio of depleted ozone.

In the vortex edge region, it was assumed that the volume mixing ratio of depleted ozone is a linear function of PV, decreasing as the PV values inside the edge region increase (Section 6.4). This assumption is probably only good as a first approximation. A more detailed study of the ozone depletion, both in the vortex core and the edge region, would significantly raise confidence in our results.

7.6.2   Advection

In this step, there are two possible sources of uncertainties. The computational errors are negligible, as discussed in Section 3.5. The errors arising from the uncertainties in the wind fields were tested in an additional run performed with the perturbed zonal and meridional winds (Section 7.3.1). The results show that the corresponding uncertainties in midlatitude depletion range between 4–14 % (Table 7.1), and are less than the uncertainties associated with the choice of the initial day. The sensitivity of the results to perturbations in heating rates was not studied.

7.6.3   Numerical Calculations

In the numerical calculations of depletion in midlatitudes, two critical steps were examined. First, the number of isentropes chosen for the integration of ozone depletion was discussed in Section 6.5. The results show that that any possible increase in the precision of the calculations, introduced by a greater number of isentropic surfaces, is masked by the uncertainties arising from the uncertainties in temperatures. The estimated temperature uncertainty of the depletion results is $\sim$5 %.

Second, non-conservation of mass, which is an inherent problem in the Lagrangian models, was analyzed, and a scaling method was introduced (Section 7.1.1). The method consists of two parts. In the first part, a fraction of the vortex mass inside the model domain on any given day is derived. The complement ratios, which represent "leakage" of the vortex material through the lower boundary of the model, agree well with the studies of *Li et al.* (2002) and *Öllers et al.* (2002). In the next step, mass conservation is forced by comparing the total number of depleted ozone molecules inside the domain, and the total number of ozone depleted molecules that the calculations yield.

7.6.4   Limitations of the Method

The results presented in this work capture only one aspect of the influence of the ozone depletion in the Antarctic ozone hole – how much more ozone there would have been in southern midlatitudes, had ozone inside the vortex not been depleted. In answering this question, a possibility that the stratospheric circulation was altered by the ozone deficit was neglected. Likewise, chemistry along parcel trajectories was not included, resulting

in exclusion of additional ozone depletion and photochemical recovery. Furthermore, mixing between parcels was not explicitly represented in RDF calculations. Even the one aspect examined is limited by the fact that the calculations were performed for the 375–725 K layer, and only for the time period between 15 October and 15 January of the following year. A brief discussion of these limitations is given here.

Changes in the SH Circulation

Mahlman et al. (1994) showed that in the presence of the Antarctic ozone hole, the whole meridional circulation in the Southern Hemisphere is expected to change, with the effect being most pronounced in spring, and considerably less when averaged over a year. *Prather et al.* (1990) showed that transport from the upper stratosphere would not be significantly changed, but that an increased transport from the tropics and a decreased transport into the troposphere would synergistically lead to ozone recovery. Any possible change in the SH circulation was neglected in this work, as the observed winds from the Met Office analyses were used.

Additional Ozone Depletion

Transport of active substances into midlatitudes, and the ensuing ozone destruction, was extensively studied by *Prather and Jaffe* (1990). They demonstrated that the amount of ozone depletion occurring in midlatitudes depends on the amount of ozone already depleted and the level of denitrification in exported air, as well as on the degree of isolation of exported air. If air is already severely depleted of ozone (as is the case with air parcels leaving the Antarctic vortex after September), then the additional ozone loss is not significant. Interestingly though, in the denitrified environment, ozone loss through the NO_x cycle (Table 2.1) is hindered, leading to recovery.

Knudsen and Grooß (2000) argued that in the Northern Hemisphere, export of chemically perturbed air during winter poses only a minor factor in total dilution. First, the depleting potential of active forms is reduced outside the vortex, and second, the ozone-depleted air undergoes photochemical recovery. In winter, export of vortex air into southern midlatitudes is less than in the NH (Section 2.3), hence this effect is not expected to have a significant impact.

Photochemical Recovery

Knudsen and Grooß (2000) showed that ~18 % of the ozone-depleted air in northern midlatitudes photochemically recovers after about seven weeks. This result is somewhat higher than the result for southern midlatitudes of *Prather et al.* (1990), indicating a

recovery of $\sim$14 % during October and November, and of $\sim$20 % from October to mid-January.

Mixing

In this study, the process of mixing was not specifically included. In other words, there was no explicit representation of mixing in RDF calculations. However, mixing is implicitly included through averaging depletion in the whole midlatitude region. Here, a brief discussion of the importance of mixing is given.

The assumption that the volume mixing ratio of depleted ozone in a spatial box assigned to a vortex parcel is always the same, implies that the box was isolated from the surrounding air. The isolation prevents any exchange of material, whereby depleted ozone in the box would be partly replenished, and the surrounding air would be partly depleted in ozone. The validity of our method hence relies on the length of time during which vortex air can be considered isolated.

A complication in quantifying the time of isolation lies in the fact that our method does not distinguish between different vortex air masses. In other words, a vortex parcel can be a part of the vortex protruding into midlatitudes (often seen before the vortex breakdown, see Section 7.2), or a part of a vortex filament, or a part of a vortex remnant. In the first case, mixing can be completely ignored, and the method realistically captures the reduction in ozone. On the other hand, when a filament or a remnant is situated in midlatitudes, mixing must be taken into account.

The level of isolation of a filament or a remnant depends on its size and on the background flow. The PV barrier associated with those structures prevents mixing in the same fashion as in the vortex. Hence, to a large extent, mixing of ozone-poor air depends on the persistence of the PV anomaly. The large-scale wind field causes stretching and folding of the structures, reducing their size and enabling mixing in the horizontal plane (*Hess*, 1991). Furthermore, as the vertical thickness of the structures decreases, the vertical gradient of ozone is increased, and mixing is facilitated (*Hess*, 1991; *Haynes and Anglade*, 1997). The decrease in the thickness of the structures is aided by the vertical wind sheer leading to tilting of the structures (*Orsolini et al.*, 1995). The rate of dissipation of the PV anomalies also depends on the radiative heating they experience. Radiative cooling assists persistence of the structures, while radiative warming enables dissipation (*Waugh and Rong*, 2002).

The estimated time for the disappearance of large-scale PV anomalies is about a month (*Sutton*, 1994; *Waugh et al.*, 1997; *Waugh and Rong*, 2002). On the other hand, *Waugh and Rong* (2002) argued that after vortex breakdown, remnants of chemical species can be longer lived than PV remnants. This was mentioned in Section 5.5, where Figure

5.9 showed a faster increase in the PV values than in the ozone values that POAM III measured during December 1998.

Without a doubt, a significant improvement in our results would be obtained if mixing processes were explicitly presented in the calculations. Still, it is important to stress that our method implicitly includes mixing, and that there are only two instances when exclusion of mixing leads to errors. Mixing is implicitly included in the method by averaging depletion in the whole midlatitude region. The calculated mean value is insensitive to the amount of actual mixing that has occurred so long as the air remains in midlatitudes – it is the same, no matter whether ozone-depleted air is completely mixed into midlatitudes, or isolated in a region. The errors arise only when already diluted vortex air enters or leaves the region under examination. If vortex air leaves the region, in the calculations it is assumed that it carries away undiluted depletion. In this case our result underestimates the total depletion. On the other hand, if already diluted vortex air enters the region, the result overestimates the depletion. As transport across the boundaries of subregions is larger, the results for subregions are more sensitive to mixing than the results for midlatitudes.

Vertical Limits of the Model Domain

The set vertical domain of the model did not allow an analysis of the influence of dilution outside the domain. In southern midlatitudes, three distinct regions were excluded from the domain, the region above $725\,K$, the lowermost stratosphere (between $375\,K$ and the tropopause), and the troposphere. As discussed in Section 6.3, no vortex air was ascending, hence the exclusion of the stratosphere above $725\,K$ should not influence the results. Therefore, only the presence of ozone-depleted air in the lowermost stratosphere and the troposphere was effectively excluded from the analysis.

According to *Prather et al.* (1990), the ozone reduction around the tropopause is $\sim6\,\%$, and in the troposphere $\sim10\,\%$ (see also *Brasseur et al.* (1997)). A rough estimate of the combined contribution of depletion in those two regions, taking the total column of ozone in midlatitudes in December as $300\,DU$ (Figure 7.25), and the column of ozone in the troposphere and the lowermost stratosphere as $16\,DU$ each (based on the December climatological ozone over Lauder), is another $\sim0.8\,\%$ of the total column ozone. This means that without the dilution of the Antarctic ozone hole, there would have been ~5–$7\,\%$ more ozone, and that the dilution is responsible for as much as 60–$70\,\%$ of the change since 1979.

Length of the Examined Period

The results presented here give only an immediate causal relationship between ozone depletion in the vortex and dilution in midlatitudes. In other words, persistence of the ozone reduction in the polar region and midlatitudes after 15 January is beyond the scope of this work. Model studies of *Prather et al.* (1990), *Mahlman et al.* (1994), *Eckman et al.* (1996) and *Chipperfield* (1999) all show that ozone levels, both in the polar region and in midlatitudes, do not fully recover from depletion within a year.

On the other hand, *Bodeker et al.* (2002) argued that over the period 1981–2000, in the polar region, there was no negative trend in ozone before the onset of the Antarctic ozone hole, and concluded that there was no cumulative loss. Furthermore, *Fioletov and Shepherd* (2003) showed that midlatitude (35°–60°) ozone levels strongly depend on the ozone buildup during winter and spring. The correlation they found between the spring ozone values and ozone in other months can fully explain total ozone trends in the Northern Hemisphere. In the Southern Hemisphere, the total ozone trend is significantly stronger than the trend predicted from the correlation in all of the seasons except winter. *Fioletov and Shepherd* (2003) indicated that the disagreement between the trends is caused by the transport of ozone-depleted air from the Antarctic vortex. The fact that the trends are the same in winter suggests that there is no cumulative effect of the depletion even in midlatitudes.

With the results of *Bodeker et al.* (2002) and *Fioletov and Shepherd* (2003), showing no accumulation of ozone depletion, it can be concluded that our method fully (with the exception of other limitations) captures the dilution effect.

7.7   Conclusion

The dilution of the Antarctic ozone hole into southern midlatitudes between 15 October and 15 January of the years 1998, 1999 and 2000, has been analyzed, using diabatic RDF calculations for parcels initialized on a 1° longitude by 1° latitude grid (between 30°S and 60°S), on seven potential temperature surfaces (400–700 K, with 50 K spacing). A method for calculating reduction in ozone caused by the presence of the Antarctic vortex parcels has been presented. Within the method, two distinct regions of the vortex, the core and the edge region, have been considered. A scaling procedure has been introduced to mitigate non-conservation of mass arising from the employment of the Lagrangian model.

The results for the years 1998, 1999, and 2000 show that on average, over the 15 October – 15 January period, 18%, 19%, and 17%, respectively, of midlatitude air parcels originated inside the Antarctic vortex. The corresponding reduction in ozone is 15 DU, 17 DU, and 18 DU, respectively. The reduction caused by the presence of air parcels

originating in the vortex edge region is significant, especially in the early part of the period under examination. The results for four subregions in midlatitudes (spanning longitude regions of 90°, starting from 0°) are also presented. These results show that, on average, in the region encompassing New Zealand and Australia ozone reduction is less than in the other subregions during spring, but by summer the reduction is effectively the same in all subregions.

Tests have been performed for the year 1998 to examine the sensitivity of the results to uncertainties in the wind fields, and to the choice of the initial day. The results indicate that the method is more sensitive to the initial conditions, including the size of the vortex and the amount of filamentation, than to introduced perturbations in the winds. The corresponding ozone reduction uncertainties range from 37–65 %, and 4–14 %, respectively. The uncertainties are generally larger for subregions.

The combined uncertainties in the number of parcels and in depletion, arising from the uncertainties in the wind perturbations, the choice of the initial day, and in the temperature fields used here (not applicable for the number of vortex parcels), are 23–40 % and 38–67 %, respectively. In midlatitudes as well as in subregions, the interannual variability in the number of vortex parcels and in depletion, is within the uncertainties of the results for the year 1998.

The absolute ozone reduction has been compared to the TOMS measurements of column ozone to derive relative changes in the total ozone. The results show that without the dilution effect, ozone levels in southern midlatitudes would be 4–6 % higher. The reduction in ozone due to dilution is estimated to have caused an increase of ~6 % in erythemal UV radiation. Moreover, comparison of the calculated ozone reduction with ozone levels in 1979 demonstrates that 50–60 % of the change in the total column ozone can be attributed to the dilution effect. These results present a lower limit of the impact, as dilution in the lowermost stratosphere and troposphere is not captured in the calculations presented here.

Chapter 8

Conclusions

The results presented in this thesis show unambiguously that the Antarctic ozone hole has a significant impact on the vertical distribution and total amount of ozone in southern midlatitudes. An analysis given in the thesis consists of two different, but complementary, approaches. In Chapter 5, a detailed study of an altered ozone profile over Lauder in late December 1998, has been presented. In Chapter 7, an analysis of the dilution effect on southern midlatitudes, for spring- and summertime of the years 1998, 1999 and 2000, has been given.

The results presented in Chapter 5 demonstrate that a vortex remnant situated above New Zealand on the potential temperature surfaces of 550 K and 600 K, was responsible for the atypical vertical profile of ozone. The vortex remnant air on the 550 K isentrope ascended from the ozone hole region, while the 600 K air originated from higher altitudes and was not subjected to ozone-depleting chemical reactions.

In addition to the above results, a novel method for producing high-resolution ozone maps has also been introduced in Chapter 5. The method combines the PV/O_3 fitting technique and RDF calculations. The high-resolution ozone maps have been used to illustrate the highly structured state of the atmosphere during and after the Antarctic vortex breakdown in 1998.

The results given in Chapter 7 show that the dilution of the Antarctic ozone hole into southern midlatitudes significantly decreases midlatitude ozone levels. The results are summarized in Table 8.1.

The results show that on average, between 15 October and 15 January, 17–19 % of midlatitude air parcels originated inside the Antarctic vortex. The corresponding reduction in ozone was 15–18 DU. The influence of the Antarctic ozone hole was most pronounced in the geographical regions encompassing South America and Africa. The interannual variability of the results is within the uncertainties calculated for the year 1998.

A comparison of the ozone depletion results with the total column ozone measured by TOMS indicate that the total column ozone would have been 4–6 % higher had ozone-depleted air not been transported into midlatitudes. Furthermore, the ozone depletion results indicate that on average 50–60 % of the change in the total column ozone since 1979 can be attributed to the dilution effect.

Region	Number of parcels (%)	Depletion (DU)
SH midlatitudes	18	16
Africa	20	19
Aust+NZ	14	13
Pacific	15	14
S.America	21	20

Table 8.1: Mean total number of parcels (%) and mean total depletion (DU) in midlatitudes and subregions, averaged over 1998–2000.

The above results offer a quantification of the Antarctic ozone hole dilution effect that has not been done previously. In each examined year, the results are explicitly based on ozone depletion that occurred in the Antarctic vortex during spring of that same year. Furthermore, the results cover a relatively long period of three months, including the time around the summer solstice when the impact of ozone on UV is greatest.

8.1   Further Remarks

Future work can cover a number of issues, either not adequately presented in this study, or not examined at all. An improvement of the method would be to include mixing and chemistry. Both of these processes could be modelled within the method (e.g. *Pierce et al.*, 1997; *Fairlie et al.*, 1999; *Pierce et al.*, 1999; *Knudsen and Groß*, 2000; *McKenna et al.*, 2002), but would lead to an increased demand on computational resources.

A straight-forward extension of the results would be to include more years. The identical technique could be applied for the years 1994–1996, and 2001–2002, for which the POAM ozone measurements are available. The year 2002 would be of special interest, as in late September the Antarctic ozone hole split in two, with one part disappearing after a few days, and the other part reestablishing over the pole (e.g. *Allen et al.*, 2003; *Hoppel et al.*, 2003).

Another possible direction would be to apply the method to examine the influence of the Arctic ozone hole on northern midlatitudes. Studies of *Knudsen et al.* (1998a) and *Knudsen and Groß* (2000) utilized a method similar to the method presented in this work, to analyze ozone reduction caused by the transport of ozone-depleted air in the boreal springs of 1995 and 1997. The results of our analysis could therefore be directly compared to the results of *Knudsen et al.* (1998a) and *Knudsen and Groß* (2000).

Furthermore, obtaining the results for northern midlatitudes would allow a detailed study of the hemispheric differences.

References

Ajtić, J., B. J. Connor, C. E. Randall, B. N. Lawrence, G. E. Bodeker, J. E. Rosenfield, and D. N. Heuff, Antarctic air over New Zealand following vortex breakdown in 1998, *Ann. Geophys.*, *21*(11), 2175–2183, 2003.

Allaart, M. A. F., H. Kelder, and L. C. Heijboer, On the relation between ozone and potential vorticity, *Geophys. Res. Lett.*, *20*(9), 811–814, 1993.

Allen, D. R., and N. Nakamura, A seasonal climatology of effective diffusivity in the stratosphere, *J. Geophys. Res.*, *106*(D8), 7917–7935, 2001.

Allen, D. R., R. M. Bevilacqua, G. E. Nedoluha, C. E. Randall, and G. L. Manney, Unusual stratospheric transport and mixing during the 2002 Antarctic winter, *Geophys. Res. Lett.*, *30*(12), doi:10.1029/2003GL017117, 2003.

Atkinson, R. J., and R. A. Plumb, Three-dimensional ozone transport during the ozone hole breakup in December 1987, *J. Geophys. Res.*, *102*(D1), 1451–1466, 1997.

Atkinson, R. J., W. A. Matthews, P. A. Newman, and R. A. Plumb, Evidence of the mid-latitude impact of Antarctic ozone depletion, *Lett. Nat.*, *340*, 290–294, 1989.

Austin, J., N. Butchart, and K. P. Shine, Possibility of an Arctic ozone hole in a doubled-CO_2 climate, *Nature*, *360*, 221–225, 1992.

Becker, G., R. Müller, D. S. McKenna, M. Rex, and K. S. Carslaw, Ozone loss rates in the Arctic stratosphere in the winter 1991/92: Model calculations compared with Match results, *Geophys. Res. Lett.*, *25*(23), 4325–4328, 1998.

Becker, G., R. Müller, D. S. McKenna, M. Rex, K. S. Carslaw, and H. Oelhaf, Ozone loss rates in the Arctic stratosphere in the winter 1994/1995: Model simulations underestimate results of the Match analysis, *J. Geophys. Res.*, *105*(D12), 15175–15184, 2000.

Bevilacqua, R. M., et al., POAM II ozone observations in the Antarctic ozone hole in 1994, 1995, and 1996, *J. Geophys. Res.*, *102*(D19), 23643–23657, 1997.

Bodeker, G. E., I. S. Boyd, and W. A. Matthews, Trends and variability in vertical ozone and temperature profiles measured by ozonesondes at Lauder, New Zealand: 1986-1996, *J. Geophys. Res.*, *103*(D22), 28661–28681, 1998.

Bodeker, G. E., J. C. Scott, K. Kreher, and R. L. McKenzie, Global ozone trends in potential vorticity coordinates using TOMS and GOME intercompared against the Dobson network: 1978-1998, *J. Geophys. Res.*, *106*(D19), 23029–23042, 2001.

Bodeker, G. E., H. A. Struthers, and B. J. Connor, Dynamical containment of Antarctic ozone depletion, *Geophys. Res. Lett.*, *29*(7), doi:10.1029/2001GL014206, 2002.

Bowman, K. P., Large-scale isentropic mixing properties of the Antarctic polar vortex from analyzed winds, *J. Geophys. Res.*, *98*(D12), 23013–23027, 1993.

Brasseur, G., and S. Solomon, *Aeronomy of the Middle Atmosphere*. D. Reidel Publishing Company, second edn., 1986.

Brasseur, G. P., X. X. Tie, P. J. Rasch, and F. Lefèvre, A three-dimensional simulation of the Antarctic ozone hole: Impact of anthropogenic chlorine on the lower stratosphere and upper troposphere, *J. Geophys. Res.*, *102*(D7), 8909–8930, 1997.

Bregman, A., M. van den Broek, K. S. Carslaw, R. Müller, T. Peter, M. P. Scheele, and J. Lelieveld, Ozone depletion in the late winter lower Arctic stratosphere: Observations and model results, *J. Geophys. Res.*, *102*(D9), 10815–10828, 1997.

Brewer, A. W., Evidence for a world circulation provided by the measurements of helium and water vapour distribution in the stratosphere, *Q. J. R. Meteorol. Soc.*, *75*, 351–363, 1949.

Brinksma, E. J., et al., Analysis of record-low ozone values during the 1997 winter over Lauder, New Zealand, *Geophys. Res. Lett.*, *25*(15), 2785–2788, 1998.

Brinksma, E. J., J. Ajtic, J. B. Bergwerff, G. E. Bodeker, I. S. Boyd, J. F. de Haan, W. Hogervorst, J. W. Hovenier, and D. P. J. Swart, Five years of observations of ozone profiles over Lauder, New Zealand, *J. Geophys. Res.*, *107*(D14), doi:10.1029/2001JD000737, 2002.

Brühl, C., P. J. Crutzen, and J.-U. Grooß, High-latitude, summertime NO_x activation and seasonal ozone decline in the lower stratosphere: Model calculations based on observations by HALOE on UARS, *J. Geophys. Res.*, *103*, 3587–3597, 1998.

Butchart, N., and E. E. Remsberg, The area of the stratospheric polar vortex as a diagnostic for tracer transport on an isentropic surface, *J. Atmos. Sci.*, *43*(13), 1319–1339, 1986.

Cacciani, M., G. Fiocco, P. Colagrande, P. Di Girolamo, A. di Sarra, and D. Fuà, Lidar observations of polar stratospheric clouds at the South Pole 1. Stratospheric unperturbed conditions, 1990, *J. Geophys. Res.*, *102*(D11), 13937–12943, 1997.

Chapman, S., On ozone and atomic oxygen in the upper atmosphere, *Philos. Mag.*, *10*, 369–383, 1930.

Chen, P., The permeability of the Antarctic vortex edge, *J. Geophys. Res.*, *99*(D10), 20563–20571, 1994.

Chen, P., J. R. Holton, A. O'Neill, and R. Swinbank, Quasi-horizontal transport and mixing in the Antarctic stratosphere, *J. Geophys. Res.*, *99*(D8), 16851–16866, 1994.

Chipperfield, M. P., Multiannual simulations with a three-dimensional chemical transport model, *J. Geophys. Res.*, *104*(D1), 1781–1805, 1999.

Chou, M.-D., Broadband water vapor transmission functions for atmospheric IR flux computations, *J. Atmos. Sci.*, *41*, 1775–1778, 1984.

Chou, M.-D., and L. Kouvaris, Calculations of transmission functions in the infrared CO_2 and O_3 bands, *J. Geophys. Res.*, *96*, 9003–9012, 1991.

Collins, R. L., K. P. Bowman, and C. S. Gardner, Polar stratospheric clouds at the South Pole in 1990: Lidar observations and analysis, *J. Geophys. Res.*, *98*(D1), 1001–1010, 1993.

Crutzen, P. J., The influence of nitrogen oxides on the atmospheric ozone content, *Q. J. R. Meteorol. Soc.*, *96*, 320–325, 1970.

Crutzen, P. J., Ozone production rates in oxygen-hydrogen-nitrogen oxide atmosphere, *J. Geophys. Res.*, *76*, 7311–7327, 1971.

Crutzen, P. J., Estimates of possible future ozone reductions from continued use of fluoro-chloro-methanes, *Geophys. Res. Lett.*, *1*, 205–208, 1974.

Danilin, M. Y., et al., Trajectory hunting as an effective technique to validate multiplat-form measurements: Analysis of the MLS, HALOE, SAGE-II, ILAS, and POAM-II data in October-November 1996, *J. Geophys. Res.*, *107*(D20), doi:10.1029/2001JD002012, 2002.

Dave, J. V., Meaning of successive iteration of the auxiliary equation of radiative transfer, *Astrophys. J.*, *140*, 1292–1303, 1964.

Deniel, C., R. M. Bevilacqua, J. P. Pommereau, and F. Lefèvre, Arctic chemical ozone depletion during the 1994-1995 winter deduced from POAM II satellite observations and the REPROBUS three-dimensional model, *J. Geophys. Res.*, *103*(D15), 19231–19244, 1998.

Deshler, T., D. J. Hofmann, D. J. Hereford, and C. B. Sutter, Ozone and temperature profiles over McMurdo station Antarctica in the spring of 1989, *Geophys. Res. Lett.*, *17*, 151, 1990.

Dobson, G. M. B., Observations of the amount of ozone in the Earth's atmosphere and its relation to other geophysical conditions, *Proc. R. Soc. London, Ser. A.*, *129*, 411, 1930.

Eckman, R. S., W. L. Grose, R. E. Turner, and W. T. Blackshear, Polar ozone depletion: A three-dimensional chemical modeling study of its long-term global impact, *J. Geophys. Res.*, *101*(D17), 22977–22989, 1996.

Fairlie, T. D., R. B. Pierce, J. A. Al-Saadi, W. L. Grose, J. M. Russell III, M. Proffitt, and C. R. Webster, The contribution of mixing in Lagrangian photochemical predictions of polar ozone loss over the Arctic in summer 1997, *J. Geophys. Res.*, *104*(D21), 26597–26609, 1999.

Farman, J. C., B. G. Gardiner, and J. D. Shanklin, Large losses of total ozone in Antarctica reveal seasonal ClO_x/NO_x interaction, *Nature*, *315*, 207–210, 1985.

Fioletov, V. E., and T. G. Shepherd, Seasonal persistence of midlatitude total ozone anomalies, *Geophys. Res. Lett.*, *30*, doi:10.1029/2002GL016739, 2003.

Fromm, M. D., J. D. Lumpe, R. M. Bevilacqua, E. P. Shettle, J. Hornstein, S. T. Massie, and K. H. Fricke, Observations of Antarctic polar stratospheric clouds by POAM II: 1994–1996, *J. Geophys. Res.*, *102*(D19), 23659–23672, 1997.

Glaccum, W., et al., The Polar Ozone and Aerosol Measurement instrument, *J. Geophys. Res.*, *101*(D9), 14479–14487, 1996.

Godin, S., V. Bergeret, S. Bekki, C. David, and G. Mégie, Study of the interannual ozone loss and the permeability of the Antarctic polar vortex from aerosol and ozone lidar measurements in Dumont d'Urville (66.4° S, 140° E), *J. Geophys. Res.*, *106*(D1), 1311–1330, 2001.

Godin, S., M. Marchand, A. Hauchecorne, and F. Lefèvre, Influence of Arctic polar ozone depletion on lower stratospheric ozone amounts at Haute-Provence Observatory (43.92° N, 5.71° E), *J. Geophys. Res.*, *107*(D20), doi: 10.1029/2001JD000516, 2002.

Hansen, G., T. Svenøe, M. P. Chipperfield, A. Dahlback, and U.-P. Hoppe, Evidence of substantial ozone depletion in winter 1995/96 over Northern Norway, *Geophys. Res. Lett.*, *24*(7), 799–802, 1997.

Harris, N. R. P., M. Rex, F. Goutail, B. M. Knudsen, G. L. Manney, R. Müller, and P. von der Gathen, Comparison of empirically derived ozone losses in the Arctic vortex, *J. Geophys. Res.*, *107*(D20), doi: 10.1029/2001JD000482, 2002.

Haynes, P., and J. Anglade, The vertical-scale cascade in atmospheric tracers due to large-scale differential advection, *J. Atmos. Sci.*, *54*(9), 1121–1136, 1997.

Haynes, P., and E. Shuckburgh, Effective diffusivity as a diagnostic of atmospheric transport, 1. Stratosphere, *J. Geophys. Res.*, *105*(D18), 22777–22794, 2000a.

Haynes, P., and E. Shuckburgh, Effective diffusivity as a diagnostic of atmospheric transport, 2. Troposphere and lower stratosphere, *J. Geophys. Res.*, *105*(D18), 22795–22810, 2000b.

Hess, P. G., Mixing processes following the final stratospheric warming, *J. Atmos. Sci.*, *48*(14), 1625–1641, 1991.

Hofmann, D. J., and S. Solomon, Ozone destruction through heterogeneous chemistry following the eruption of El Chichón, *J. Geophys. Res.*, *94*, 5029–5041, 1989.

Hofmann, D. J., J. W. Harder, S. R. Rolf, and J. M. Rosen, Balloon-borne observations of the development and vertical structure of the Antarctic ozone hole in 1986, *Nature*, *326*, 59–62, 1987.

Holton, J. R., P. H. Haynes, M. E. McIntyre, A. R. Douglass, R. B. Rood, and L. Pfister, Stratosphere-troposphere exchange, *Rev. Geophys.*, *33*(4), 403–439, 1995.

Hoppel, K., et al., POAM III observations of arctic ozone loss for the 1999/2000 winter, *J. Geophys. Res.*, *107*(D20), doi:10.1029/2001JD000476, 2002.

Hoppel, K. W., R. M. Bevilacqua, D. R. Allen, G. Nedoluha, and C. E. Randall, POAM III observations of the anomalous 2002 Antarctic ozone hole, *Geophys. Res. Lett.*, *30*(7), doi:10.1029/2003GL016899, 2003.

Jacobson, M. Z., *Fundamentals of Atmospheric Modeling*. Cambridge University Press, 1999.

Juckes, M. M., and M. E. McIntyre, A high-resolution one-layer model of breaking planetary waves in the stratosphere, *Nature*, *328*, 590–596, 1987.

Kelly, K. K., et al., Dehydration in the lower Antarctic stratosphere during the late winter and early spring 1987, *J. Geophys. Res.*, *94*(D9), 11317–11358, 1989.

Kent, G. S., C. R. Trepte, U. O. Farrukh, and M. P. McCormick, Variation in the stratospheric aerosol associated with the north cyclonic polar vortex as measured by the SAM II satellite sensor, *J. Atmos. Sci.*, *42*(14), 1536–1551, 1985.

Kiehl, J. T., B. A. Boville, and B. P. Briegleb, Response of a general circulation model to a prescribed Antarctic ozone hole, *Nature*, *332*, 501–504, 1988.

Kirchhoff, V. W. J. H., Y. Sahai, C. A. R. Casiccia S., F. Zamorano B., and V. Valderrama V., Observations of the 1995 ozone hole over Punta Arenas, Chile, *J. Geophys. Res.*, *102*(D13), 16109–16120, 1997.

Klenk, K. F., P. K. Bhartia, E. Hilsenrath, and A. J. Fleig, Standard ozone profiles from baloon and satellite data sets, *J. Climate Appl. Meteorol.*, *22*, 2012–2022, 1983.

Knight, J. R., J. Austin, R. G. Grainger, and A. Lambert, A three-dimensional model simulations of the imapct of Mt. Pinatubo aerosol on the Antarctic ozone hole, *Q. J. R. Meteorol. Soc.*, *124*, 1527–1558, 1998.

Knudsen, B. M., and J.-U. Grooß, Northern midlatitude stratospheric dilution in spring modeled with simulated mixing, *J. Geophys. Res.*, *105*(D5), 6885–6890, 2000.

Knudsen, B. M., W. A. Lahoz, A. O'Neill, and J.-J. Morcrette, Evidence for a substantial role for dilution in northern mid-latitude ozone depletion, *Geophys. Res. Lett.*, *25*(24), 4501–4504, 1998a.

Knudsen, B. M., et al., Ozone depletion in and below the Arctic vortex for 1997, *Geophys. Res. Lett.*, *25*(5), 627–630, 1998b.

Lacis, A. A., and J. E. Hansen, A parametrization for the absorption of solar radiation in the Earth's atmosphere, *J. Atmos. Sci.*, *31*, 118–133, 1990.

Lait, L. R., An alternative form for potential vorticity, *J. Atmos. Sci.*, *51*(12), 1754–1759, 1994.

Lait, L. R., et al., Reconstruction of O_3 and N_2O fields from ER-2, DC-8, and balloon observations, *Geophys. Res. Lett.*, *17*(4), 521–524, 1990.

Lee, A. M., H. K. Roscoe, A. E. Jones, P. H. Haynes, E. F. Shuckburgh, M. W. Morrey, and H. C. Pumphrey, The impact of the mixing properties within the Antarctic stratospheric vortex on ozone loss in spring, *J. Geophys. Res.*, *106*(D3), 3203–3211, 2001.

Leovy, C. B., C.-R. Sun, M. H. Hitchman, E. E. Remsberg, J. M. Russell III, L. L. Gordley, J. C. Gille, and L. V. Lyjak, Transport of ozone in the middle stratosphere: Evidence for planetary wave breaking, *J. Atmos. Sci.*, *42*(3), 230–244, 1985.

Li, S., E. C. Cordero, and D. J. Karoly, Transport out of the Antarctic polar vortex from a three-dimensional transport model, *J. Geophys. Res.*, *107*(D11), doi:10.1029/2001JD000508, 2002.

Lucke, R. L., et al., The Polar Ozone and Aerosol Measurement (POAM) III instrument and early validation results, *J. Geophys. Res.*, *104*(D15), 18785–18799, 1999.

Lumpe, J. D., R. M. Bevilacqua, K. W. Hoppel, and C. E. Randall, POAM III retrieval algorithm and error analysis, *J. Geophys. Res.*, *107*(D21), doi:10.1029/2002JD002137, 2002.

Lumpe, J. D., et al., Comparison of POAM III ozone measurements with correlative aircraft and balloon data during SOLVE, *J. Geophys. Res.*, *108*(D5), doi:10.1029/2001JD000472, 2003.

MacKenzie, I. A., R. S. Harwood, L. Froidevaux, W. G. Read, and J. W. Waters, Chemical loss of polar vortex ozone inferred from UARS MLS measurements of ClO during the Arctic and Antarctic late winters of 1993, *J. Geophys. Res.*, *101*(D9), 14505–14518, 1996.

Mahlman, J. D., J. P. Pinto, and L. J. Umscheid, Transport, radiative, and dynamical effects of the Antarctic ozone hole: A GFDL "SKYHI" model experiment, *J. Atmos. Sci.*, *51*(4), 489–508, 1994.

Manney, G. L., L. Froidevaux, J. W. Waters, and R. W. Zurek, Evolution of microwave limb sounder ozone and the polar vortex during winter, *J. Geophys. Res.*, *100*(D2), 2953–2972, 1995.

Manney, G. L., M. L. Santee, L. Froidevaux, J. W. Waters, R. W. Zurek, W. G. Read, D. A. Flower, and R. F. Jarnot, Arctic ozone depletion observed by UARS MLS during the 1994-95 winter, *Geophys. Res. Lett.*, *23*, 85–88, 1996.

Mariotti, A., C. R. Mechoso, B. Legras, and V. Daniel, The evolution of the ozone "collar" in the Antarctic lower statosphere during early August 1994, *J. Atmos. Sci.*, *57*, 402–414, 2000.

Mauldin, L. E., III, N. H. Zaun, M. P. McCormick, J. H. Guy, and W. R. Vaughn, Stratospheric Aerosol and Gas Experiment II instrument: A functional description, *Opt. Eng.*, *24*, 307–312, 1985.

McKenna, D. S., P. Konopka, J.-U. Grooß, G. Günther, R. Müller, R. Spang, D. Offermann, and Y. Orsolini, A new chemical Lagrangian model of the stratosphere

(CLaMS): 1. Formulation of advection and mixing, *J. Geophys. Res.*, *107*(D16), doi:10.1029/2000JD000114, 2002.

McKenzie, R., B. Connor, and G. Bodeker, Increased summertime UV radiation in New Zealand in response to ozone loss, *Science*, *285*, 1709–1711, 1999.

McKenzie, R., D. Smale, G. Bodeker, and H. Claude, Ozone profile differences between Europe and New Zealand: Effects on surface UV irradiance and its estimation from satellite sensors, *J. Geophys. Res.*, *108*(D6), doi:10.1029/2002JD002770, 2003.

McPeters, R. D., D. F. Heath, and P. K. Bhartia, Average ozone profiles for 1979 from the NIMBUS-7 SBUV instrument, *J. Geophys. Res.*, *84*, 5199–5214, 1984.

McPeters, R. D., et al., Earth Probe Total Ozone Mapping Spectrometer (TOMS) data products user's guide, technical publication 1998-206895, NASA, Goddard Space Flight Center, Greenbelt, Maryland 20771, USA, 1998.

Molina, M. J., and F. S. Rowland, Stratospheric sink for chlorofluoromethanes: Chlorine atom catalyzed destruction of ozone, *Nature*, *249*, 810, 1974.

Morris, G. A., et al., Trajectory mapping and applications to data from the Upper Atmosphere Research Satellite, *J. Geophys. Res.*, *100*(D8), 16491–16505, 1995.

Morris, G. A., J. F. Gleason, J. Ziemke, and M. R. Schoeberl, Trajectory mapping: A tool for validation of trace gas observations, *J. Geophys. Res.*, *105*(D14), 17875–17894, 2000.

Nash, E. R., P. A. Newman, J. E. Rosenfield, and M. R. Schoeberl, An objective determination of the polar vortex using Ertel's potential vorticity, *J. Geophys. Res.*, *101*(D5), 9471–9478, 1996.

Nedoluha, G. E., R. M. Bevilacqua, K. W. Hoppel, J. D. Lumpe, and H. Smit, POAM III measurements of water vapour in the upper troposphere and lowermost stratosphere, *J. Geophys. Res.*, *107*, doi:10.1029/2001JD000793, 2002.

Newman, P. A., et al., Measurements of polar vortex air in the midlatitudes, *J. Geophys. Res.*, *101*(D8), 12879–12891, 1996.

Norton, W. A., Breaking Rossby waves in a model stratosphere diagnosed by a vortex-following coordinate system and a technique for advecting material contours, *J. Atmos. Sci.*, *51*, 654–673, 1994.

Norton, W. A., and M. P. Chipperfield, Quantification of the transport of chemically activated air from the northern hemisphere polar vortex, *J. Geophys. Res.*, *100*(D12), 25817–25840, 1995.

Öllers, M. C., P. F. J. van Velthoven, H. M. Kelder, and L. P. J. Kamp, A study of the leakage of the Antarctic polar vortex in late austral winter and spring using isentropic and 3-D trajectories, *J. Geophys. Res.*, *107*(D17), doi: 10.1029/2001JD001363, 2002.

Orsolini, Y., P. Simon, and D. Cariolle, Filamentation and layering of an idealized tracer by observed winds in the lower stratosphere, *Geophys. Res. Lett.*, *22*(7), 839–842, 1995.

Paparella, F., A. Babiano, C. Basdevant, A. Provenzale, and P. Tanga, A Lagrangian study of the Antarctic polar vortex, *J. Geophys. Res.*, *102*(D6), 6765–6773, 1997.

Parrish, A., R. L. de Zafra, P. M. Solomon, J. W. Barrett, and E. R. Carlson, Chlorine oxide in the stratospheric ozone layer: Ground-based detection and measurement, *Science*, *211*, 1158–1161, 1981.

Paur, R. J., and A. M. Bass, The ultraviolet cross-sections of ozone: II. Results and temperature dependance, in *Atmospheric Ozone*, edited by C. S. Zerefos, and A. Ghazi, pp. 611–616. Reidel, 1985.

Pérez, A., E. Crino, I. A. de Cárcer, and F. Jaque, Low-ozone events and three-dimensional transport at midlatitudes of South America during springs of 1996 and 1997, *J. Geophys. Res.*, *105*(D4), 4553–4561, 2000.

Pierce, R. B., and T. D. A. Fairlie, Chaotic advection in the stratosphere: Implications for the dispersal of chemically perturbed air from the polar vortex, *Geophys. Res. Lett.*, *98*, 18589–18595, 1993.

Pierce, R. B., W. L. Grose, J. M. Russell III, and A. F. Tuck, Evolution of southern hemisphere spring air masses observed by HALOE, *Geophys. Res. Lett.*, *21*(3), 213–216, 1994.

Pierce, R. B., J.-U. Grooss, W. L. Grose, J. M. Russell III, P. J. Crutzen, T. D. Fairlie, and G. Lingenfelser, Photochemical calculations along air mass trajectories during ASHOE/MAESA, *J. Geophys. Res.*, *102*(D11), 13153–13167, 1997.

Pierce, R. B., J. A. Al-Saadi, T. D. Fairlie, J. R. Olsin, R. S. Eckman, G. S. Lingenfelser, and J. M. Russell III, Large-scale stratospheric ozone photochemistry and transport during the POLARIS Campaign, *J. Geophys. Res.*, *104*(D21), 26525–26545, 1999.

Prather, M., and A. H. Jaffe, Global impact of the Antarctic ozone hole: Chemical propagation, *J. Geophys. Res.*, *95*(D4), 3473–3492, 1990.

Prather, M., M. M. Garcia, R. Suozzo, and D. Rind, Global impact of the Antarctic ozone hole: Dynamical dilution with a three-dimenesional chemical transport model, *J. Geophys. Res.*, *95*(D4), 3449–3471, 1990.

Press, W. H., B. P. Flannery, S. A. Teukolsky, and W. T. Vetterling, *Numerical recipes: The art of scientific computing*. Cambridge University Press, 1989.

Proffitt, M. H., et al., A chemical definition of the boundary of the Antarctic ozone hole, *J. Geophys. Res.*, *94*(D9), 11437–11448, 1989a.

Proffitt, M. H., K. K. Kelly, J. A. Powell, B. L. Gary, M. Loewenstein, J. R. Podolske, S. E. Strahan, and K. R. Chan, Evidence for diabatic cooling and poleward transport within and around the 1987 Antarctic ozone hole, *J. Geophys. Res.*, *94*, 16797–16813, 1989b.

Proffitt, M. H., et al., In situ ozone measurements within the 1987 Antarctic ozone hole from a high-altitude ER-2 aircraft, *J. Geophys. Res.*, *94*(D14), 16547–16555, 1989c.

Ramanathan, V., and R. D. Cess, Radiative transfer within the mesospheres of venus and mars, *Astrophys. J.*, *188*, 407–416, 1974.

Randall, C. E., et al., Preliminary results for POAM II: Stratospheric ozone at high northern latitudes, *Geophys. Res. Lett.*, *22*(20), 2733–2736, 1995.

Randall, C. E., R. M. Bevilacqua, J. D. Lumpe, and K. W. Hoppel, Validation of POAM III aerosols: Comparison to SAGE II and HALOE, *J. Geophys. Res.*, *106*, 27525–27536, 2001.

Randall, C. E., et al., Reconstruction of three-dimensional ozone fields using POAM III during SOLVE, *J. Geophys. Res.*, *107*(D20), doi:10.1029/2001JD000471, 2002.

Rex, M., R. J. Salawitch, M. L. Santee, J. W. Waters, K. Hoppel, and R. Bevilacqua, On the unexplained stratospheric ozone losses during cold Arctic Januaries, *Geophys. Res. Lett.*, *30*(1), doi:10.1029/2002GL016008, 2003.

Rosenfield, J. E., A simple parametrization of ozone infrared absorption for atmospheric heating rate calculations, *J. Geophys. Res.*, *96*, 9065–9074, 1991.

Rosenfield, J. E., and M. R. Schoeberl, On the origin of polar vortex air, *J. Geophys. Res.*, *106*(D824), 33485–33497, 2001.

Rosenfield, J. E., P. A. Newman, and M. R. Schoeberl, Computations of diabatic descent in the stratospheric polar vortex, *J. Geophys. Res.*, *99*(D8), 16677–16689, 1994.

Russell, J. M., et al., The Halogen Occultation Experiment, *J. Geophys. Res.*, *98*, 10777–10797, 1993.

Salawitch, R. J., et al., Loss of ozone in the Arctic vortex for the winter of 1989, *Geophys. Res. Lett.*, *17*(4), 561–564, 1990.

Schauffler, S. M., L. E. Heidt, W. H. Pollock, T. M. Gilpin, J. F. Vedder, S. Solomon, R. A. Lueb, and E. L. Atlas, Measurements of halogenated organic compounds near the tropical tropopause, *Geophys. Res. Lett.*, *20*, 2567–2570, 1993.

Schoeberl, M. R., and D. L. Hartmann, The dynamics of the stratospheric polar vortex and its relation to springtime ozone depletions, *Science*, *251*, 46–52, 1991.

Schoeberl, M. R., and L. R. Lait, Conservative-coordinate transformations for atmospheric measurements., in *The Use of EOS for the Study of Atmospheric Physics*, edited by J. Gille, and G. Visconti, pp. 419–430. International School of Physics "Enrico Fermi", 1992.

Schoeberl, M. R., and P. A. Newman, A multiple-level trajectory analysis of vortex filaments, *J. Geophys. Res.*, *100*(D12), 25801–25815, 1995.

Schoeberl, M. R., and L. C. Sparling, Trajectory modelling., in *Diagnostic Tools in Atmospheric Science*, edited by G. Visconti, pp. 289–305. International School of Physics "Enrico Fermi", 1995.

Schoeberl, M. R., et al., Reconstruction of the constituent distribution and trends in the Antarctic polar vortex from ER-2 flight observations, *J. Geophys. Res.*, *94*(D14), 16815–16845, 1989.

Schoeberl, M. R., L. R. Lait, P. A. Newman, and J. E. Rosenfield, The structure of the polar vortex, *J. Geophys. Res.*, *97*, 7859–7882, 1992.

Schoeberl, M. R., et al., The evolution of ClO and NO along air parcel trajectories, *Geophys. Res. Lett.*, *20*(22), 2511–2514, 1993.

Schoeberl, M. R., A. R. Douglass, S. R. Kawa, A. E. Dessler, P. A. Newman, R. S. Stolarski, A. E. Roche, J. W. Waters, and J. M. Russell III, Development of the Antarctic ozone hole, *J. Geophys. Res.*, *101*(D15), 20909–20924, 1996.

Shindell, D. T., D. Rind, and P. Lonergan, Increased polar stratospheric ozone losses and delayed eventual recovery owing to increasing greenhouse-gas concentrations, *Lett. Nat.*, *392*, 589–592, 1998.

Solomon, S., Stratospheric ozone depletion: A review of concepts and history, *Rev. Geophys.*, *37*(3), 275–316, 1999.

Solomon, S., S. Borrmann, R. R. Garcia, R. Portmann, L. Thomason, L. R. Poole, D. Winker, and M. P. McCormick, Heterogeneous chlorine chemistry in the tropopause region, *J. Geophys. Res.*, *21*(102), 411–421, 1997.

Sparling, L. C., J. A. Kettleborough, P. H. Haynes, M. E. McIntyre, J. E. Rosenfield, M. R. Schoeberl, and P. A. Newman, Diabatic cross-isentropic dispresion in the lower stratosphere, *J. Geophys. Res.*, *102*(D22), 25817–25829, 1997.

Stohl, A., Computation, accuracy and applications of trajectories – A review and bibliography, *Atm. Env.*, *32*(6), 947–966, 1998.

Strobel, D. F., Parametrization of the atmospheric heating rate from 15 to 120 km due to O_2 and O_3 absorption of solar radiation, *J. Geophys. Res.*, *83*, 6225–6230, 1978.

Sutton, R., Lagrangian flow in the middle atmosphere, *Q. J. R. Meteorol. Soc.*, *120*, 1299–1321, 1994.

Sutton, R. T., H. Maclean, R. Swinbank, A. O'Neill, and F. W. Taylor, High-resolution stratospheric tracer fields estimated from satellite observations using Lagrangian trajectory calculations, *J. Atmos. Sci.*, *51*(20), 2995–3005, 1994.

Swinbank, R., and A. O'Neill, A stratosphere-troposphere data assimilation system, *Mon. Wea. Rev.*, *122*, 686–702, 1994.

Tao, X., and A. F. Tuck, On the distribution of cold-air near the vortex edge in the lower stratosphere, *J. Geophys. Res.*, *99*(D2), 3431–3450, 1994.

Tuck, A. F., Synoptic and chemical evolution of the Antarctic vortex in late winter and early spring, 1987, *J. Geophys. Res.*, *94*, 16687–16737, 1989.

Tuck, A. F., and M. H. Proffitt, Comment on "On the magnitude of transport out of the Antarctic polar vortex" by Wiel M. F. Wauben et al., *J. Geophys. Res.*, *102*(D23), 28215–28218, 1997.

UNEP, Enviromental Effects of Ozone Depletion: 1998 Assesment, Tech. rep., United Nations Enviroment Programme, 1998.

Viggiano, A. A., R. A. Morris, K. Gollinger, and F. Arnold, Ozone destruction by chlorine: The impracticality of mitigation through ion chemistry, *Science*, *267*, 82–84, 1995.

von der Gathen, P., et al., Observational evidence for chemical ozone depletion over the Arctic in winter 1991-92, *Lett. Nat.*, *375*, 131–134, 1995.

Waugh, D. W., Elliptical diagnostics of stratospheric polar vortices, *Q. J. R. Meteorol. Soc.*, *123*, 1725–1748, 1997.

Waugh, D. W., and R. A. Plumb, Contour advection with surgery: A technique for investigating finescale structure in tracer transport, *J. Atmos. Sci.*, *51*(4), 530–540, 1994.

Waugh, D. W., and W. J. Randel, Climatology of Arctic and Antarctic polar vortices using elliptical diagnostics, *J. Atmos. Sci.*, *56*, 1594–1613, 1999.

Waugh, D. W., and P.-P. Rong, Interannual variability in the decay of lower stratospheric Arctic vortices, *J. Meteor. Soc. Japan*, *80*(4B), 997–1012, 2002.

Waugh, D. W., et al., Mixing of polar vortex air into middle latitudes as revealed by tracer-tracer scatterplots, *J. Geophys. Res.*, *102*(D11), 13119–13134, 1997.

Waugh, D. W., W. J. Randel, S. Pawson, P. A. Newman, and E. R. Nash, Persistence of the lower stratospheric polar vortices, *J. Geophys. Res.*, *104*(D22), 27191–27201, 1999.

Wayne, R. P., *Chemistry of Atmospheres*. Oxford University Press, New York, second edn., 1992.

WMO, Scientific Assessment of Ozone Depletion: 1998, Global Ozone Research and Monitoring Project – Report No. 44, World Meteorological Organization, Geneva, 1999.

WMO, Scientific Assessment of Ozone Depletion: 2002, Global Ozone Research and Monitoring Project – Report No. 47, World Meteorological Organization, Geneva, 2003.

Woyke, T., R. Müller, F. Stroh, D. S. McKenna, A. Engel, J. J. Margitan, M. Rex, and K. S. Carslaw, A test of our understanding of the ozone chemistry in the Arctic polar vortex based on in situ measurements of ClO, BrO, and O_3 in the 1994/95 winter, *J. Geophys. Res.*, *104*(D15), 18755–18768, 1999.

Wu, J., and A. E. Dessler, Comaprisons between measurements and models of Antarctic ozone loss, *J. Geophys. Res.*, *106*(D3), 3195–3201, 2001.

Zhou, S., M. E. Gelman, A. J. Miller, and J. P. McCormack, An inter-hemisphere comparison of the persistent stratospheric polar vortex, *Geophys. Res. Lett.*, *27*(8), 1123–1126, 2000.